Sveučilište u Rijeci
POMORSKI FAKULTET U RIJECI
FACULTY OF MARITIME STUDIES RIJEKA
University of Rijeka

University of Zagreb
Faculty of Transport
and Traffic Sciences

Royal Institute of Navigation
Science Technology Practice

ISSN 1849-7306

11th Annual Baška GNSS Conference

PROCEEDINGS

Baška, Krk Island, Croatia
7 – 9 May 2017

Sveučilište u Rijeci
POMORSKI FAKULTET U RIJECI
FACULTY OF MARITIME STUDIES RIJEKA
University of Rijeka

University of Zagreb
Faculty of Transport
and Traffic Sciences

Royal Institute of Navigation
Science Technology Practice

11th Annual Baška GNSS Conference

PROCEEDINGS

Baška, Krk Island, Croatia

7 – 9 May 2017

Published by:

University of Rijeka, Faculty of Maritime Studies, Rijeka, Croatia

The Royal Institute of Navigation, London, UK

For the Publisher:

Associate Professor Alen Jugović, Ph. D., Dean, University of Rijeka,
Faculty of Maritime Studies, Rijeka, Croatia

Publishing Associates:

Captain James B. Taylor, OBE RN, President, The Royal Institute of Navigation

John Pottle, FRIN, Director, The Royal Institute of Navigation, London, UK, Chair

Editors:

Assist. Prof. David Brčić, Ph. D., MRIN, University of Rijeka, Faculty of Maritime Studies

Assist. Mia Filić, mag. inf. et. math., MRIN, University of Zagreb, Faculty of Electrical Engineering and Computing

Assoc. Prof. Alen Jugović, Ph. D., University of Rijeka, Faculty of Maritime Studies

Academician Serdjo Kos, Ph. D., FRIN, University of Rijeka, Faculty of Maritime Studies

Front-page photo credits:

David Brčić: Moonwalk

Text formatting:

Tempora, Rijeka

Print:

AKD d.o.o. Zagreb

Address:

University of Rijeka, Faculty of Maritime Studies
Studentska 2
51000 Rijeka
Croatia
Phone: +385 (0)51 338 411
Fax: +385 (0)51 336 755
URL: http://www.pfri.uniri.hr/
E-mail: dekanat@pfri.hr

ISSN 1849-7306

CONTENTS

International Programme and Organising Committee:

John Pottle, FRIN, Director, The Royal Institute of Navigation, London, UK, Chair
Serdjo Kos, FRIN, Faculty of Maritime Studies, University of Rijeka, Croatia, Co-chair
Hrvoje Gold, Faculty of Transportation and Traffic Sciences, University of Zagreb, Croatia, Co-chair
Tomislav Kos, FRIN, Faculty of Electrical Engineering and Computing, University of Zagreb, Croatia, Co-chair
James B Taylor, FRIN, President, The Royal Institute of Navigation, London, UK
David Brčić, MRIN, Faculty of Maritime Studies, University of Rijeka, Croatia
Ljiljana R Cander, Rutherford Appleton Laboratory, Chilton, UK
Olja Čokorilo, Faculty of Transport and Traffic Engineering, University of Belgrade, Serbia
Jordi Corbera, Institut Cartogràfic i Geològic de Catalunya, Barcelona, Spain
Giovanni E Corazza, University of Bologna, Italy
Robert Crane, National Coordination Office for Space-Based PNT, Washington, DC, USA
Franc Dimc, Faculty of Maritime Studies and Transport, University of Ljubljana, Portorož, Slovenia
Shaoujun Feng, FRIN, Imperial College, London, UK
Mia Filić, MRIN, satellite navigation, SDR and deep networks specialist, Sesvete, Zagreb, Croatia
Renato Filjar, FRIN, satellite navigation, SDRand space weather specialist, Kalinovac, Croatia
Sharafat Gadimova, UN Office of Outer Space Affairs, Vienna, Austria
Luka Grubišić, Faculty of Science, University of Zagreb, Croatia
Darko Huljenić, MRIN, Ericsson Nikola Tesla, Zagreb, Croatia
Siniša Krajnović, LM Ericsson, Stockholm, Sweden
Bal Krishna, Coordinates Journal, Delhi, India
Marta Krywanis-Brzostowska, European GNSS Agency, Prague, Czech Republic
David Last, FRIN, Consultant Engineer and Expert Witness, Conwy, UK
Kristijan Lenac, MRIN, Faculty of Engineering, University of Rijeka, Croatia
Andrea Lučić, MRIN, satellite navigation and SDRspecialist, Rijeka, Croatia
Anastasia Lyubimova, GLONASS/GNSS Forum Association, Moscow, Russia
Roger A McKinley, Consultant, Leatherhad, UK
Terry Moore, FRIN, University of Nottingham, UK
Washington Y Ochieng, FRIN, Imperial College, London, UK
Majda Petrić, School of Electrical Engineering, University of Belgrade, Serbia
Ivan Rumora, Croatian Navy, Pula, Croatia
Laura Ruotsalainen, Finnish Geodetic Institute, Masala, Finland
Nenad Sikirica, Polytechnic Hrvatsko Zagorje Krapina, Krapina, Croatia
Enik Shytermeja, Ecole Nationale de l'Aviation Civile, Toulouse, France
Grigory Stupak, Russian Space Systems, Moscow, Russia
Marko Ševrović, MRIN, Faculty of Transport and Traffic Sciences, University of Zagreb, Croatia
Adam Weintrit, FRIN, Faculty of Navigation, Gdynia Maritime University, Gdynia, Poland
Jingnong Weng, Beihang University of Aeronautics and Astronautics, Beijing, China

List of reviewers:

Tomislav Kos (Croatia), David Brčić (Croatia), Luka Grubišić (Croatia), Josip Vuković (Croatia), Franc Dimc (Slovenia), Tanja Brcko (Slovenia), Mario Muštra (Croatia), Diego Sušanj (Croatia), Dawit Tegbaru (USA), Laura Ruotsalainen (Finland).

Sveučilište u Rijeci
POMORSKI FAKULTET U RIJECI
FACULTY OF MARITIME STUDIES RIJEKA
University of Rijeka

University of Zagreb
Faculty of Transport
and Traffic Sciences

Royal Institute of Navigation
Science Technology Practice

11th Annual Baška GNSS Conference

PROCEEDINGS

Sveučilište u Rijeci
POMORSKI FAKULTET U RIJECI
FACULTY OF MARITIME STUDIES RIJEKA
University of Rijeka

University of Zagreb
Faculty of Transport
and Traffic Sciences

Royal Institute of Navigation
Science Technology Practice

11th
Annual
Baška GNSS
Conference

IMPROVEMENT OF STANDARD GPS POSITION ESTIMATION ALGORITHM THROUGH UTILIZATION OF WEIGHTED LEAST-SQUARE APPROACH

Mia Filić[1], **Luka Grubišić**[1], **Renato Filjar**[2,3]

[1] Faculty of Science, University of Zagreb, Croatia
E-mail: luka.grubisic2@gmail.com (Corresponding author)
[2] Faculty of Maritime Studies, University of Rijeka, Croatia
[3] Faculty of Engineering, University of Rijeka, Croatia

ABSTRACT

This paper covers the analysis of (reference) position estimation procedures in the navigation application domain, discovering of potential weaknesses and suggesting the improvement. The algorithm analysis involves practical performance and rating of the algorithm performance quality using measured pseudorange. For the empirical comparison, we used GPS receiver's observations collected from IGS reference station located in Padua, Italy. We present a quantitative performance comparison of the modified and the standard algorithm, based on simulations conducted in R environment for statistical computing.

Key words: *GNSS position estimation algorithm, weighted least-square method, GPS ionospheric error*

1 INTRODUCTION AND MOTIVATION

The most frequently used global positioning system is the American GPS system. Its widespread utilisation results from its ability to provide globally available and continuous positioning and timing signals of sufficient quality for a range of relates services to users equipped only with an appropriate receivers. The fact that this service is provided at no extra charge (Petrovski and Tsujii, 2012, Sanz Subirana *et al*, 2013), is one of the main reasons for its ubiquitous presence. As a result, GPS and services based on it are considered as a globally available infrastructure. Its performance directly impacts tackling of a broad scope of societal challenges (Canon *et al*, 2013, Thomas *et al*, 2011, Grzebellus, Filjar and Kusters, 2013). Although, GPS system mostly operates reliably it can experience service outages due to both internal and external factors (Thomas *et al*, Baraniuk, 2016a, Baraniuk, 2016b, 2011, Celestrack, 2016). In this note we consider the sensitivity of the standard positioning estimator on the choice of the numerical method used in estimation process. We propose a preconditioning technique, which stabilises the numerical procedure, based on geometrical properties of the satellite constellation used for solving the positioning problem. We present the algorithm and discuss its properties in a case study based on real positioning data from the IGS reference station in Padua (IGS, 2017), with the case-scenario of mitigation of GPS ionospheric effects.

2 DESCRIPTION OF THE PROBLEM AND THE PROPOSED SOLUTION APPROACH

The causes of GPS positioning quality deterioration can be grouped into Geometric Dilution of Precision (caused by inadequate and uneven spatial distribution of visible satellites), and User Equivalent Ranging Error (comprising all the sources of satellite signal delay and, consequently, wrong estimation of pseudorange) components (Sanz Subirana *et al*, 2013). The accuracy needed for societally relevant applications, like Intelligent Transportation Systems range from 1 m – 5 m for Emergency Services, to 10 m – 50 m for Traffic Information Services, (Thomas *et al*, 2011, SaPPART, 2015). This accuracy is frequently achieved by a combination of precision boosting techniques. The first step is always to compute an estimator of a solution to the standard positioning equation. This is typically done by computing an unbiased estimator of the position by solving a non-linear least squares problem (Björck, 1996). A

linearised Taylor series-based method is often referred to as the standard position estimation model for position estimation in navigation (application) domain for its mathematical and computational simplicity (Tian *et al*, 2012). This estimator usually does not have a sufficient precision for any of the above listed applications and further techniques are employed in improving the accuracy of the estimator.

Ionospheric delay is considered the principal contributor to GNSS positioning error budget. The amount of the GPS ionospheric delay is directly related to the number of ionised particles encountered by the satellite signal on its path, expressed by Total Electron Content (TEC) variable. Actual TEC encountered by the satellite signal travelling at real elevation angle in regard to the GPS receiver aerial is commonly called Slant TEC (STEC), while its normal component is commonly known as Vertical TEC (VTEC). The nature of GPS ionospheric delay is complex, and involves bias, systematic and stochastic components, thus leaving the GPS ionospheric error mitigation a daunting task. Mitigation approaches range from acceptance of the errors as negligible and utilisation of GPS ionospheric delay correction models (Klobuchar etc.) in GPS pseudorange pre-conditioning (corrections), to advanced signal processing methods in base-band domain, depending on the utilisation scenario. The correct estimation of the GPS ionospheric error requires a very detailed description of the whole ionosphere. Numerous correction models attempts to simplify the correction estimation task by estimation of the VTEC first, then extending it to the actual STEC. Although simple, this approach leaves an unknown and potentially large amount of the GPS ionospheric error uncorrected.

The purpose of this paper is to propose the advancement and discuss the performance of the least squares positioning estimator of the position in relation to several preconditioning techniques which will be employed to solve the problem. The accuracy threshold level is to be determined based on the requirements for the performance characteristic of the measuring device employed. Also, we will discuss the use of appropriate measures of the sensitivity of the positioning problem to Geometric Dilution of Precision by analysing the structure of the least squares solution method. Developed approach is considered from the perspective of the case-scenario of integrated approach for GPS ionospheric effects mitigation. The direct utilisation of the elevation angle into position estimator brings the information of the actual TEC spatio-temporal variations in a simple and efficient manner. This allows for

direct mitigation of the actual TEC (STEC), rather than dealing with it indirectly through VTEC estimation first and with the effects of the broader region of local atmosphere not considered. The alternative position estimator proposed here maintains the mathematical and computational simplicity at the level of the standard approach, thus leaving it applicable in large number of use-case scenarios and equipment. The alternative model proposed her is in a sense of position estimation-related linear mode (Gustafsson, 2012).

3 STANDARD POSITIONING ALGORITHM

The standard positioning algorithm is based on the solution of the system

$$d_1 = \sqrt{(x - x_1)^2 + (y - y_1)^2 + (z - z_1)^2} + d + v_1 \tag{1}$$

$$d_2 = \sqrt{(x - x_2)^2 + (y - y_2)^2 + (z - z_2)^2} + d + v_2 \tag{2}$$

$$d_3 = \sqrt{(x - x_3)^2 + (y - y_3)^2 + (z - z_3)^2} + d + v_3 \tag{3}$$

$$d_4 = \sqrt{(x - x_4)^2 + (y - y_4)^2 + (z - z_4)^2} + d + v_4 \tag{4}$$

using iterative least squares method. Here $d = cd_T$ and the vector

$$\boldsymbol{v} = \begin{bmatrix} v_1 \\ v_2 \\ v_3 \\ v_4 \end{bmatrix} \tag{5}$$

represents the errors in the process on which we assume standard statistical restrictions (independence and centralized Gaussian distribution). Let us introduce the following notation

$$\boldsymbol{x} = \begin{bmatrix} x_1 \\ x_2 \\ x_3 \\ x_4 \end{bmatrix} = \begin{bmatrix} x_s \\ x_t \end{bmatrix} \in \mathbb{R}^4 = \mathbb{R}^3 \times \mathbb{R}, \tag{6}$$

where $x_s = [x\ \ y\ \ z]^t \in \mathbb{R}^3$. We also define

$$\boldsymbol{\rho} = \begin{bmatrix} d_1 \\ d_2 \\ d_3 \\ d_4 \end{bmatrix}. \tag{7}$$

This is the vector of distances to the sources s_i, defined by $s_i = [x_i\ \ y_i\ \ z_i]^t$, $i \in \mathbb{N}$. The vector of residual errors associated to the observations s_i, $i = 1, 2, 3, 4$ is

$$h(\boldsymbol{x}) = \begin{bmatrix} ||s_1 - x_s|| + x_t c \\ ||s_2 - x_s|| + x_t c \\ ||s_3 - x_s|| + x_t c \\ ||s_4 - x_s|| + x_t c \end{bmatrix}. \tag{8}$$

We can now write the nonlinear positioning system of equations in the vector notation as

$$\boldsymbol{\rho} = h(\boldsymbol{x}) + \boldsymbol{v}. \tag{9}$$

Let us define the residual of the position estimation system as $p(x) := \rho - h(x)$. Under the standard statistical assumptions on the measurement error υ, the minimiser x_c of the norm of the residual defined by

$$\boldsymbol{x_c} := \underset{\boldsymbol{x}}{\operatorname{argmin}}\, p(\boldsymbol{x})^t p(\boldsymbol{x}) \tag{10}$$

is an unbiased estimator od the solution x of the positioning system of equations.

Since this is a quadratic minimization problem it possesses a unique solution. To solve this nonlinear minimization problem we construct, starting from $x_0 \in \mathbb{R}^3$, the sequence

$$\boldsymbol{x}_{k+1} = \boldsymbol{x}_k - (J_k^t J_k)^{-1} J_k^t p(\boldsymbol{x}_k). \tag{11}$$

In this formula, we used the Jacobi matrices $J_k = D_p(x_k)$. We note that the matrix $(J_k^t J_k)^{-1} J_k^t$ is sometimes denoted by J_k^+ and is called the generalized inverse of J_k.

The method which we used to construct this sequence is called the Newton-Gauss method. Its convergence is understood in the sense that

$$\boldsymbol{x}_c = \lim_{k\to\infty} \boldsymbol{x}_k. \tag{12}$$

However, unlike the standard Newton method the convergence of the Gauss-Newton method is not guaranteed, not even locally (under the assumption that the initial approximation is fine enough). It is however shown that if the method converges, then the limit of x_k is the stationary point of the error function $p(x)^t p(x)$. For details see (Björck, 1996).

The rate of the convergence of the method can approach quadratic convergence rate. However, the method might not converge if the initial guess is far from the stationary point, or if the approximate Hessian ($J_k^t J_k$) is ill conditioned. In the cases of slow convergence the method is typically improved by employing relaxation in the search for the descent direction and a trust region approach like Levenberg–Marquardt approach.

Instead of minimizing the function $F(x) = p(x)^t p(x)$ we will be minimizing the function $F'(x) = p'(x)^t p'(x)$, where squared residual is defined as

$$p'(\boldsymbol{x}) = \begin{bmatrix} (d_1 - x_t c)^2 - (x_1 - x)^2 - (y_1 - y)^2 - (z_1 - z)^2 \\ (d_2 - x_t c)^2 - (x_2 - x)^2 - (y_2 - y)^2 - (z_2 - z)^2 \\ (d_3 - x_t c)^2 - (x_3 - x)^2 - (y_3 - y)^2 - (z_3 - z)^2 \\ (d_4 - x_t c)^2 - (x_4 - x)^2 - (y_4 - y)^2 - (z_4 - z)^2 \end{bmatrix} \tag{13}$$

The functions $F(x)$ and $F'(x)$ have the same minimizers, but the gradient of $F'(x)$ has a more convenient form. The gradient matrix of the function $p'(x)$ will be denoted by $J'(x, y, z, x_t)$ and is given in the factorized form by

$$D_x p' = J'^{(x,y,z,x_t)} = 2\begin{bmatrix} (x_1 - x) & (y_1 - y) & (z_1 - z) & (d_1 - x_t c) \\ (x_2 - x) & (y_2 - y) & (z_2 - z) & (d_2 - x_t c) \\ (x_3 - x) & (y_3 - y) & (z_3 - z) & (d_3 - x_t c) \\ (x_4 - x) & (y_4 - y) & (z_4 - z) & (d_4 - x_t c) \end{bmatrix} \begin{bmatrix} 1 & 0 & 0 & 0 \\ 0 & 1 & 0 & 0 \\ 0 & 0 & 1 & 0 \\ 0 & 0 & 0 & -c \end{bmatrix}. \tag{14}$$

The sequence of matrices which we construct is again given by the rule

$$\boldsymbol{x}'_{k+1} = \boldsymbol{x}'_k - \left(J'^{\,t}_k J'_k\right)^{-1} J'^{\,t}_k \, p'(\boldsymbol{x}'_k). \tag{15}$$

The sequence can converge, if it converges, to the same collection of stationary points however the conditioning of the Jacobian matrices J'_k is possibly different. In the next section, we will present another possibility to influence the convergence rate.

4 WEIGHTED LEAST SQUARES APPROACH

In this section, we will explore the possibility to precondition the Jacobian matrix of the positioning system by diagonal scaling. This scaling will have the effect of changing the nature of the least squares minimization so that we will be considering the weighted liest squares problem. We will use the geometrical concept of the elevation angle to precondition the positioning equations. This choice also can be motivated by the consideration of the expected errors in the receiver.

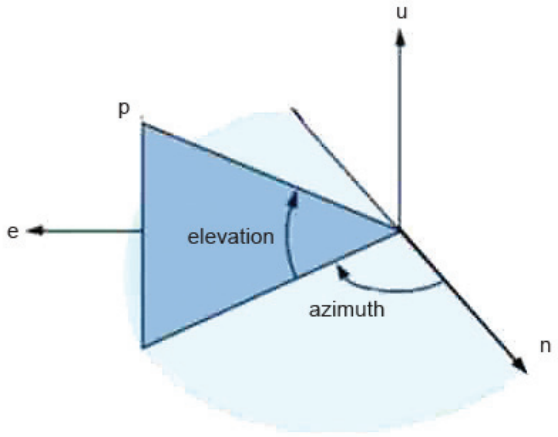

Figure 1. Elevation angle

First, let us define the necessary concepts. The elevation angle of a GPS satellite determined by coordinates $s_i = [x_i \quad y_i \quad z_i]^t$ and the receiver with coordinates $s_k = [x_k \quad y_k \quad z_k]^t$ in the reference WGS84 coordinate system is defined as

$$\theta(s_i, s_k) = \left(\frac{\pi}{2} - \lambda_i(s_i, s_k)\right) \tag{16}$$

where

$$\cos\lambda_i(s_i,s_k)=\frac{[x_i-x_k \quad y_i-y_k \quad z_i-z_k][x_i \quad y_i \quad z_i]^t}{\left|\left|[x_i-x_k \quad y_i-y_k \quad z_i-z_k]\right|\right|\cdot\left|\left|[x_i \quad y_i \quad z_i]\right|\right|}. \tag{17}$$

Here we assumed $\lambda_i(s_i, s_k) > 0$, in the case in which $\lambda_i(s_i, s_k) < 0$ we use

$$\theta(s_i,s_k)=\left(\frac{\pi}{2}+\lambda_i(s_i,s_k)\right). \tag{18}$$

To precondition the positioning problem, we will consider the modified minimization problem

$$F_W(\boldsymbol{x})=p'(\boldsymbol{x})^t W p'(\boldsymbol{x}). \tag{19}$$

As a position estimator we seek the minimizer

$$\boldsymbol{x_w}:=\underset{\boldsymbol{x}}{\operatorname{argmin}}\, p'(\boldsymbol{x})^t W p'^{(\boldsymbol{x})}. \tag{20}$$

We solve this system also by Newton Gauss method which now reads

$$\boldsymbol{x}_{k+1}=\boldsymbol{x}_k-(J_k^t W\, J_k)^{-1}J_k^t W p'^{(x_k)}. \tag{21}$$

As diagonal preconditioners we will use the following weighting matrices

$$W_1=\begin{bmatrix}\frac{1}{\sin\theta(s_1,s_k)} & 0 & 0 & 0\\ 0 & \frac{1}{\sin\theta(s_2,s_k)} & 0 & 0\\ 0 & 0 & \frac{1}{\sin\theta(s_3,s_k)} & 0\\ 0 & 0 & 0 & \frac{1}{\sin\theta(s_4,s_k)}\end{bmatrix}, \tag{22}$$

$$W_2=\begin{bmatrix}1+\frac{2}{\sin\theta(s_1,s_k)} & 0 & 0 & 0\\ 0 & 1+\frac{2}{\sin\theta(s_2,s_k)} & 0 & 0\\ 0 & 0 & 1+\frac{2}{\sin\theta(s_3,s_k)} & 0\\ 0 & 0 & 0 & 1+\frac{2}{\sin\theta(s_4,s_k)}\end{bmatrix}, \tag{23}$$

$$W_3 = \begin{bmatrix} \frac{1}{\left(\frac{1}{2}+\sin(\theta(s_1,s_k))\right)^2} & 0 & 0 & 0 \\ 0 & \frac{1}{\left(\frac{1}{2}+\sin(\theta(s_2,s_k))\right)^2} & 0 & 0 \\ 0 & 0 & \frac{1}{\left(\frac{1}{2}+\sin(\theta(s_3,s_k))\right)^2} & 0 \\ 0 & 0 & 0 & \frac{1}{\left(\frac{1}{2}+\sin(\theta(s_4,s_k))\right)^2} \end{bmatrix}. \quad (24)$$

We were motivated in the construction of these matrices by the fact that depending on the length of the path of the signal through ionosphere, more errors could be expected. However, also the angle between the columns of the matrix J_k has a direct influence on the ill conditioning of the evaluation of the pseudo inverse J_k^+. The columns which span a smaller angle, lead to more ill conditioned pseudo inverse. Subsequently, using diagonal matrices W_i and computing

$$J_k^{+W} = (J_k^t W_i J_k)^{-1} J_k^t W_i. \quad (25)$$

might lead to a better conditioned matrix then when computing $J_k^+ = (J_k^t J_k)^{-1} J_k^t$. We will assess this claim in an empirical case study in the next section.

Finally, let us return to the Jacobian matrix $D_x p'$. This matrix should be used in the algorithm in the factorized form. The condition number of the matrix $D_x p'$, defined by

$$\kappa = \| D_x p' \| \| (D_x [\![p']\!])^{-1} \|, \quad (26)$$

can be estimated as $\kappa = 0(c) = 0(1e + 19)$, and so

$$\| (D_x [\![p']\!])^{-1} (D_x [\![p']\!])^{-t} \| = O(c^2) = O(1e + 18). \quad (27)$$

On the other hand, the matrix

$$J_k' \,\mathrm{diag}(1,1,1,c^{-1}) = \begin{bmatrix} (x_1 - x) & (y_1 - y) & (z_1 - z) & (d_1 - x_t c) \\ (x_2 - x) & (y_2 - y) & (z_2 - z) & (d_2 - x_t c) \\ (x_3 - x) & (y_3 - y) & (z_3 - z) & (d_3 - x_t c) \\ (x_4 - x) & (y_4 - y) & (z_4 - z) & (d_4 - x_t c) \end{bmatrix} = T_{s,k} \quad (28)$$

can have a considerably smaller condition number. In the examples which we considered

$$\| T_{s,k} \| = O(1e1) \tag{29}$$

and so an algorithm which computes the pseudo inverse in the factorized form, assuming Γ = diag(1,1,1,c^{-1}) is the diagonal scaling matrix, reads

$$\left(J_k'^{t} J_k'\right)^{-1} J_k^t = \Gamma(T_s^* T_s)^{-1} T_s^t \tag{30}$$

and the inverse $(T_s^*\, T_s)^{-1}$ is a much better-behaved object.

5 NUMERICAL EXPERIMENTS

A simulation framework for numerical experiments was developed using the open-source R environment for statistical computing. The empirical assessment was conducted using the set of benchmark GPS receiver's experimental single-frequency GPS pseudorange observations collected from the IGS reference station located in Padua, Italy (IGS 2017). The IGS benchmark (reference) stations collect data on the regular basis, 24-hours a day, with the 30 s-sampling interval.

We used three different computational models for the assessment of computational simplicity of the proposed alternative approach in estimation of GPS positions based on experimental GPS pseudoranges, and in the case-scenario addressing the GPS ionospheric delay mitigation, as follows.

Model 1 was developed in R environment for statistical computing, based on utilisation of the normal equations system (Gustafsson, 2012).

Model 2 was developed in R environment for statistical computing, based on utilisation of the QR decomposition (Gustafsson, 2012).

Model 3 was developed in R environment for statistical computing, based on utilisation of the Singular Value Decomposition (SVD) (Gustafsson, 2012).

All three models required the iterative process deployment. In the performance assessment procedure, we set targeted GPS positioning accuracy/the value of norm of the correction vector (10 m) as the iteration process control parameter, and observed the number of iterations and computational time required for reaching targeted positioning accuracy.

The assessment results are presented in Table 1.

Table 1. Assessment results of models

MODEL	1	2	3
Timing	0.12	0.46	0.08
Iteration count	38	192	14

We see that the number of iterations necessary to achieve the convergence criterion significantly depends on the scaling matrix W (Fieller, 2016). The error of the positioning estimate was in kilometres, which can be improved by other methods to achieve the usual accuracy of less than 10 meters. Furthermore, it should be pointed out that the choice of the method to compute the next iterate in the Newton – Gauss algorithm considerably influences the convergence behaviour (Gulliksson *et al*, 1992, Nielsen, 2013, Gander *et al*, 2014). Also, the implementation of the chosen algorithm for computing the weighted pseudo inverse significantly influences the performance (Fieller, 2016).

6 CONCLUSION AND FUTURE WORK

In this note we present the direct implementation of the generalized weighted pseudo-inverse method for a mathematically and computationally simple GPS position estimator in navigation (application) domain. We also performed several preliminary tests on alternative implementation of the algorithm. Initial experiments, where the weighted pseudo inverse was computed using the weighted QR decomposition method, as cited, show far superior performance to the direct evaluation which we presented in this note. The results are still in the raw form, so we will just outline the expectations. There the convergence could be achieved in as little as 5 iterations with the measure of the error in tens of meters. Reporting on this development, as well as on a thorough discussion of the conditioning (dilution of the precision measure) of the method will be the topic of the follow up report.

Acknowledgment

The work presented in this manuscript resulted partly from the activities performed within the COST Action TU1302 *Satellite Positioning Performance Assessment for Road Transport*. The participation of L.G. in the conference has been supported by Croatian mathematical society and the Croatian mathematical electronic journal (http://e.math.hr).

References

Celestrak. (2016). Notice Advisory to Navstar Users (NANU) No. 2016008. Available at: https://celestrak.com/GPS/NANU/2016/nanu.2016008.txt, accessed on 19 August, 2016.

Cannon, P *et al.* (2013). Extreme space weather: impacts on engineered systems and infrastructure. Royal Academy of Engineering. London, UK. Available at: http://bit.ly/11OdBNN. accessed on 4th November, 2017.

Fieller, N. (2016). Basics of Matrix Algebra for Statistics with R. CRC Press, Taylor & Francis Group. Boca Raton, FL.

Gander, W. *et al*. (2014). Scientific Computing – An Introduction using Maple and MATLAB.

Grzebellus, M, Filjar, R. and Kusters, M M. (2013). An initial experimental validation of the eCall service performance. *Proc of European ITS Congress 2013* (on CD, 12 pages). Dublin, Ireland.

Gulliksson, M. and Wedin, P. (1992). Modifying the QR-Decomposition to Constrained and Weighted Linear Least Squares-SIAM J. Matrix Anal. & Appl., 13(4), 1298–1313.

Gustafsson, F. (2012). Statistical Sensor Fusion. Sutudentlitteratur. Lund, Sweden.

IGS. (2017). International GNSS Service observations archive and products. Available at: http://www.igs.org, accessed on: 4th November, 2017.

Nielsen, A A. (2013). Least Squares Adjustment: Linear and Nonlinear Weighted Regression Analysis (technical note). Technical University of Denmark. Lyngby, Denmark.

Petrovski, I G. and Tsujii, T. (2012). Digital Satellite Navigation and Geophysics: A Practical Guide with GNSS Signal Simulator and Receiver Laboratory. Cambridge University Press. Cambridge, UK.

Sanz Subirana, J *et al*. (2013). GNSS Data Processing – Volume I: Fundamentals and Algorithms. ESA. Noordwijk, The Netherlands.

SaPPART. (2015). SaPPART White Paper: Better use of Global Navigation Satellite Systems for safer and greener transport. Available at: http://bit.ly/1N3wO5L, accessed on 19 August, 2016.

Tian, A *et al*. (2013). GPS Single Point Positioning Algorithm Based on Least Sqauers. Proc of sixth International Symposium on Computational Intelligence and Design. Hangzhou, China.

Takasu, T. (2013). RTKLIB: An Open Source Program Package for GNSS Positioning. Software and documentation available at: http://www.rtklib.com, accessed on 19 August, 2016.

Thomas, M *et al*. (2011). Global Navigation Space Systems: reliance and vulnerabilities. Royal Academy of Engineering. London, UK. Available at: http://bit.ly/1vrIenu, accessed on 19 August, 2016.

Sveučilište u Rijeci
POMORSKI FAKULTET U RIJECI
FACULTY OF MARITIME STUDIES RIJEKA
University of Rijeka

University of Zagreb
Faculty of Transport
and Traffic Sciences

Royal Institute of Navigation
Science Technology Practice

11th
Annual
Baška GNSS
Conference

INFLUENCE OF THE INBUILT TROPOSPHERIC CORRECTIONS TO GPS POSITIONING PERFORMANCE

Ivan Rumora[1], **Serdjo Kos**[2], **Tomislav Josip Mlinarić**[3]

[1] Croatian Navy, Pula, Croatia
E-mail: ivan.rumora@yahoo.com (Corresponding author)
[2] Faculty of Maritime Studies, University of Rijeka, Croatia
[3] Faculty of Transport and Traffic Sciences, University of Zagreb, Croatia

ABSTRACT

Satellite navigation has become a component of national infrastructure, with a growing number of applications, systems and services relying upon its Positioning, Navigation and Timing (PNT) services performance. Throughout the years, the main sources of the absolute GPS positioning error budget were identified, with the aim to determine the influence of the inbuilt tropospheric corrections to GPS positioning performance. The GPS tropospheric delay is commonly understood a minor and often negligible GPS positioning error source for various applications. Here we examine the foundations of that presumption through analysis of the real GPS positioning performance as experienced by a commercial-grade single-frequency GPS receiver with utilisation of several tropospheric correction scenarios (no correction, Saastamoinen). The study was based on real raw GPS pseudorange observations that were later post-processed using a GPS Software Defined Radio (SDR) that simulates a real receiver. Test period was 24 hours. Ionospheric corrections were not applied. We found noticeable effects of GPS tropospheric delay on GPS positioning performance for categories of various GPS applications, importance of tropospheric delay correction model deployment, and staged subject for future research aimed at improvement of GNSS positioning performance. Ionospheric corrections for this work are not included but also they could be included in some other paper because in this paper we are arguing about the difference (Δ) between the corrected and uncorrected tropospheric delay.

Key words: *GNSS, positioning performance deterioration, tropospheric correction*

1 INTRODUCTION

The rising market share of satellite navigation equipment causes the satellite navigation performance to become the essential quality parameter for a diversity of various applications and services (Thomas *et al*, 2011). In due course, studying the GNSS positioning performance in different utilisation scenarios and positioning environments gains the importance in assessing the potential risks of GNSS utilisation as the underlying enabling technology (Filjar and Huljenić, 2012). Further refinement of the subject of the GNSS-based applications and services development has been found recently in matching the required level of positioning accuracy with the positioning performance observed in the suitable configured GNSS receiver that simulates the specific positioning environment conditions.

2 PROBLEM DESCRIPTION AND PREVIOUS RESEARCH

Tropospheric delay of the GNSS radio signals has been identified as a contributor to the over-all GNSS positioning error budget since the times of introduction of satellite navigation systems. It consists of a large systematic error, and small random error components. While reasonably important in precise surveying applications, tropospheric GPS error seemed to have a negligible effect on navigation related GPS positioning applications, primarily due to theoretical ability of correction models to successfully mitigate the effects of tropospheric delay on the over-all GPS positioning error budget.

The GPS tropospheric delay results from the effects of the lower atmosphere (troposphere) at the heights between the Earth's sea level and the 18 km top-side boundary of the troposphere (Stull, 2015). Although the troposphere is (mostly) not an ionised media in the sense that it may cause noticeable effects on the satellite signal propagation characteristics, the effects due to variation of the air temperature and humidity cause the satellite signal delay in microwave portion of the spectrum (Petrovski, 2014).

The proportion of the systematic error in the over-all GPS positioning error budget has already been exploited in development of the GPS tropospheric error correction models. A comprehensive review of GPS tropospheric correction model was given by (Kos, Markezic and Botincan, 2009), and (Sanz Subirana *et al*, 2013). The Saastamoinen model (Sanz Subirana *et al*, 2013) has been

recognised as the most suitable and the de facto standard GPS tropospheric error correction model. Outlined in equations (1) to (3) are for calculation of standard atmospheric conditions while Saastamonien model (4) can correct up to 90% of the overall GPS tropospheric delay effect.

$$p = 1013.25 \cdot (1 - 2.2557 \cdot 10^{-5} h)^{5.2568} \quad (1)$$

$$T = 15.0 - 6.5 \cdot 10^{-3} h + 273.15 \quad (2)$$

$$e = 6.108 \cdot exp\left\{\frac{17.15T - 4684.0}{T - 38.45}\right\} \cdot \frac{h_{rel}}{100} \quad (3)$$

$$T_r^s = \frac{0.002277}{\cos z}\left\{p + \left(\frac{1255}{T} + 0.05\right)e - \tan^2 z\right\} \quad (4)$$

$$z = \frac{\pi}{2} - El_r^s \quad (5)$$

Parameters of the model are referred to as:

p … total surface air pressure in [hPa]

h … height above the sea level

h_{rel} … relative humidity

T … air temperature in [K]

z … zenith angle [rad]

El_r^s … elevation angle of the s-th satellite, as seen from the user's perspective [rad]

e … partial vapour pressure

T_r^s … Tropospheric delay of the s-th satellite

Based on the knowledge of tropospheric positioning environment parameters, the model is predominantly used with the estimations provided by the standard model of the atmosphere, embedded in every commercial GNSS receiver.

Still, the ability of the Saastamoinen model to mitigate GPS tropospheric error in order to comply with the requirements of emerging GPS applications remains unconfirmed, and have been attempted to be addressed in this study for various scenarios.

3 A CASE-STUDY DESCRIPTION AND METHODOLOGY

We challenged the problem by conducting a research in determination of the GPS positioning performance as observed by a commercial single-frequency receiver in a common weather conditions, and assessing the potential effects affecting a range of characteristic GPS applications.

The research methodology was simulation-based one of a commercial-grade GPS receiver, that utilise a Software-Defined GNSS receiver RTKLIB for postprocessing of experimentally collected raw single-frequency GPS pseudorange observations (Takasu, 2013), as detailed in (Filić, Filjar and Routsalainen, 2016). Raw pseudoranges were corrected for satellite an ephemeris clock errors using the corrections broadcast by GPS system at the time of the experimental data collection. The ionospheric corrections were not applied (Figure 1).

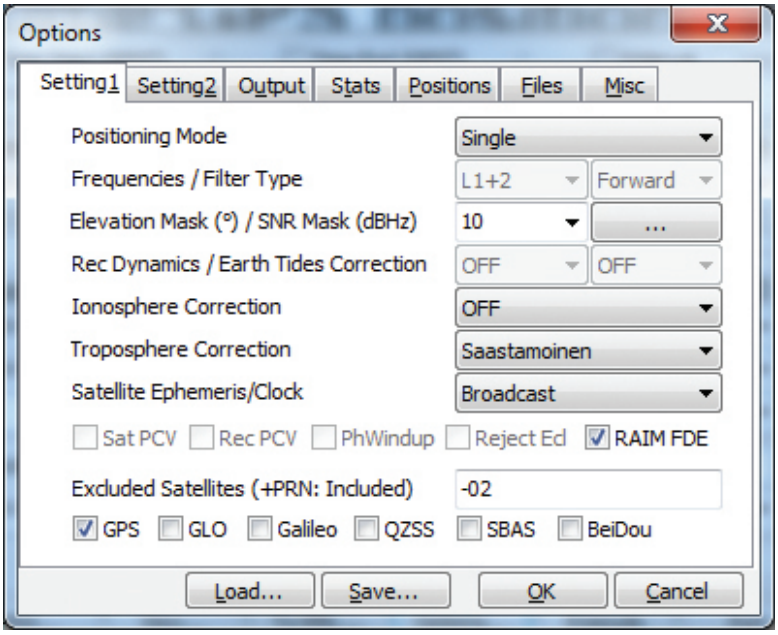

Figure 1. Configuration of the RTKLIB/RTKPOS GNSS Software-Defined Radio (SDR) receiver

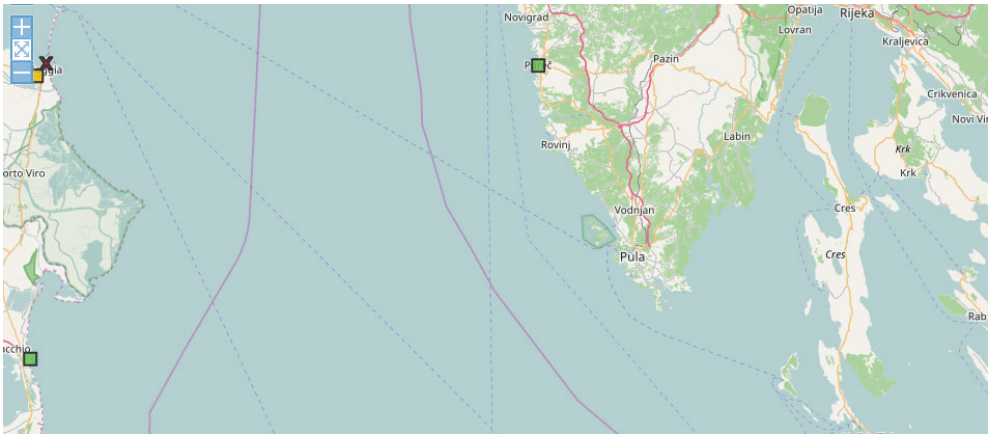

Figure 2. Reference station Porto Garibaldi, Ferrara, Italy (marked with X)

Two scenarios were simulated, one leaving the tropospheric GPS delay uncorrected, and the other one with Saastamoinen correction model based on standard atmosphere applied.

The GPS pseudoranges taken at the stationary-positioned reference station Porto Garibaldi (Figures 2 and 3), Ferrara, Italy (N44.67694444, E12.24916660) taken on 13th May, 2015 in deteriorating spring weather conditions and moderate wind (Sonel, 2017) were fed to the RTKLIB GNSS SDR in order to produce a time series of the GPS position and positioning error (in regard to the actual position of the reference station) time series. Time series of northing, easting, and vertical GPS positioning errors were then examined using a dedicated home-made software, developed in the R environment for statistical computing (R development core team, 2017, Crawley, 2013).

Figure 3. The Porto Garibaldi reference station set-up

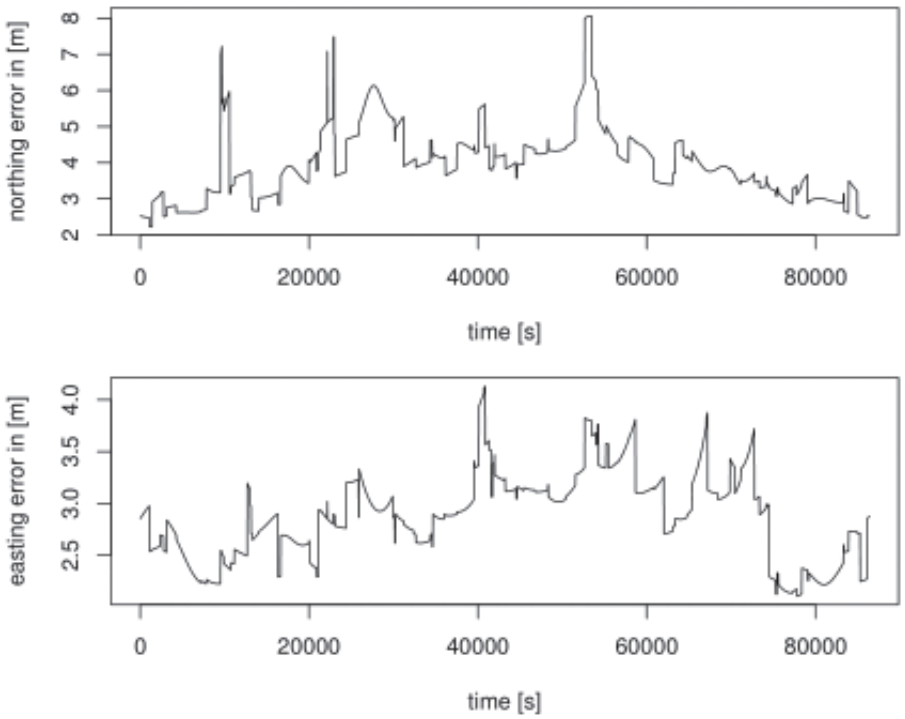

Figure 4. Time series of northing (upper diagram) and easting (lower diagram) single-frequency un-corrected GPS tropospheric positioning errors at Porto Garibaldi on 13th May, 2015

4 RESEARCH RESULTS

Research results of the single-frequency GPS positioning performance in two positioning environments (un-corrected tropospheric effects, and Saastamoinen-corrected tropospheric effects) are presented in this section.

Time series and histograms (estimates of statistical distributions) of northing, easting, and vertical GPS positioning errors are depicted in diagrams that follow.

4.1 Scenario 1: GPS positioning performance of the simulated Saastaimoinen-corrected single-frequency commercial-grade GPS receiver.

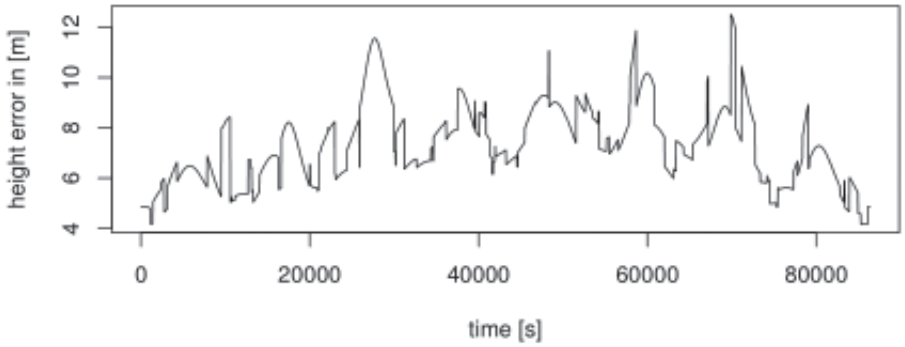

Figure 5. Time series of vertical single-frequency un-corrected tropospheric GPS positioning errors at Porto Garibaldi on 13th May, 2015

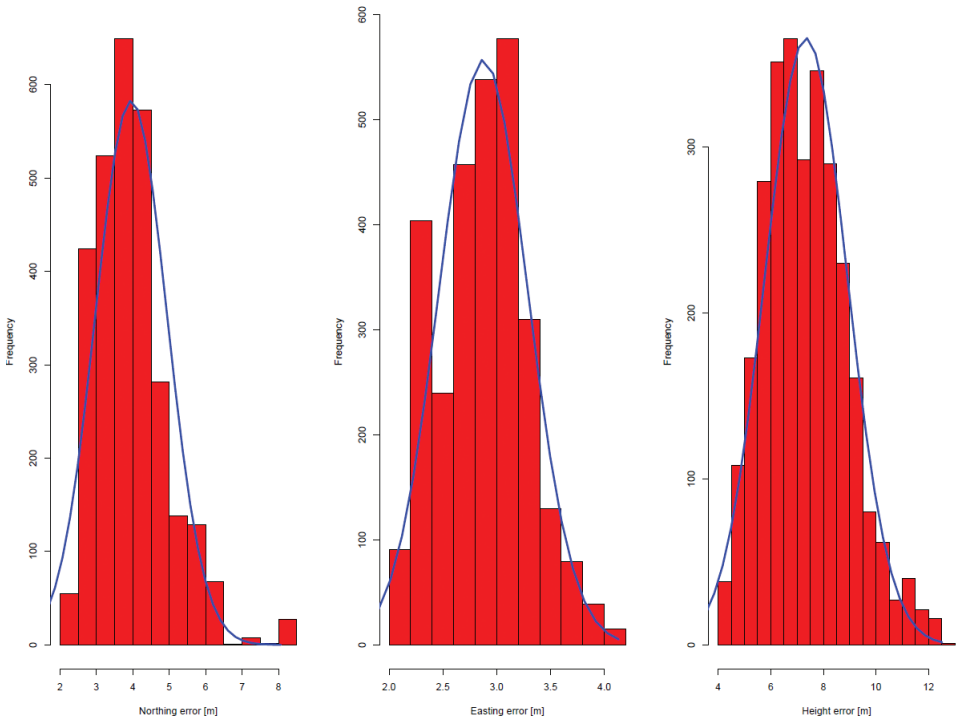

Figure 6. Histograms of northing (left), easting (middle), and vertical (right) single-frequency un-corrected GPS tropospheric positioning errors at Porto Garibaldi on 13th May, 2015

4.2 Scenario 2: *GPS positioning performance of the simulated tropospheric un-corrected single-frequency commercial-grade GPS receiver.*

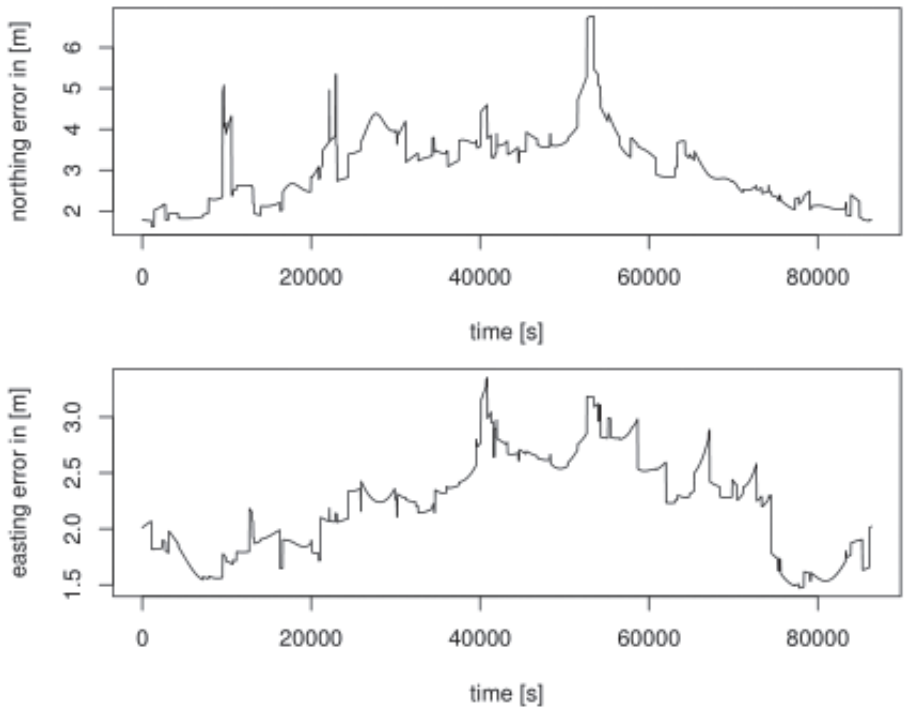

Figure 7. Time series of northing (upper diagram) and easting (lower diagram) single-frequency Saastamoinen-corrected GPS positioning errors at Porto Garibaldi on 13th May, 2015

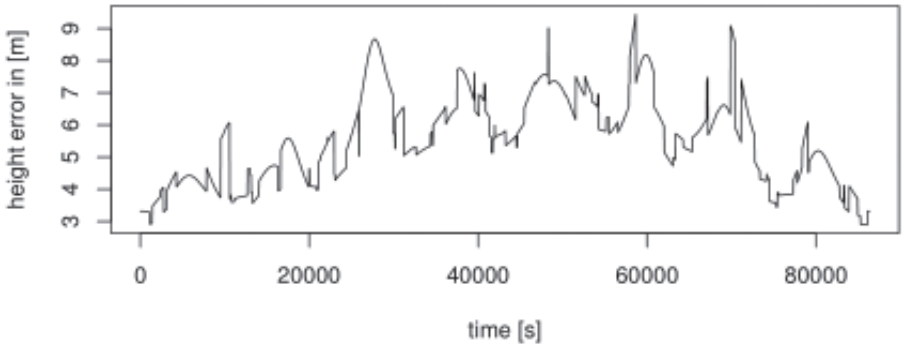

Figure 8. Time series of vertical single-frequency Saastamoinen-corrected GPS positioning errors at Porto Garibaldi on 13th May, 2015

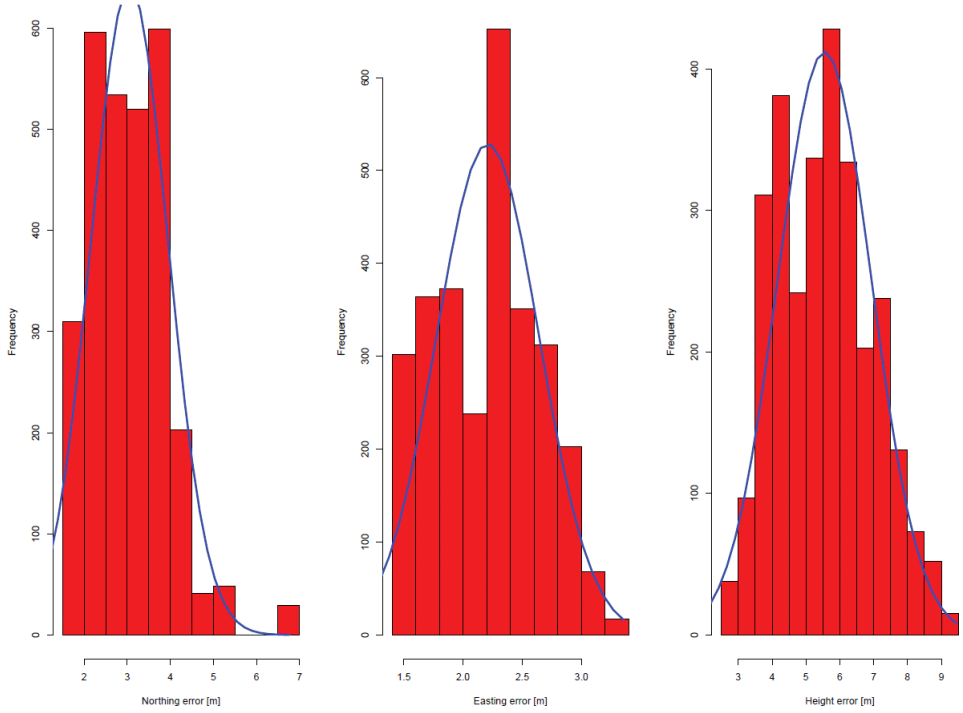

Figure 9. Histograms of northing (left), easting (middle), and vertical (right) single-frequency un-corrected tropospheric GPS positioning errors at Porto Garibaldi on 13th May, 2015

5 DISCUSSION

Deployment of Saastamoinen model reduces the over-all GPS positioning error for over a meter (vertical accuracy), compared with un-corrected GPS positioning performance Table 1). However, the Saastamoinen model utilisation is based on standard model of the atmosphere. The description of the actual situation in the troposphere may differ from those produced by the standard atmosphere utilisation. At the same time, having a met watch on vessels has become a common practice, with majority of vessels conducting a thorough met watch with high-quality met equipment.

Table 1. Summary statistics of observed GPS positioning performance in two scenarios of tropospheric effects considerations

Northing	No corrections	Saastamoinen
Mean error (m)	3.953947	3.052242
Standard deviation (m)	0.985753	0.8948904

Easting	No corrections	Saastamoinen
Mean error (m)	2.876094	2.208376
Standard deviation (m)	0.4122836	0.4343528

Over all vertical positioning error	No corrections	Saastamoinen
Mean error (m)	4.889337	3.767374
Standard deviation (m)	1.068497	0.9947317

Considering the circumstances and the results of our simulation, we propose the utilisation of the real meteorological observations in correction of the GPS tropospheric delay.

Still, the advanced methods for taming GPS tropospheric error still may be needed for high-accuracy and very high-accuracy maritime navigation applications, such as:

- Search And Rescue (SAR) operations,
- Autonomous vessels navigation,
- High-accuracy commercial services (laying underwater cables).

6 CONCLUSION

The analysis of the deterioration weather case scenario reveals the tropospheric impact on GPS positioning performance. The order of actual GPS tropospheric error magnitude in the zenith direction and the mapping function of error increasing for lower elevation satellites were not analysed. Utilisation of the standard (Saastamoinen model) significantly improves GPS positioning accuracy. While Saastamoinen model relies upon standard atmosphere values, more improved corrections can be obtained from the actual met values observed regularly on vessels, thus allowing for high-accuracy GPS application, such as those in autonomous vessels, critical safety operations (like SAR applications), and high-accuracy commercial services (like: laying underwater cables).

References

Brown, R G, and Hwang, P W C. (2009). Introduction to Random Signals and Applied Kalman Filtering (3rd ed). John Wiley & Sons. New York, NY.

Crawley, M J. (2013). The R Book (2nd ed). John Wiley & Sons. Chichester, UK.

Davis, K. (1990). Ionospheric Radio. Peter Peregrinus Ltd. London, UK.

Filić, M, Filjar, R, and Ruotsalainen, L. (2016). An SDR-based Study of Multi-GNSS Positioning Performance During Fast-developing Space Weather Storm. *TRANSNAV*, 10(3), 395 – 400. DOI: 10.12716/1001.10.03.03. Available at: http://bit.ly/2fxAvph, accessed on 5 May, 2017.

Filjar, R and Huljenić, D. (2012). The importance of mitigation of GNSS Vulnerabilities and Risks. *Coordinates*, 8(5), 14–16.

Kos, T, Markezic, I, and Botincan, M. (2009). Evaluation of EGNOS Tropospheric Delay Model in South-Eastern Europe. J of Navigation, 62, 148–154.

Petrovski, I G. (2014). GPS, GLONASS, Galileo, and Beidou for Mobile Devices: From Instant to Precise Positioning. Cambridge University Press. Cambridge, UK.

R Development Core Team (2017). R: A language and environment for statistical computing. R Foundation for Statistical Computing, Vienna, Austria. ISBN 3-900051-07-0. Available at: http://www.R-project.org, accessed on 5 May, 2017.

Rumora, I, Sikirica, N, and Filjar, R. (2017). An experimental identification of multipath effect in GPS positioning error. Presented at TRANSNAV 2017 Congress. Gydnya, Poland.

Sanz Subirana, J *et al*. (2013). GNSS Data Processing – Vol. I: Fundamentals and Algorithms. European Space Agency (ESA). Nordwijk, The Netherlands. Available at: http://bit.ly/1QV4KAL, accessed on 5 May, 2017.

Sonel. (2017). The global network GNSS assembly data centre for the Global Sea Level Observing System (GLOSS). Available at: http://www.sonel.org/?lang=en, accessed on 10 February, 2017.

Stull, R. (2015). Meteorology for scientists and engineers (3rd ed). The University of British Columbia. Vancouver, Canada. Available at: http://www.eos.ubc.ca/books/Practical_Meteorology/, accessed on 1 May, 2017.

Takasu, T. (2013). RTKLIB: An Open Source Program Package for GNSS Positioning. Software and documentation available at: http://www.rtklib.com/ , accessed on 5 May, 2017.

Thomas, M *et al*. (2011). Global Navigation Space Systems: reliance and vulnerabilities. The Royal Academy of Engineering. London, UK. Available at: http://bit.ly/1vrIenu, accessed on 5 May, 2017.

Sveučilište u Rijeci
POMORSKI FAKULTET U RIJECI
FACULTY OF MARITIME STUDIES RIJEKA
University of Rijeka

University of Zagreb
Faculty of Transport
and Traffic Sciences

Royal Institute of Navigation
Science Technology Practice

11th
Annual
Baška GNSS
Conference

A COMPARATIVE STUDY OF FORECASTING METHODS FOR SPACE WEATHER – CAUSED GNSS POSITIONING PERFORMANCE DEGRADATION

Mia Filić[1], **Jingnong Weng**[2], **Renato Filjar**[1]

[1] Faculty of Engineering, University of Rijeka, Croatia
E-mail: filicmia@gmail.com (Corresponding author)

[2] Regional Centre for Space Science and Technology Education in Asia and the Pacific (China), Beihang University, Beijing, China

ABSTRACT

Space weather and ionospheric dynamics have a profound effect on the positioning performance of Global Satellite Navigation System (GNSS). However, the quantification of that effect is still the subject of scientific activities around the world. In the latest contribution to the understanding of the space weather and ionospheric effects on GNSS positioning performance, we conducted a comparative study of several candidates for forecasting method for space weather-induced GNSS positioning performance deterioration. First, a moderately large set of experimentally collected data was established, encompassing space weather and ionospheric activity indices (including: the readings of the Sudden Ionospheric Disturbance (SID) monitors, components of geomagnetic field strength, planetary geomagnetic K (Kp) index, Total Electron Content (TEC), and sunspot number) and observations of GPS positioning error components (northing, easting and height) derived from the International GNSS Service (IGS) reference stations' Receiver Independent Exchange Format (RINEX) files in low solar activity periods. This data set was split into the training and test sub-sets. Then, the selected two supervised machine learning methods (Decision Tree Model – DTM, and Artificial Neural Network – ANN) were applied to the experimentally collected data set in order to establish the appropriate forecasting models for space weather-induced GNSS positioning

performance deterioration. The forecasting models were developed in R/rattle statistical programming environment. The forecasting quality of the examined forecasting models was assessed and the conclusions on the advantages and shortcomings of the proposed forecasting models for space weather-caused GNSS positioning performance deterioration were drawn.

Key words: *space weather, GNSS, horizontal positioning error*

1 INTRODUCTION AND MOTIVATION

Satellite navigation has been recognised as a part of national infrastructure (UN OOSA, 2012). An increasing number of technology and socio-economic systems rely upon satellite navigation systems for their Positioning, Navigation and Timing (PNT) services. Robust and reliable Global Navigation Satellite Systems' (GNSS) positioning performance is the foundation of the GNSS development and operation.

Space weather disturbances have been identified as the principal source of GNSS positioning performance degradation. It affects both the quality of the GNSS PNT performance, and the GNSS core system operation. The GNSS system operators take the challenge of mitigation of space weather effects on GNSS system operation, and support the overcoming of the GNSS positioning performance deterioration due to space weather effects.

Understanding the space weather effects on GNSS positioning performance is a daunting task. It is supposed to yield a model capable of forecasting GNSS positioning performance degradation based on space weather status description that can serve as a basis for GNSS application Quality of Service (QoS) assurance and assessment of GNSS utilisation risk. However, the complexity of relationship between space weather processes and GNSS positioning performance descriptors has prevented a successful development of such a model.

Here we present our contribution to the space weather-induced GNSS positioning performance deterioration model development. We used a methodology of utilisation of advanced statistical learning methods for forecasting of GNSS positioning performance degradation due to space weather, in a scenario of quiet space weather to low solar activity conditions, and based on a data set we assembled from trusted sources and our own measurements of space weather, geomagnetic, ionospheric, and GNSS positioning performance data.

The manuscript is structured as follows. The problem description and a brief survey of previous research are given in Section 2. The case scenario assessed in the study is outlined in Section 3. A data set assembled by our team is described in Section 4.

2 PROBLEM DESCRIPTION AND PREVIOUS RESEARCH

Natural stochastic processes affect GNSS positioning performance through introduction of GNSS positioning errors of complex nature. Related effects have been identified in the User Equivalent Ranging Error (UERE) segment, that comprises the effects that cause the satellite positioning signal delay, thus undermining the accuracy of GNSS positioning measurements, and causing the over-all GNSS positioning estimation errors. Ionospheric effects on satellite signal propagation comprise the ionospheric propagation delay and ionospheric scintillation, and are considered the most influential single cause of GNSS positioning performance degradation.

Statistical description of such processes offers a qualitative insight into the underlying mechanisms of GNSS positioning errors generation, thus allowing for development process description models, as an essential pre-requisite for forecasting model development that can be used with confidence in GNSS utilisation risk assessment, and GNSS application Quality of Service definition (Petrovski and Tsujii, 2012).

A complex relationship between space weather processes, as the prime source of ionospheric causes of GNSS positioning errors, and GNSS positioning performance prevents development of a simple and accurate forecasting model, required by both scientific and engineering communities. A traditional approach in modelling, through linearisation and simplification of the complex relationship and utilisation of sparse computing resources provided by a GNSS receiver, has not achieved required results. Figure 1 captures an environment for space weather impacts on GNSS position performance degradation.

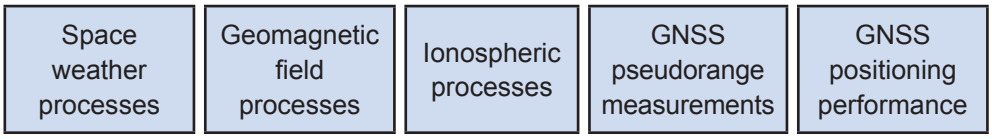

Figure 1. Environment for space weather impact on GNSS positioning performance

The quest of descriptive and forecasting models development of the interrelationships within space weather impact on GNSS positioning performance, depicted in Figure 1, has been addressed in scientific literature (Davis, 1991). The literature gives a comprehensive view on traditional methodology for space weather forecasting model development, as well as of the established models of interrelationship between space weather and geomagnetic field, geomagnetic field and ionosphere, and ionospheric and GNSS pseudorange measurement processes. Established models are based on simplifications and linearization of theoretical models (Maxwell equations and Appleton formula) based on real environment characterisation (Davis, 1991), and on understanding of space weather disturbances development (Mendillo, 2006), in particular. Advanced model development methods that would be capable of addressing of complexity and non-linearity of processes under scrutiny were applied only partially, attempting to describe the specific interrelationships between the components of space weather impact on GNSS positioning performance, rather than as the whole system (Cander, 1998).

The relationship between the quality of GNSS pseudorange measurements and the GNSS positioning performance (accuracy, availability, integrity, and continuity) has been and remains a subject of study. A wide variety of deteriorating conditions requires thorough study of utilisation scenarios, as the foundation for knowledge and understanding development of the underlying processes (Filić, Filjar and Ruotsalainen, 2016).

The general descriptive model of the environment for space weather impact on GNSS positioning performance is still to be developed, thus allowing for establishment of a suitable forecasting model of GNSS positioning performance deterioration due to space weather disturbances.

3 SOFTWARE BASED GNSS POSITIONING EFFECTS FORECASTING USING THE EXTENDED SET OF SW DATA

We addressed the problem of the SW – GNSS positioning performance forecasting model development with focusing our study to the particular scenario of GNSS utilisation in the specific category of a GNSS positioning environment. Quiet to low solar activity space weather conditions scenario was chosen for the reason of identification of systematic error sources (those facilitating bias, trend and seasonality). It leaves the causes of stochastic (random) errors for the later stages of our research.

An experimental data set including space weather and GNSS performance indices from trusted internet-based sources was assembled for the purpose of this study. The data set comprises measurable descriptors (independent variables) of space weather, geomagnetic field, ionospheric, GNSS pseudorange measurements and GNSS positioning performance accuracy dynamics, as outlined in Table 1. With the aim to identify independent variables that affect horizontal GNSS accuracy, a GNSS positioning performance descriptor, we applied a statistical learning methodology (James *et al*, 2015) to the assembled data set. Moreover, we deployed two forecasting model approaches, Decision Tree Model (DTM) and Artificial Neural Network (ANN), to develop the GNSS positioning performance deterioration forecast model for the scenario of low solar activity space weather conditions.

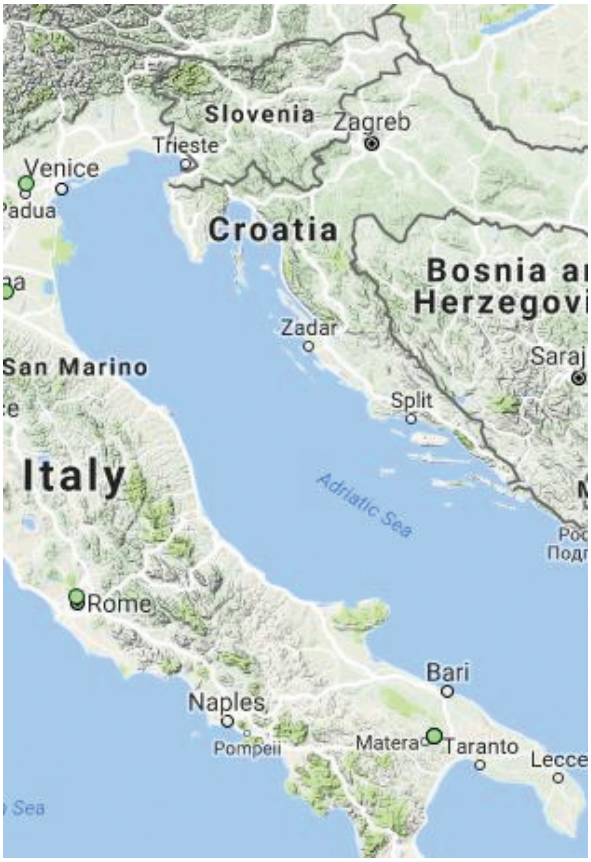

Figure 2. Position of the Matera, Italy GPS reference station, near Taranto in southern Italy

The collected data addresses the period between days 167 and 172 in 2007, for which quiet space weather to low solar activity conditions were identified. This choice allowed us to assess the long-term (mostly systematic) effects of GNSS positioning error sources. The GNSS positioning performance scrutinise the case of positioning in Mediterranean area (southern Italy), with the available data from the IGS reference station in Matera, Italy (IGS, 2017), with position depicted in Figure 2.

4 DATA SET DESCRIPTION

The data set was assembled of independent measurable variables describing all the processes establishing the environment of GNSS positioning (Figure 1), as outlined in Table 1. Trusted independent sources of variables observations were used, with the addition of SID (Sudden Ionospheric Disturbance) monitor observations taken by our team.

Table 1. A comprehensive description of input data

Input variables	Description	Relation	Source
DOY	Time stamp	None – serves for identification	
Bx	Earth's magnetic field density - x component at Lonjsko Polje, Croatia reference station	Geomagnetic field	(INTERMAGNET, 2017)
By	Earth's magnetic field density - y component at Lonjsko Polje, Croatia reference station	Geomagnetic field	(INTERMAGNET, 2017)
Bz	Earth's magnetic field density - z component at Lonjsko Polje, Croatia reference station	Geomagnetic field	(INTERMAGNET, 2017)
SFD	Solar flux density	Space weather	(NOAA SWPC, 2017)
SSN	Sunspot number	Space weather	(NOAA SWPC, 2017)
Ap	Planetary geomagnetic A index	Geomagnetic field	(NOAA SWPC, 2017)
Kp	Planetary geomagnetic K index	Geomagnetic field	(NOAA SWPC, 2017)
Dst	Disturbance storm time index	Ionosphere	(Kyoto University, 2017)
f0F2	Critical frequency of the F2 layer	Ionosphere	(NOAA SWPC, 2017)
f0Es	Critical frequency of the Es layer	Ionosphere	(NOAA SWPC, 2017)

Input variables	Description	Relation	Source
SID	Rijeka Reference station signal strength observed with Sudden Ionospheric Disturbance (SID) monitor	Ionosphere	Measurements taken by our team
d_plane	Observed equivalent positioning error (horizontal plane) [m]	GPS positioning performance	Output variable

Exploratory analysis was performed on the assembled data set in the R environment for statistical computing. It revealed a common dynamics of horizontal GPS positioning error time series, with occasional outliers reaching values of up to 25 m (Figure 3). Initial presumption of quiet space weather to low solar activity conditions in the period observed were confirmed with the assessment of Kp variable time series, that revealed just occasional mild geomagnetic disturbances at worst during the period observed.

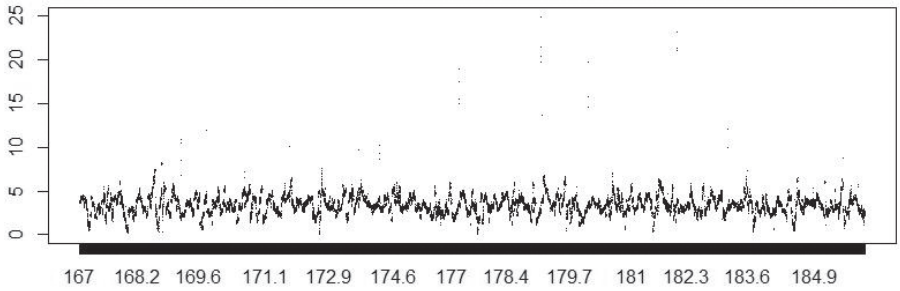

Figure 3. Horizontal GPS positioning error during the period (of year 2007) under observation

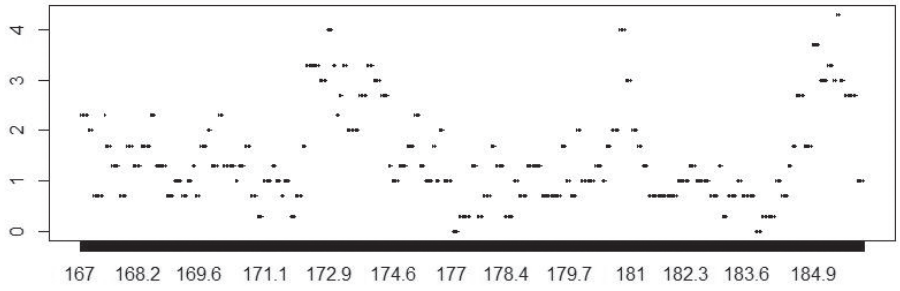

Figure 4. Planetary Kp index of geomagnetic activity during the period (of year 2007) under observation

5 METHODOLOGY

5.1 General methodology. *S*tatistical/machine learning methods were applied on structured data describing space weather-influenced GNSS positioning environment and performance, as derived from experimentally collected raw GNSS pseudoranges. We used RTKLIB/RTKPOST (Takasu, 2013), an open source GNSS Software-Defined Radio (SDR) receiver configured as a single-frequency commercial-grade GPS receiver with standard correction models, to simulate GNSS positioning performance based on experimental (real) GNSS pseudorange observations in a procedure described elsewhere (Filić, Filjar and Ruotsalainen, 2016). RTKLIB/RTKPOST GNSS SDR was set in post-processing mode, supplied with broadcast navigation message, and fed with raw GNSS pseudoranges collected at Matera, Italy IGS reference station. Standard GPS correction models were applied based on navigation message data to correct ionospheric (Klobuchar model), tropospheric (reference atmosphere-based Saastamoinen model) and satellite clock errors in a manner of a single-frequency commercial-grade GPS receiver (Sanz Subirana *et al*, 2013), (Filić, Filjar, and Routsalainen, 2016). Post-processing returned series of position and positioning error (northing, easting, and height) estimates in 30 s intervals. GPS northing and easting positioning errors time series were used to derive horizontal GPS positioning error samples which are then added to the data set.

Assembled data sets were then analysed, and related data-driven models developed in the R environment for statistical computing, an open source programming environment, with the utilisation of a dedicated *rattle* R package (Williams, 2016).

5.2 Decision Tree Model (DTM) for regression was selected as a control model in the presented study, with the assumption of the observation-based prediction to be achieved through stratification of the predictor space into a number of well-defined simple regions. Additionally, DTM is a simple model capable of adding an interpretation to the process. Supporting methodology followed usual description (James *et al*, 2015) and was applied in the R-based *rattle* package.

5.3 Artificial Neural Networks (ANN) was selected as the working observation-based model development method. A neural network is a highly parametrised model, motivated with the analogy with biological neural networks, and capable of modelling smooth relationships of various levels of complexity based on the set of learning data (Ephron and Hastie, 2016), (Lin and Tegmark, 2016). We

developed a 10-2-1 neural network (10 inputs, 2 hidden layers, and 1 output) in the R environment, using its *rattle* package (Williams, 2016).

6 AN OUTLINE OF RESEARCH RESULTS

Decision Tree and Artificial Neural Network Models developed and validated based on the assembled data set (Sections 3 and 4) are presented in this section. Performance assessment results for both models are given here, as well.

6.1 Decision Tree Model developed in the R environment is presented in Figure 5.

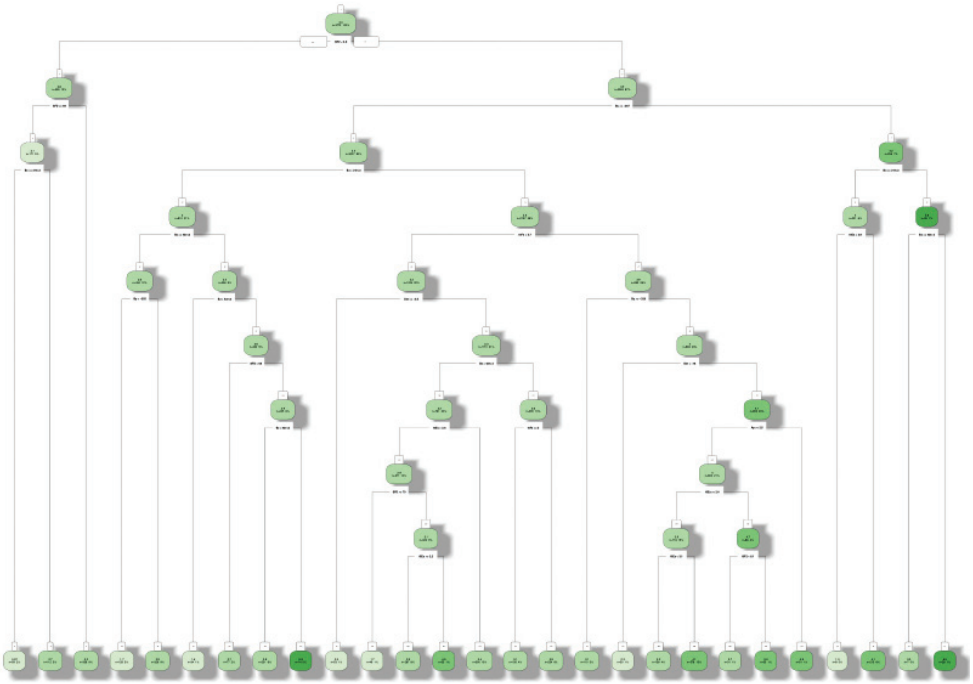

Figure 5. Decision Tree Model based on the assembled data set

The DTM derived is a GNSS positioning performance degradation forecasting model for quiet space weather to low solar activity conditions based on stratification of the predictor space in the regions determined by interval values of geomagnetic, ionospheric and space weather variables.

Model performance was assessed through Prediction-Observation Diagram (POD), presented for DTM in Figure 6. Pseudo R-square coefficient reached a moderate value. The DTM POD shows clearly visible evidence of stratification based on interval values.

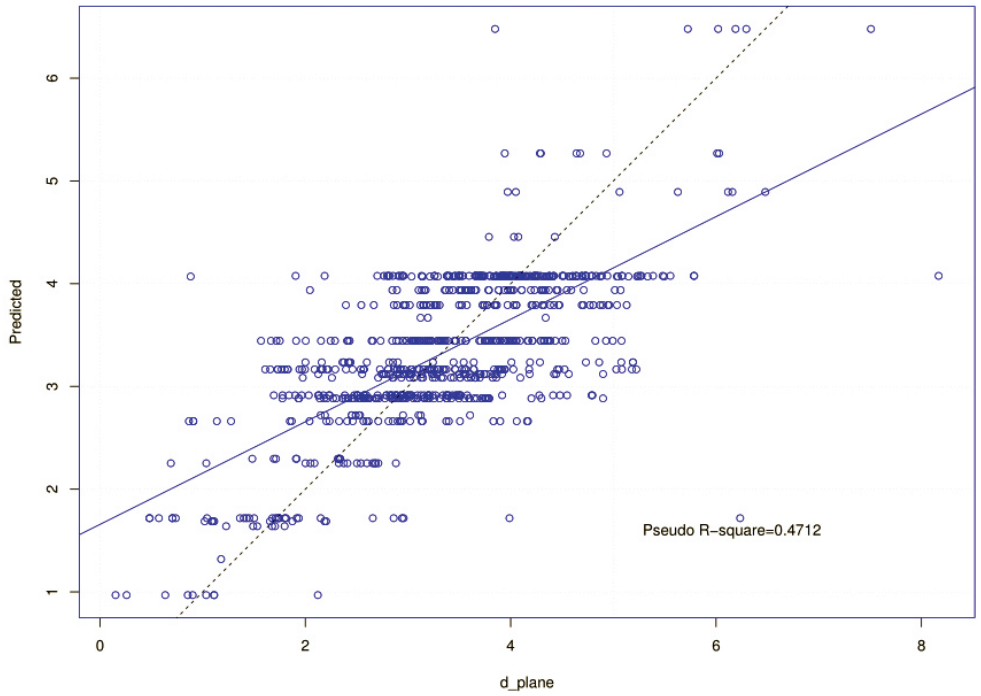

Figure 6. Prediction-Observation Diagram (POD) for DTM

6.2 Artificial Neural Network (ANN). A 10-2-1 ANN model was developed based on the assembled data set, with the resulting 35 weights presented in Figure 7.

POD of the ANN GPS positioning performance deterioration forecasting model in quiet space weather to low solar activity conditions revealed a rather poor performance. The Fitted-to-Points line differs significantly from the referenced P-O line, while spatial distribution of Observation-Prediction pairs show improvement over the control DTM.

```
   b  represents the bias associated with a node
   h1 represents hidden layer node 1
   i1 represents input node 1 (i.e., input variable 1)
   o  represents the output node

Weights for node h1:
  b->h1  i1->h1  i2->h1  i3->h1  i4->h1  i5->h1  i6->h1  i7->h1  i8->h1  i9->h1
  -0.66    0.23    0.29   -0.31   -0.68   -0.36    0.27    0.23   -0.31   -0.18
i10->h1
   0.31

Weights for node h2:
  b->h2  i1->h2  i2->h2  i3->h2  i4->h2  i5->h2  i6->h2  i7->h2  i8->h2  i9->h2
  -0.02    0.29   -0.50    0.39    0.25   -0.16   -0.55   -0.52    0.25   -0.65
i10->h2
  -0.15

Weights for node o:
   b->o   h1->o   h2->o   i1->o   i2->o   i3->o   i4->o   i5->o   i6->o   i7->o
-135.33   -0.20 -135.00    0.01   -0.01    0.00   -0.05   -0.01   -0.08    0.00
  i8->o   i9->o  i10->o
   0.13   -0.02    0.04
```

Figure 7. Architecture of the resulting 10-2-1 ANN forecasting model

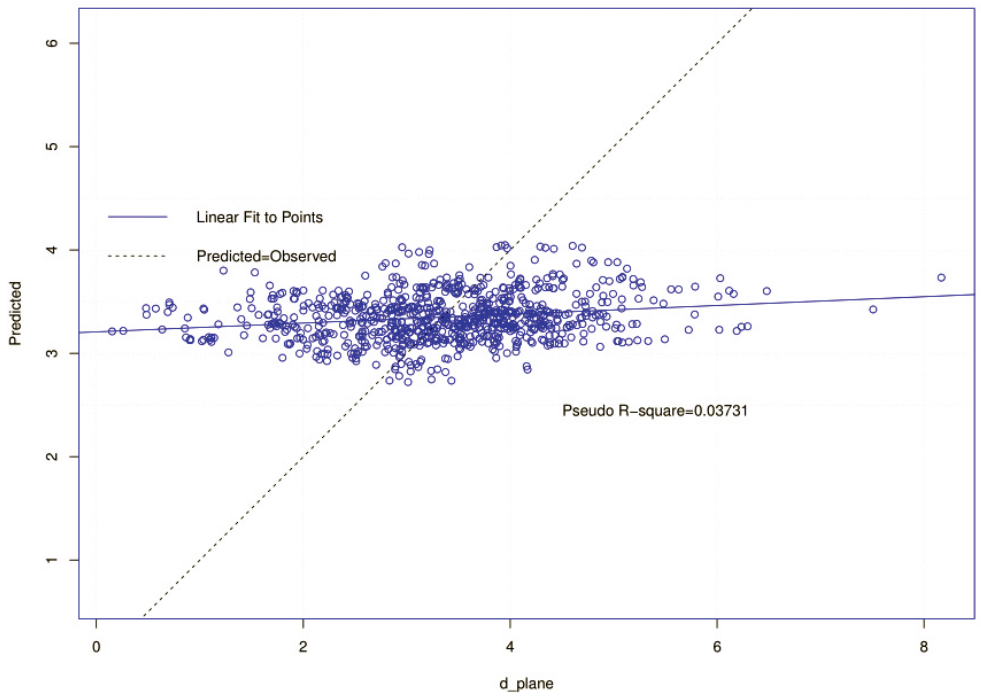

Figure 8. Prediction-Observation Diagram (POD) for the resulting ANN forecasting model

7 DISCUSSION

A research was conducted on the assembled multi-variable data set extending to the time-span of 6 days in 2007 with quiet space weather to low solar activity conditions. The scenario for study was chosen with the aim to explore the causes of systematic errors. Those of the random (stochastic) nature were suppressed by the nature of methodology. The assembled data set consisted of experimentally collected real data covering all the components of the GPS positioning environment (Figure 1), with the exception of the GPS pseudorange measurement process. Cross-correlation between the pairs of descriptors (input variables) was generally insignificant, pointing to the complex nature of the coupling, and potentially inappropriate definition of influencing descriptors. Discussion on appropriate choice of descriptors is given in (Filjar, Filić and Mirakhmudov, 2017).

The choice of data and methodology resulted in moderate forecasting performance of DTM, and a poor performance of ANN forecasting models. In general, the measured variables have nonlinear relations and low correlation. Additionally, variability of cases was limited due to the very choice of the quiet space weather to low solar activity scenario. Finally, statistical learning methods were applied on carefully prepared data set, but probably too sparse for some statistical learning methods to discover the underlying dynamics. DTM performed far better than ANN model, confirming the choice for a control model. In our understanding, the ANN model performed poorly partly because of the failure from the lack of a descriptor of GPS pseudorange measurement process, and would perform better with different set up and improved descriptor's variable set.

8 CONCLUSION AND FUTURE RESEARCH

A study was conducted and its results were presented. The study addresses the problem of the GPS positioning performance forecasting model development, that considers the effects of space weather dynamics. Two models (DTM, and ANN) were developed and examined for their performance in forecasting GPS positioning performance deterioration, based on the scenario of quiet to low solar activity space weather conditions. Based on GPS positioning error time series derived from experimentally collected GPS pseudoranges, models were supposed to allow for forecasting the GPS positioning performance deterioration

caused by systematic (long-term) effects that remain during quiet to low solar activity space weather conditions.

This study revealed a moderate performance of DTM, considered a control model, and a poor performance of the ANN model. We argue that poor results of the ANN model resulted from low correlation of measured descriptors of the component chain of the environment for satellite-based positioning, and possible short time-span selected for the study.

Further research is to be conducted on the development and the performance of a variety of statistical learning-based models to forecast GPS positioning performance in moderately disturbed and significantly disrupted space weather conditions, based on expanded experimental data set, extending to much larger time-spans.

References

Cander, L R. (1998). Artificial neural network applications in ionospheric studies. *Annali di Geofisica*, 5-6, 757-766.

Davis, K. (1991). Ionospheric Radio. Peter Peregrinus Ltd. London, UK.

Efron, B, and Hastie, T. (2016). Computer Age Statistical Inference: Algorithms, Evidence, and Data Science. Cambrdige University Press. Cambridge, UK.

Filić, M, Filjar, R. and Ruotsalainen, L. (2016). An SDR-based Study of Multi-GNSS Positioning Performance During Fast-developing Space Weather Storm. T*ransNav*, 10, 395-400. doi: 10.12716/1001.10.03.03

Filjar, R, Filić, M and Mirakhmudov, E. (2017). Categorisation of space weather and GNSS positioning quality indicators for estimation of GNSS positioning quality degradadtion. This Proceedings. 11th Annual Baška GNSS Conference. Baška, Krk Island, Croatia.

IGS. (2017). International GNSS Service archive and products. Available at: http://www.igs.org, accessed on: 4 April, 2017.

INTERMAGNET. (2017). Internet database of geomagnetic indices observations. Available at: http://www.intermagnet.org/data-donnee/data-eng.php, accessed on 2 November, 2017.

James, G *et al*. (2015). An Introduction to Statistical Learning (6 th printing). Springer Verlag. New York, NY.

Kyoto University. (2017). Internet database of geomagnetic equatorial Dst index. Available at: http://wdc.kugi.kyoto-u.ac.jp/dstdir/, accessed on 2 November, 2017.

Lin, H W, and Tegmark, M. (2016). Why does deep and cheap learning work so well? arXiv pre-print archive. Available at: https://arxiv.org/abs/1608.08225, accessed on: 2 May, 2017.

Mendillo, M. (2006), Storms in the ionosphere: Patterns and processes for total electron content, *Rev Geophys*, 44, RG4001, doi:10.1029/2005RG000193.

NOAA Space Weather Prediction Center (SWPC). (2017). Internet database of space weather indices observations. Available at: http://www.swpc.noaa.gov, accessed on 2 November, 2017.

Petrovski, I G, and Tsujii, T. (2012). Digital Satellite Navigation and Geophysics: A Practical Guide with GNSS Signal Simulator and Receiver Laboratory. Cambridge University Press. Cambridge, UK

Sanz Subirana, J *et al*. (2013). GNSS Data Processing – Vol. I: Fundamentals and Algorithms. European Space Agency (ESA). Nordwijk, The Netherlands. Available at: http://bit.ly/1QV4KAL, accessed on 5 February, 2017.

Takasu, T. (2013). RTKLIB: An Open Source Program Package for GNSS Positioning. Software and documentation available at: http://www.rtklib.com/, accessed on 5 April, 2017.

UN OOSA ICG. (2012). Current and Planned Global and Regional Navigation Satellite Systems and Satellite-based Augmentations Systems. Available at: http://bit.ly/2m7jjGJ, accessed on 8 March, 2017.

Williams, G *et al*. (2016). Rattle: Graphical User Interface for Data Mining in R. Available at: https://cran.r-project.org/web/packages/rattle/index.html, accessed on 4 April, 2017.

Sveučilište u Rijeci
POMORSKI FAKULTET U RIJECI
FACULTY OF MARITIME STUDIES RIJEKA
University of Rijeka

University of Zagreb
Faculty of Transport
and Traffic Sciences

Royal Institute of Navigation
Science Technology Practice

11th
Annual
Baška GNSS
Conference

A CASE OF GNSS POSITIONING PERFORMANCE DETERIORATION AND ITS EFFECTS ON MARITIME NAVIGATION

Nenad Sikirica[1], **Boris Sviličić**[2], **Serdjo Kos**[2]

[1] University of Applied Sciences Velika Gorica, Croatia
E-mail: sikirica01@gmail.com (Corresponding author)
[2] Faculty of Maritime Studies, University of Rijeka, Croatia

ABSTRACT

Satellite navigation positioning performance should not be considered in absolute terms, but rather matched with the requirements for GNSS-based applications. Here, we present a study of the positioning performance of a commercial-grade single-frequency un-aided GPS receiver for maritime navigation applications in the period of moderate space weather disturbances. Matching the GPS positioning performance results with the maritime navigation applications requirements, we found that the category of GNSS receivers concerned does not meet the requirements of the high-quality maritime navigation applications. We presented and discussed the potential shortcomings caused by such situations and proposed the recommendations that will allow for utilisation of GNSS receivers in high-quality and critical marine navigation applications.

Key words: *GNSS, positioning performance deterioration, maritime navigation*

1 INTRODUCTION

Satellite navigation has become a pillar of modern civilisation and a component of national infrastructure, with the increasing number of technology and socio-economic systems relying on Global Navigation Satellite System (GNSS) operation performance. These facts have brought the GNSS stability and resilience to disturbing effects into the focus of the GNSS application development research. With the satellite navigation system performance positioned in the foundation of the risk assessment of GNSS utilisation, the assessment of positioning error effects for specific applications gains interest and respect. It has become paramount not to achieve the best positioning performance in the absolute terms, but to match the required level of positioning accuracy for a specific GNSS application with the positioning performance of the application-configured GNSS receiver (Filjar and Huljenić, 2012).

The ionospheric effects have been recognised as the single major contributor to the GNSS error budget. This paper addresses the extent to which a large ionospheric event affects the GNSS-based marine navigation applications.

2 PROBLEM DESCRIPTION AND RESEARCH BACKGROUND

The ionospheric delay of a GNSS satellite signal is the major single cause of GNSS positioning errors. It results from stochastic ionisation processes driven by solar activity (Mendillo, 2006) and the Earth-environment causes (supersonic flights, atmospheric discharges, earthquakes etc.). The GNSS ionospheric delay causes the GNSS positioning error of a complex nature (Filjar, Kos and Kos, 2012, Filjar, Brčić and Kos, 2013), which comprises both systematic and stochastic components, thus making it hard to mitigate, as shown in the mathematical model (1):

$$d_{iono} = \varepsilon_{syst\_corr} + \varepsilon_{syst\_uncorr} + \varepsilon_{stoch} \quad (1)$$

where:

d_{iono} ... GNSS ionospheric delay

ε_{syst_corr} ... corrected portion of the GNSS ionospheric systematic error, after deploying a GNSS ionospheric error correction model (Klobuchar model, for instance)

$\varepsilon_{syst\_uncorr}$ ... uncorrected portion of the GNSS ionospheric systematic error, due to imperfect correction model

ε_{stoch} ... the GNSS ionospheric stochastic error

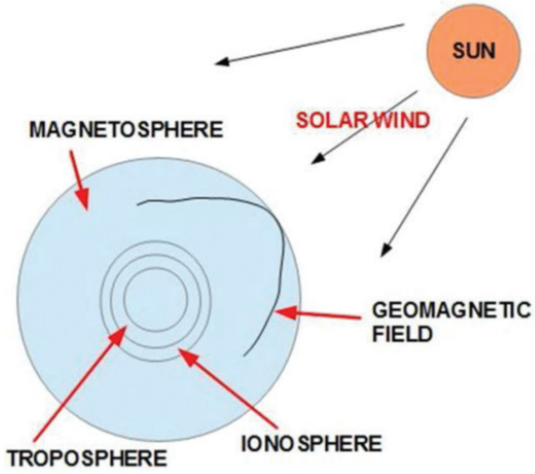

Figure 1. Sun-Earth space weather environment

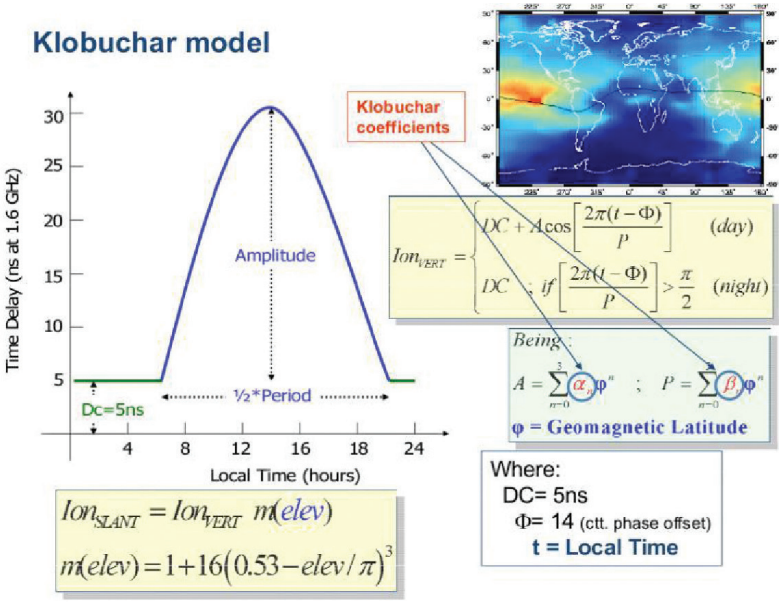

Figure 2. Klobuchar model for GPS ionospheric delay correction, from (Sanz Subirana *et al*, 2012)

Satellite navigation system deploys the correction models, aiming at partial correction of the global portion of systematic GNSS ionospheric delay errors. Global Positioning System (GPS), Global Navigation Satellite System (GLONASS) and Beidou use the so-called Klobuchar ionospheric delay model, developed on the foundation of identification of daily patterns in the GNSS ionospheric delay dynamics. The Galileo system deploys a different model based on the knowledge base of the previous ionospheric events.

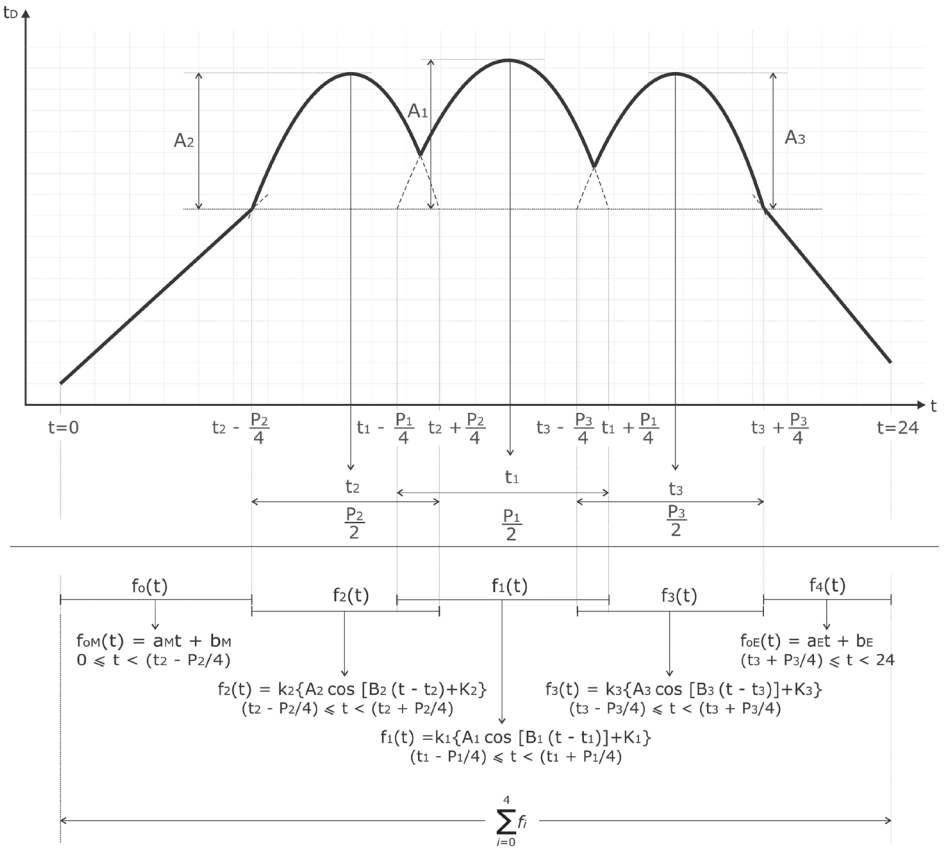

Figure 3. Brčić – Kos model for GPS ionospheric delay correction in the Northern Adriatic during the quiet space weather summer periods (after Brčić, 2015)

In the attempt to develop more accurate models of the GNSS ionospheric delay dynamics in order to use them as correction models, a number of regional and local models have been developed and deployed for specific geographical regions. For instance, Brčić and Kos (2015) have developed a local GNSS

ionospheric delay model for mitigation of systematic GNSS ionospheric delay in the Northern Adriatic region during the quiet space weather conditions in summer. The model has been developed based on the research findings and practical experience in studying the local GPS ionospheric delay dynamics and is summarised on Figure 3.

The utilisation of differential GNSS may significantly tame the impact of the GNSS ionospheric delay on the over-all GNSS positioning performance, but its utilisation requires a wide network of Differential GNSS (DGNSS) stations with affordable access and dedicated user equipment (Petrovski, 2014).

The existing GNSS ionospheric delay mitigation methods still target the GNSS positioning performance improvement in general terms, without the consideration of its deployment costs for particular GNSS applications or services.

In the meantime, various disciplines and economic segments have established the requirements for quality of service and performance of applications that may rely on satellite navigation. Thomas (*et al*, 2011) outlined an assessment of qualitative positioning performance quality requirements for categorised GNSS applications (Table 1).

Table 1. Positioning accuracy requirements for navigation applications, according to (Thomas *et al*, 2011)

Navigation application	Position accuracy requirements
Ocean navigation	Low – High
Coastal navigation	Medium – High
Inland waterway navigation	Medium – High
Tugs and pushers	High
Icebreakers	High
Automatic collision avoidance	High
Port approach	High
Port operations	High – Very high
Automatic docking	Very high
Dredging	Very high
Construction	Very high
Vessel traffic services	High – Very high
Cargo handling	Very high

Considering the practical expertise in the field, our team proposes the quantification of positioning performance requirements for marine navigation-related application, as outlined in Table 2.

Table 2. Quantification of positioning accuracy requirements

Requirement description	Numerical range
Very high accuracy	Better than 1 m
High accuracy	(1 – 3) m
Medium accuracy	(3 – 5) m
Low accuracy	(5 – 10) m

3 A CASE-STUDY DESCRIPTION AND METHODOLOGY

We set up a case for evaluation of the GPS positioning performance assessment for targeted marine navigation GNSS applications. The assessment was conducted using the experimental GPS observations (pseudo ranges and navigation messages) taken at the SONEL network (Sonel, 2017) reference station at Poreč, Croatia (Figures 4 and 5) in the Northern Adriatic. The GPS observation used were taken at the 30 s-sampling rate, and archived with the Sonel network database in Receiver Independent Exchange Format (RINEX) format.

The 7th – 10th March, 2012 period of a moderate geomagnetic (Figure 6) and ionospheric disturbance was chosen for the study in order to provide a modest but not overwhelming ionospheric impact on the GPS positioning performance.

Methodology of research was taken from (Filić, Filjar and Ruotsalainen, 2016). RTKLIB (Takasu, 2013), an open source GNSS Software-Defined Radio (SDR) receiver and GNSS observation post-processing tool, was configured to perform as a commercial-grade single frequency GPS receiver, and fed with the Poreč GNSS observations in order to provide the real-time experience of GPS positioning performance in a form of time series of GPS positioning error in northing and easting directions, and in horizontal plane (of interest to maritime navigation).

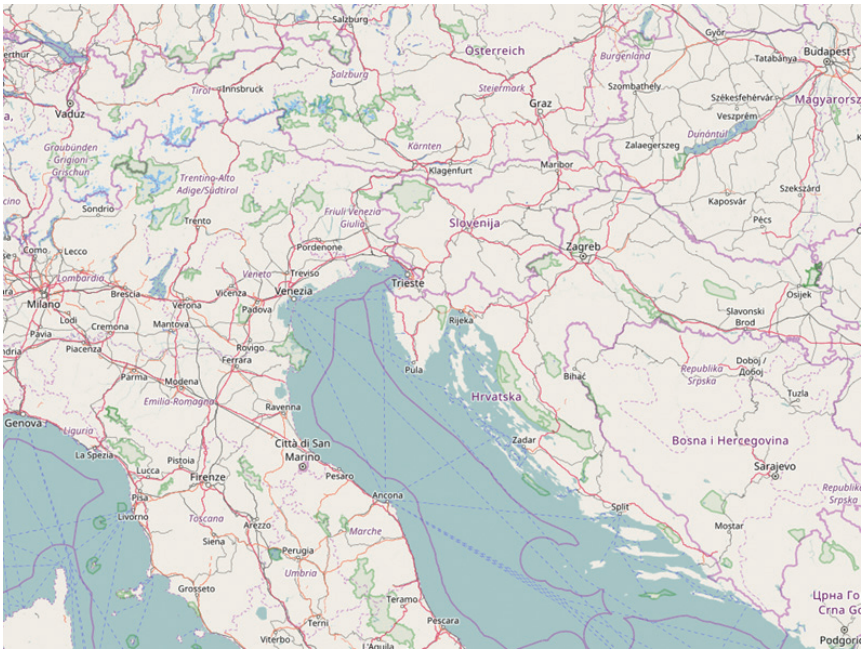

Figure 4. Poreč reference station's position on western coastline of the Istrian Peninsula

Figure 5. GPS aerial instalment for Poreč reference station

The most common models of the GPS ionospheric error mitigations were deployed in the study: GPS positioning without ionospheric corrections (thus leaving both systematic and stochastic components active), Klobuchar correction model deployment (that partly eliminates the GPS ionospheric delay systematic error, but leaves the stochastic error untamed), and dual-frequency correction deployment (that effectively removes almost all systematic and stochastic errors, but requires a specialised user equipment not applied in maritime navigation).

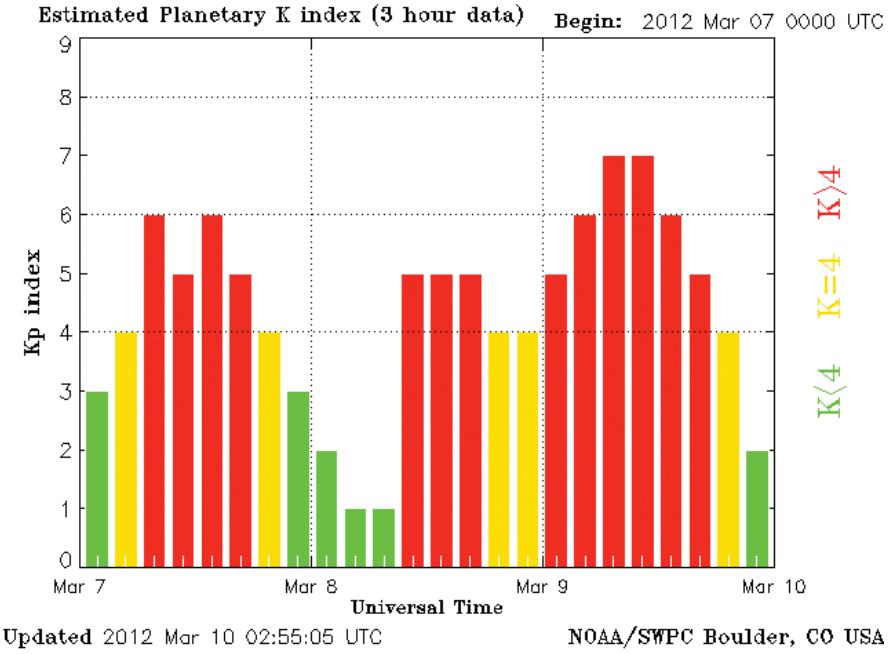

Figure 6. Time series of Kp indices in the 7 March 1012 – 10 March 2012 period under scrutiny

As we studied the effects of the GPS ionospheric delay, all the other effects on GPS positioning performance were kept mitigated in the same way (standard GPS corrections as applied in a commercial-grade single frequency GPS receiver) in all the three cases of the GPS ionospheric delay corrections. That way, we were able to identify the impact of various GPS ionospheric delay components on GPS positioning performance in a relative way, assess the overall GPS positioning error with different approaches in taming the GPS

ionospheric delay and map it on the set of GNSS positioning performance requirements for particular targeted applications in the maritime navigation segment.

4 RESEARCH RESULTS

This section contains a graphical presentation of time series and statistical descriptions of the GPS positioning performance indicators (direction-related GPS positioning errors) for given data and the observed period of time.

A case of non-correction is presented with the time series of the northing, easting (Figure 7) and horizontal (Figure 8) positioning errors. Histograms of observed values of GPS positioning error components are depicted in Figure 9.

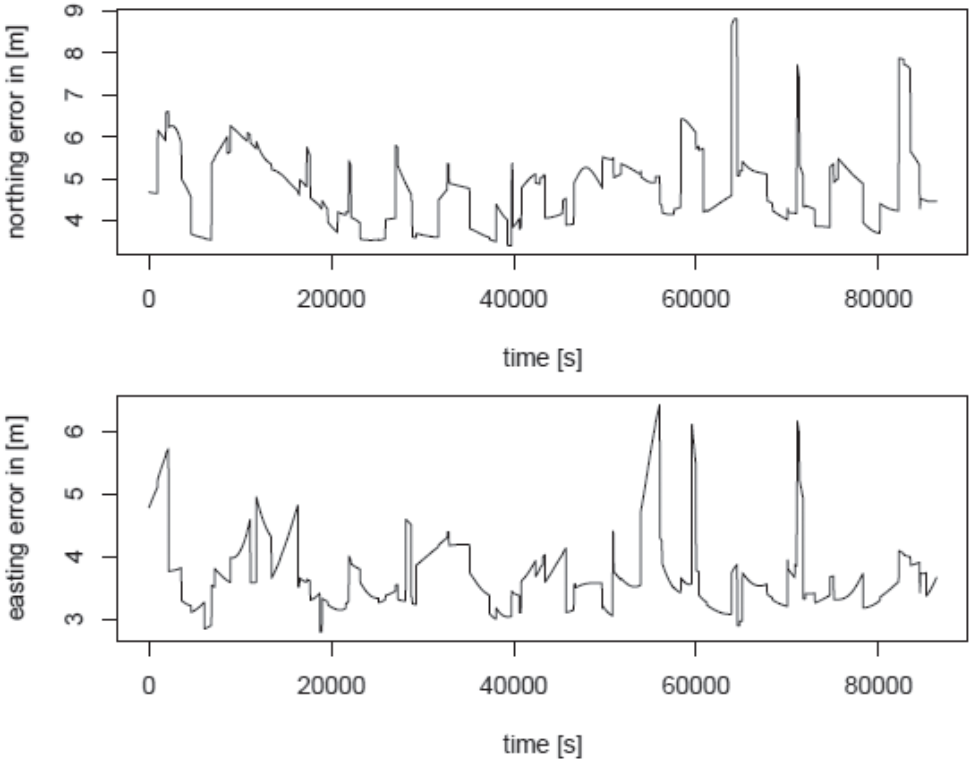

Figure 7. Time series of northing (above) and easting (below) positioning errors, as derived from RTKLIB-based post processing of 7 Mar 2012 – 10 Mar 2012 GPS observations, with no ionospheric corrections applied

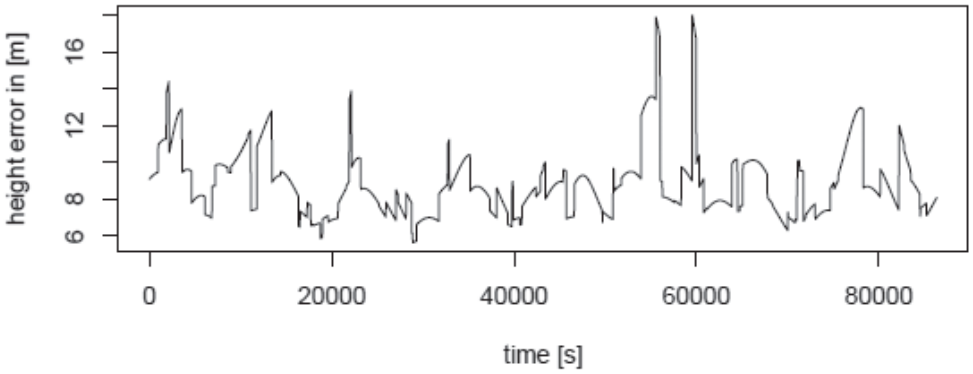

Figure 8. Time series of horizontal positioning errors, as derived from RTKLIB-based post processing of Mar 7th – 10th 2012 GPS observations, with no ionospheric corrections applied

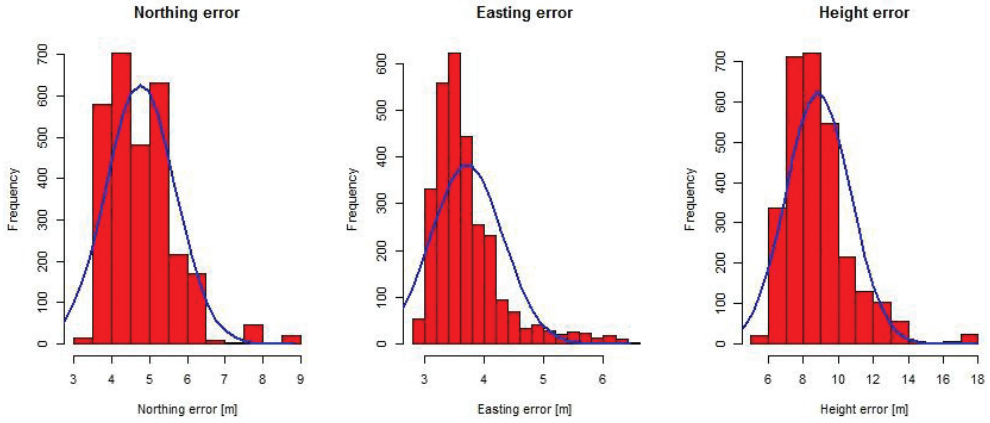

Figure 9. Histograms of northing (left), easting (middle) and horizontal (right) positioning errors, as derived from RTKLIB-based post processing of Mar 7th – 10th 2012 GPS observations, with no ionospheric corrections applied

A case of Klobuchar correction model deployment is presented with the time series of the northing, easting (Figure 10) and horizontal (Figure 11) positioning errors. Histograms of observed values of GPS positioning error components are depicted in Figure 12.

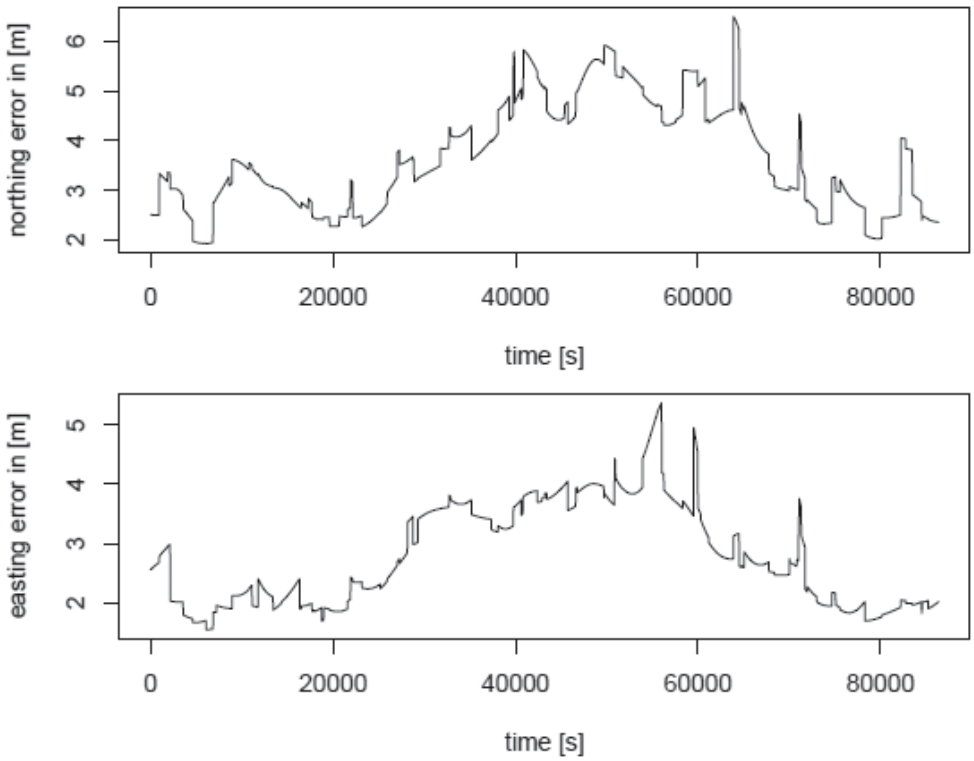

Figure 10. Time series of northing (above) and easting (below) positioning errors, as derived from RTKLIB-based post processing of Mar 7th – 10th 2012 GPS observations, with Klobuchar ionospheric corrections applied

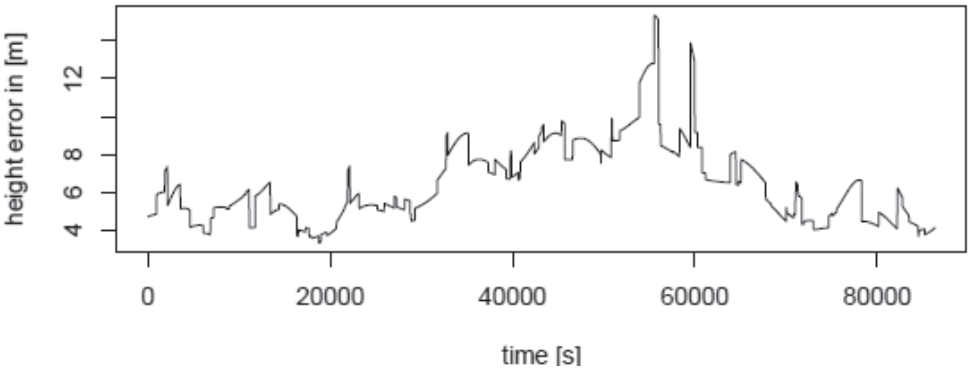

Figure 11. Time series of horizontal positioning errors, as derived from RTKLIB-based post processing of Mar 7th – 10th 2012 GPS observations, with Klobuchar ionospheric corrections applied

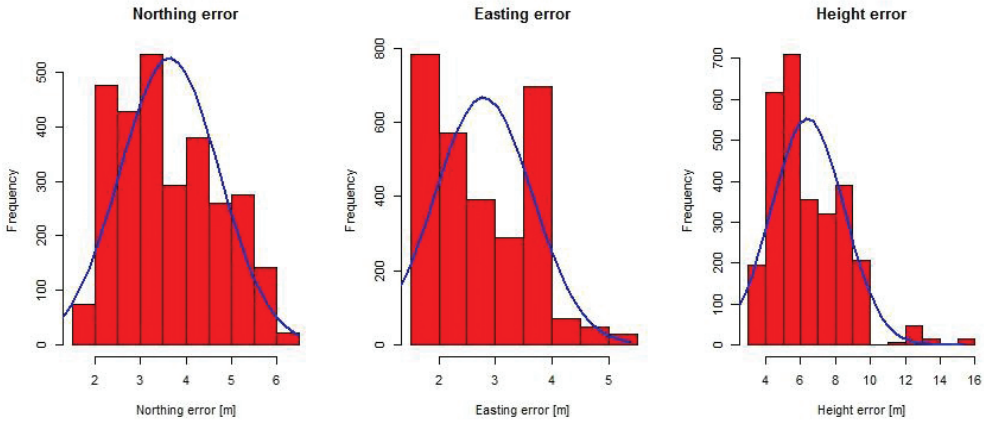

Figure 12. Histograms of northing (left), easting (middle) and horizontal (right) positioning errors, as derived from RTKLIB-based postprocessing of Mar 7th – 10th 2012 GPS observations, with Klobuchar ionospheric corrections applied

A case of dual-frequency GPS ionospheric delay correction method deployment is presented with the time series of the northing, easting (Figure 13) and horizontal (Figure 14) positioning errors. Histograms of observed values of GPS positioning error components are depicted in Figure 15.

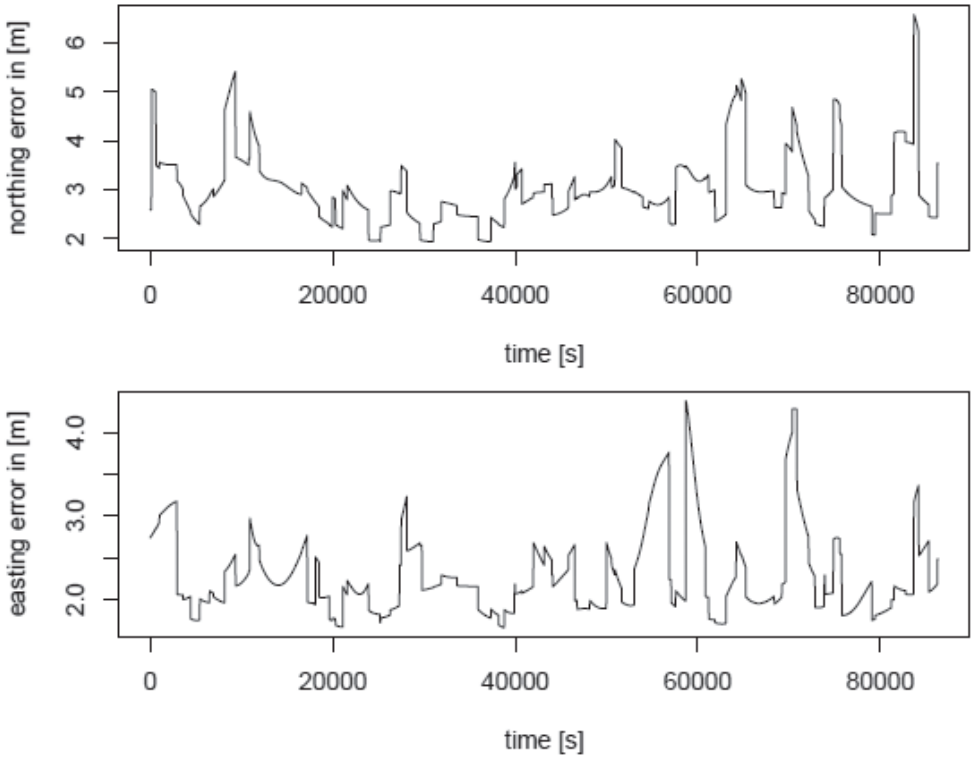

Figure 13. Time series of northing (above) and easting (below) positioning errors, as derived from RTKLIB-based post processing of Mar 7th – 10th 2012 GPS observations, with dual-frequency ionospheric corrections applied

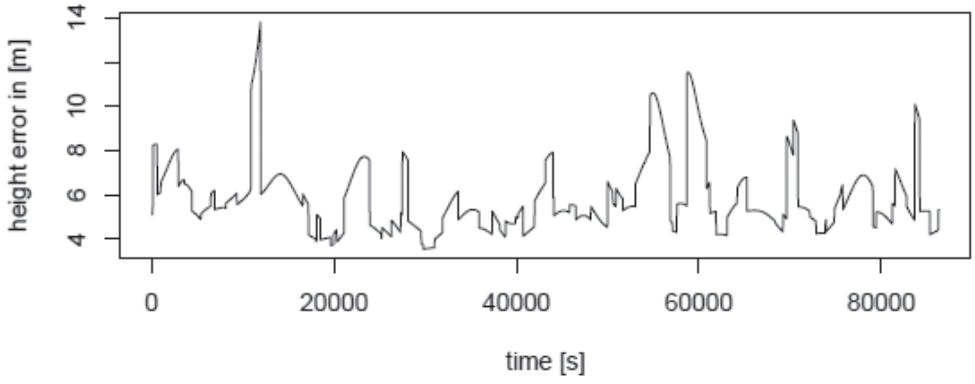

Figure 14. Time series of horizontal positioning errors, as derived from RTKLIB-based post processing Mar 7th – 10th 2012 GPS observations, with dual-frequency ionospheric corrections applied

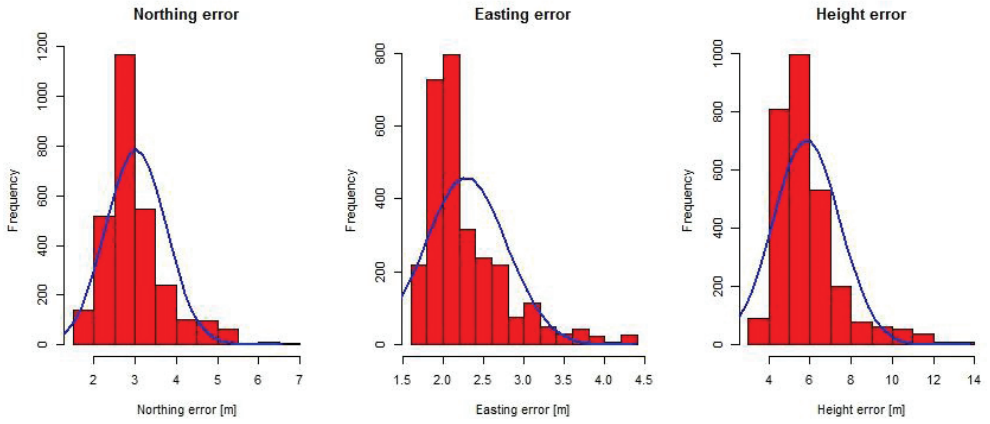

Figure 15. Histograms of northing (left), easting (middle) and horizontal (right) positioning errors, as derived from RTKLIB-based postprocessing of Mar 7th – 10th 2012 GPS observations, with dual-frequency ionospheric corrections applied

Table 3. Summary statistics of observed GPS positioning performance in three cases of ionospheric effects considerations: no corrections, Klobuchar corrections and dual-frequency corrections applied

Requirement description	Numerical range
Very high accuracy	Better than 1 m
High accuracy	(1 – 3) m
Medium accuracy	(3 – 5) m
Low accuracy	(5 – 10) m

Northing	No corrections	Broadcast (Klobuchar)	Iono-free
Mean [m]	4.766387	3.640412	3.018366
Standard dev [m]	0.9157804	1.0934	0.7318222

Easthing	No corrections	Broadcast (Klobuchar)	Iono-free
Mean [m]	3.71382	2.789641	2.280692
Standard dev [m]	0.5971461	0.8616106	0.5014245

Horizontal	No corrections	Broadcast (Klobuchar)	Iono-free
Mean [m]	6.042425	4.58636	3.783132
Standard dev [m]	1.093269	1.392083	0.8871247

The statistics of the observed GPS positioning performance in three cases of the GPS ionospheric delay mitigation during moderate space weather disturbances is presented in Table 3.

Our study shows the general inability of a commercial-grade single-frequency un-aided GPS receiver to meet the maritime navigation GNSS applications requirements for services better than those of low accuracy. Leaving the GPS receiver without any form of GPS ionospheric delay corrections will anchor it firmly into the category that satisfies the low accuracy applications requirements only. The utilisation of Klobuchar model will allow for satisfaction of the majority of requirements for medium accuracy, while the ion-free dual-frequency method will increase the positioning performance quality category of medium accuracy more firmly. Still, even the best ionospheric correction model will not allow for support of high- and very high-accuracy applications for a commercial-grade single-frequency un-aided GPS receiver.

It is also useful to note that deployment of various GPS ionospheric delay mitigation models and methods will also affect the nature of remaining GNSS positioning errors. No-correction and dual-frequency correction cases generated positioning errors that can be described as Gaussian (normal) statistical processes rather correctly. Such a characterisation opens room for deployment of various linear filtering methods (Kalman filter, for instance) that will effectively remove the remaining systematic and stochastic errors caused by GPS ionospheric delay. The utilisation of Klobuchar model will cause distraction from Gaussian process and call for different approaches in mitigation of remaining un-corrected systematic and stochastic errors due to GPS ionospheric delay, such as the particle-filtering method deployment.

Considering the interpretation of the results of our study, the utilisation of a multi-GNSS aided GNSS receiver with advanced signal processing methods and augmentation algorithms deployed is recommended for maritime applications.

5 CONCLUSION

The assessment of GPS positioning performance during moderate space weather disturbance with relation to the possible utilisation for maritime navigation applications is presented in this paper. Even moderate space weather disturbances affect the GPS positioning performance for marine navigation. Embedded GPS

ionospheric correction methods are useful in a commercial-grade single-frequency unaided GPS receiver for low- and medium-accuracy categories of the maritime navigation applications.

High-precision and very-high-precision applications require advanced methods and/or correction models for mitigating the effects of space weather and ionospheric disturbances, with the remaining importance in identification of and forecasting deteriorated ionospheric conditions.

References

Brčić, D. (2015). *A model of non-specific daily pattern of the satellite positioning signal ionospheric delay*. (PhD thesis). University of Rijeka, Faculty of Maritime Studies. Rijeka, Croatia.

Brown, R G, and Hwang, P W C. (2009). Introduction to Random Signals and Applied Kalman Filtering (3rd ed). John Wiley & Sons. New York, NY.

Crawley, M J. (2013). The R Book (2nd ed). John Wiley & Sons. Chichester, UK.

Filić, M, Filjar, R and Ruotsalainen, L. (2016). An SDR-based Study of Multi-GNSS Positioning Performance During Fast-developing Space Weather Storm. *TRANSNAV*, 10(3), 395 – 400. DOI: 10.12716/1001.10.03.03. Available at: http://bit.ly/2fxAvph, accessed on 5 May, 2017.

Filjar, R and Huljenić, D. (2012). The importance of mitigation of GNSS Vulnerabilities and Risks. *Coordinates*, 8(5), 14–16.

Filjar, R., Brčić D., and Kos, S. (2013). Single-frequency Horizontal GPS positioning Error Response to a Moderate Ionospheric Storm over Northern Adriatic. *Chapter in*: Weintrit, A. (editor) (2013). Advances in Marine Navigation. Taylor & Francis Group. London, UK.

Filjar, R, Kos, S, and Kos, T. (2012). A theoretical framework for understanding the relationship between space weather indices ad GPS ionospheric delay. *Proc of 6th GNSS Vulnerabilities and Solutions Conference*, 59–70. Baška, Krk Island, Croatia.

Mendillo, M. (2006). Storms in the ionosphere: Patterns and processes for total electron content. Rev Geophys, 44(47 pages). doi: 10.1029/2005RG000193.

Petrovski, I G. (2014).GPS, GLONASS, Galileo, and Beidou for Mobile Devices: From Instant to Precise Positioning. Cambridge University Press. Cambridge, UK.

R Development Core Team (2017). R: A language and environment for statistical computing. R Foundation for Statistical Computing, Vienna, Austria. ISBN 3-900051-07-0. Available at: http://www.R-project.org, accessed on 5 May, 2017.

Sanz Subirana, J *et al*. (2013). GNSS Data Processing – Vol. I: Fundamentals and Algorithms. European Space Agency (ESA). Nordwijk, The Netherlands. Available at: http://bit.ly/1QV4KAL, accessed on 5 May, 2017.

Sonel. (2017). The global network GNSS assembly data centre for the Global Sea Level Observing System (GLOSS). Available at: http://www.sonel.org/?lang=en, accessed on 10 February, 2017.

Takasu, T. (2013). RTKLIB: An Open Source Program Package for GNSS Positioning. Software and documentation available at: http://www.rtklib.com/, accessed on 5 May, 2017.

Thomas, M *et al*. (2011). Global Navigation Space Systems: reliance and vulnerabilities. The Royal Academy of Engineering. London, UK. Available at: http://bit.ly/1vrIenu, accessed on 5 May, 2017.

Sveučilište u Rijeci
POMORSKI FAKULTET U RIJECI
FACULTY OF MARITIME STUDIES RIJEKA
University of Rijeka

University of Zagreb
Faculty of Transport
and Traffic Sciences

Royal Institute of Navigation
Science Technology Practice

11th
Annual
Baška GNSS
Conference

CATEGORISATION OF SPACE WEATHER AND GNSS POSITIONING QUALITY INDICES FOR ESTIMATION OF GNSS POSITIONING PERFORMANCE DEGRADATION

Renato Filjar[1,2], **Mia Filić**[1], **Erkin Mirmakhmudov**[3]

[1] Faculty of Engineering, University of Rijeka, Croatia
E-mail: renato.filjar@gmail.com (Corresponding author)

[2] Faculty of Maritime Studies, University of Rijeka, Croatia

[3] National University of Uzbekistan, Tashkent, Uzbekistan

ABSTRACT

Space weather drives ionospheric dynamics, the major contributor to GNSS positioning performance, thus affecting a growing number of GNSS-related technology and socio-economic system. In development of a model capable of forecasting the GPS positioning performance deterioration caused by space weather, an appropriate choice of measurable descriptors of space weather, geomagnetic and ionospheric dynamics, GPS pseudorange measurement errors, and GPS positioning performance appeared an essential choice. Here we present the result of the study aimed at assessing the relevance of measured space weather, geomagnetic and ionospheric dynamics, GPS pseudorange measurement errors, and GPS positioning performance indices for utilisation in development of GPS positioning performance degradation forecasting model due to space weather effects. The Principal Components Analysis method is applied on the assembled set of experimental descriptors of the whole chain of the environment for satellite positioning in order to categorise the descriptors based on their individual and collective influence on the GPS positioning performance. Deployed in scenario of quiet space weather conditions to identify the systematic effects on GPS positioning performance, study results show

complexity of the whole environment for satellite positioning, with geomagnetic indices playing an important role in influencing GPS positioning performance.

Key words: *GNSS positioning performance, space weather categorisation, principal component analysis*

1 INTRODUCTION

Space weather has been understood the single most influential natural source of GNSS positioning performance degradation, accounting for both the magnitude and variability of GNSS position estimation errors (Canon *et al*, 2013). Risk assessment of satellite navigation utilisation in application and services development and operation calls increasingly for understanding the relationship between space weather and GNSS positioning performance, with GNSS already recognised as a component of national infrastructure, and a cornerstone of modern civilisation

While being described in theory, the relationship between the space weather developments and GNSS positioning performance is so complex that neither of models considered so far came close enough to the ability to allow forecasting of GNSS positioning performance deterioration due to space weather development.

Here we contribute to the subject with a case-study of categorisation of space weather and GNSS performance indices expected to serve in a later development of a forecasting model of GNSS positioning performance deterioration due to space weather development. We have taken a general approach in utilisation of statistical learning approach in describing the relationship between the state of space weather and GNSS positioning performance, attempting to develop a robust and reliable forecasting model of GNSS positioning performance degradation due to space weather activity. The results of a study represent a contribution to a larger problem solution.

This manuscript is structured as follows. After the introductory remarks in Section 1, the problem is stated and a survey of previous research outlined in Section 2. Processing methods and data set under scrutiny are presented in Section 3, while Section 4 addresses the quiet space weather-case studied. Presented results are discussed in relation to the problem in Section 5. The manuscript concludes with the outline of findings and a proposal for future scientific activities in the forecasting model developments.

2 PROBLEM STATEMENT AND PREVIOUS RESEARCH

GNSS positioning performance analysis has been considered fundamental for GNSS applications and services development. Both the identification and forecasting of GNSS positioning performance render a GNSS-based application or service robust and reliable, while allowing for estimation of its quality of service, largely determined by and reliant of the GNSS positioning performance. Various approaches failed in provision of accurate and reliable forecasts of GNSS positioning performance due to complex nature of the GNSS positioning environment and the large number of variables influencing the GNSS positioning performance indices. The GNSS positioning performance environment interweave several systems, every of them of significant spatio-temporal and complexity proportions, as depicted in Figure 1. While the existing models describe the interrelationship between the neighbouring chain components, the over-all model remains unknown.

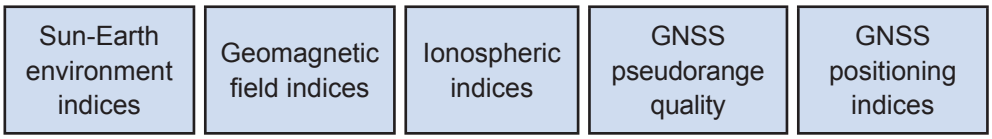

Figure 1. Environment for assessment of space weather effects on GNSS positioning performance

Statistical learning is a well-developed discipline that provides a set of indispensable tools for model development (Efron and Hastie, 2016). However, only recently it has become suitable for development of variety of model categories, bolstered by developments in computer science that allows for massive data set processing by wider segment of scientists (Efron and Hastie, 2016, James *et al*, 2015, Cadavid, Lawrence and Ruzmaikin, 2017).

Still, the existing model development projects have not been considering the over-all identification of the relevant space weather (including geomagnetic and ionospheric), and GNSS positioning performance indices for the space weather/ GNSS positioning performance relationship model development. Statistical learning methods were deployed on solar and geomagnetic data to achieve a reasonable description of the complex relationship. In addition, space weather forecasting and now-casting models with sufficient accuracy were developed.

Still, all those failed in establishing the relations with GNSS positioning performance, thus allowing for development of an over-all space weather/GNSS positioning performance forecasting model. While led by a systematic approach to modelling space weather dynamics, those models did not attempt to resolve the impact on technology systems, such as GNSS.

3 METHODOLOGY

A systematic approach has been developed by our team addressing the problem of formal description of the end-to-end (over-all) GNSS positioning environmental chain outlined in Figure 1. This approach involves a series of studies of GNSS positioning performance quality in characteristic environments for satellite positioning, determined by intensity of space weather dynamics (the conditions and variability of space weather components: Sun-Earth space weather, geomagnetic and ionospheric conditions), end-user micro-environment (urban, semi-urban, rural, mountains, maritime, air, road etc.), general geographical environment (polar, mid-latitude, equatorial, semi-equatorial regions) and a quality grade of end-user GNSS equipment.

Table 1. Indices description

Index	Description	Source	Remarks
SSN	Sunspot number	(NOAA, 2017)	Sun-Earth environment
SFD	Solar flux data	(NOAA, 2017)	Sun-Earth environment
Ap	Planetary A geomagnetic index	(NOAA, 2017)	Geomagnetic environment
Kp	Planetary K geomagnetic index	(NOAA, 2017)	Geomagnetic environment
Dst	Index of near-equatorial geomagnetic activity	(Kyoto University, 2017)	Geomagnetic environment
Bx*	x-component of geomagnetic field	(INTERMAGNET, 2017), reference station Lonjsko Polje, Croatia	Geomagnetic environment
By*	y-component of geomagnetic field	(INTERMAGNET, 2017), reference station Lonjsko Polje, Croatia	Geomagnetic environment

Index	Description	Source	Remarks
Bz*	z-component of geomagnetic field	(INTERMAGNET, 2017), reference station Lonjsko Polje, Croatia	Geomagnetic environment
f0F2	Critical frequency of F2 ionospheric layer	(NOAA, 2017)	Ionospheric environment
f0E	Critical frequency of E ionospheric layer	(NOAA, 2017)	Ionospheric environment
SID	Reading of Sudden Ionospheric Disturbance (SID) detector in Rijeka	Our own observation	Ionospheric environment
d_lam	Observed northing GPS positioning error	Derived from (IGS, 2017) GPS pseudoranges	GPS positioning performance
d_fi	Observed easting GPS positioning error	Derived from (IGS, 2017) GPS pseudoranges	GPS positioning performance

A formal approach requires a systematic development of related ontology in input data set. We developed preliminary input data ontology, based on measurable indices describing the GNSS positioning environment components (Figure 1), as detailed further in Section 3.1. In continuation of statistical learning process deployment, we used the Principal Component Analysis (PCA) method to categorise space weather and GNSS positioning quality indices, thus establishing the framework for the research described in this manuscript. An outline of PCA is given in Section 3.2.

3.1 Data description. This case scenario concerns a quiet space weather period observed in Summer 2007 (days 167 – 172). The input data set was assembled from different data sources, covering the Sun-Earth space weather, geomagnetic and ionospheric activity, as well as GNSS positioning performance data in a form of time series of northing and easting estimation errors observed with a stationary single-frequency commercial-grade GPS receiver. Indices and their sources are outlined in Table 1.

Indices SSN, SFD, Ap, Kp, Dst, Bx, By, Bz, f0F2, and f0E were taken from the internet-based scientific databases. Index SID was continually observed at Faculty of Maritime Studies, University of Rijeka, Rijeka, Croatia using a SID detector.

The GPS positioning performance indices were derived from RINEX GPS pseudorange observations taken at Padua, Italy. GPS positioning errors were calculated in relation to a known position of the Padua reference station from simulated position estimation obtained from a GNSS Software Defined Radio (SDR) RTKLIB configured to post-process pseudoranges as a single-frequency commercial-grade GPS receiver. Post-processing was conducted with broadcast satellite ephemeris and the active correction (ionospheric, tropospheric and satellite clocks) models. (Filić, Filjar, and Ruotsalainen, 2016) outlined the procedure in more details.

3.2 Principal Component Analysis (PCA) is used here for linear model dimensionality reduction and transformation of possibly correlated variables into those linearly uncorrelated. The method was developed by Prof Karl Pearson (Pearson, 1901).

> Definition: *Principal Component Analysis, known also as Karhunen-Loeve transform, is a statistical method that utilises an orthogonal transform for conversion of a set of observation of possibly correlated variables into a set of linearly uncorrelated variables called principal components.*

PCA returns principal components in descending amounts of the original observation variations covered (Abdi and Williams, 2010, Jolliffe and Cadima, 2016). The first principal component accounts for the largest portion of original variations, while the second one takes the second largest variations associated with the direction orthogonal to the first one. The application of the method continues until the whole amount of the observed variation is split among the mutually orthogonal principal components. Number of principal components is less than or equal to the lower value in the set:

$$\{\textit{the number of original variables, the number of observations}\} \quad (1)$$

The PCA method can be comprehensively presented as follows. Let **X** be a random vector of the observed variables:

$$\boldsymbol{X} = \begin{pmatrix} x_1 \\ \vdots \\ x_n \end{pmatrix} \quad (2)$$

with population variance-co-variance matrix given as:

$$var(\boldsymbol{X}) = \boldsymbol{\Sigma} = \left(\begin{pmatrix} \sigma_1^2 & \cdots & \sigma_{1p} \\ \vdots & \ddots & \vdots \\ \sigma_{p1} & \cdots & \sigma_p^2 \end{pmatrix} \right) \tag{3}$$

where:

$\sigma_i = \frac{\sum x_i^2}{N}$ … variance of elements from i-th data set,

$\sigma_{i,j} = \frac{\sum x_i x_j}{N}$ … covariance for elements from i-th and j-th data sets,

N … number of scores in a data set.

Requirement for randomness can be fulfilled easily with a prior decomposition of the observation time series (i. e. by removing systematic errors from observations).

Consider the linear system, with the e_{ij} coefficients viewed as regression coefficients, as follows:

$$\begin{aligned} Y_1 &= e_{11}X_1 + e_{12}X_2 + \ldots + e_{1p}X_p \\ Y_2 &= e_{21}X_1 + e_{22}X_2 + \ldots + e_{2p}X_p \\ &\ldots \\ Y_p &= e_{p1}X_1 + e_{p2}X_p + \ldots + e_{pp}X_p \end{aligned} \tag{4}$$

Every Y_i is a function of a random data, thus considered random itself, with population variance given as:

$$var(Y_i) = \sum_{k=1}^{p} \sum_{l=1}^{p} e_{ik} e_{il} \sigma_{kl} = e_i' \sum e_i \tag{5}$$

A population co-variance is given as:

$$cov(Y_i, Y_j) = \sum_{k=1}^{p} \sum_{l=1}^{p} e_{ik} e_{jl} \sigma_{kl} = e_i' \sum e_j \tag{6}$$

while the e_{ij} coefficients can be assembled as a vector:

$$e_i = \begin{pmatrix} e_{i1} \\ \vdots \\ e_{ip} \end{pmatrix} \tag{7}$$

The first principal component is given as the linear combination that extends the maximum variance, as given below:

$$\begin{aligned} var(Y_1) &= \sum_{k=1}^{p} \sum_{l=1}^{p} e_{1k} e_{1l} \sigma_{kl} = e_1' \sum e_1 \\ e_1' e_1 &= \sum^{p} e_{1j}^2 = 1 \end{aligned} \tag{8}$$

The second principal component accounts for as much of the remaining variance as possible, with constraint of correlation between the first and second component being equal to 0 (i. e. the two components are mutually orthogonal), as presented below:

$$\begin{aligned} var(Y_2) &= \sum_{k=1}^{p} \sum_{l=1}^{p} e_{2k} e_{2l} \sigma_{kl} = e_2' \sum e_2 \\ e_2' e_2 &= \sum_{j=1}^{p} e_{2j}^2 = 1 \end{aligned} \tag{9}$$

$$cov(Y_1, Y_2) = \sum_{k=1}^{p} \sum_{l=1}^{p} e_{1k} e_{2l} \sigma_{kl} = e_1' \sum e_2 \tag{10}$$

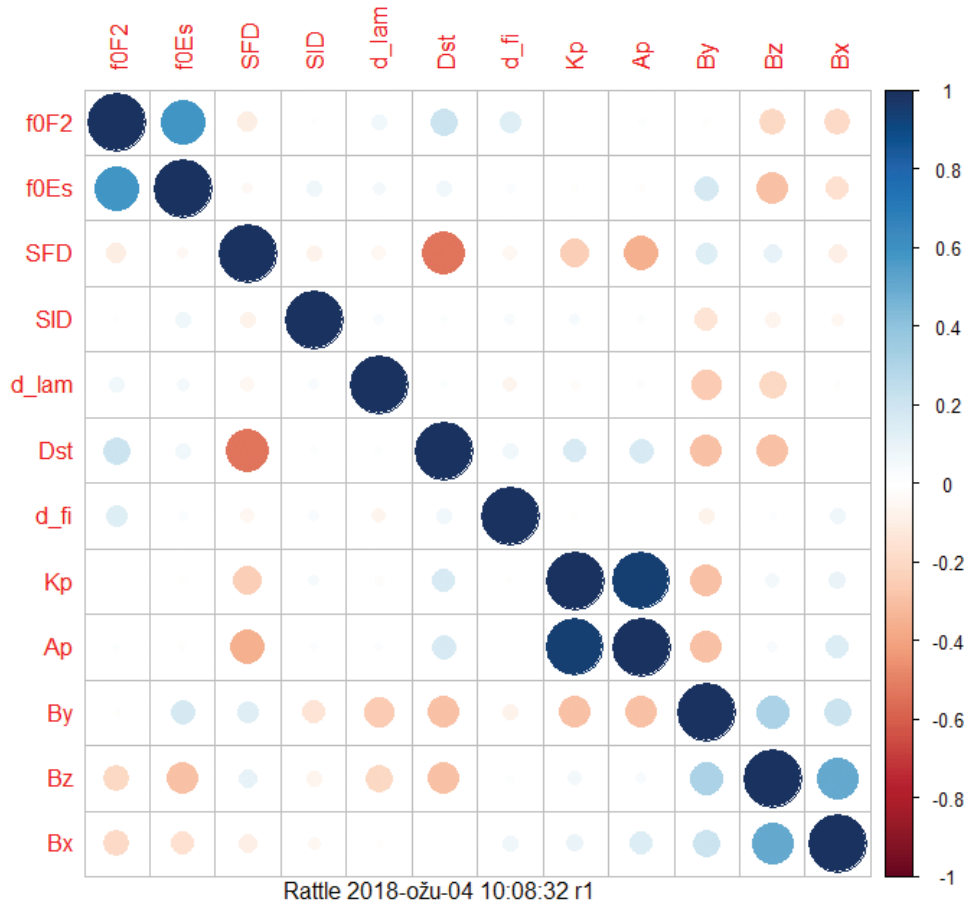

Figure 2. Correlation matrix of data set under consideration

Principal component analysis attempts to represent a data frame containing correlated variables in terms of uncorrelated components. The principal components identified account for successively smaller level of variability in the data frame. Thus, PCA reduces a large number of correlated variables into a smaller set of un-correlated components. PCA may allow for identification of the underlying structure in the data, and the provision of clues about causal connections.

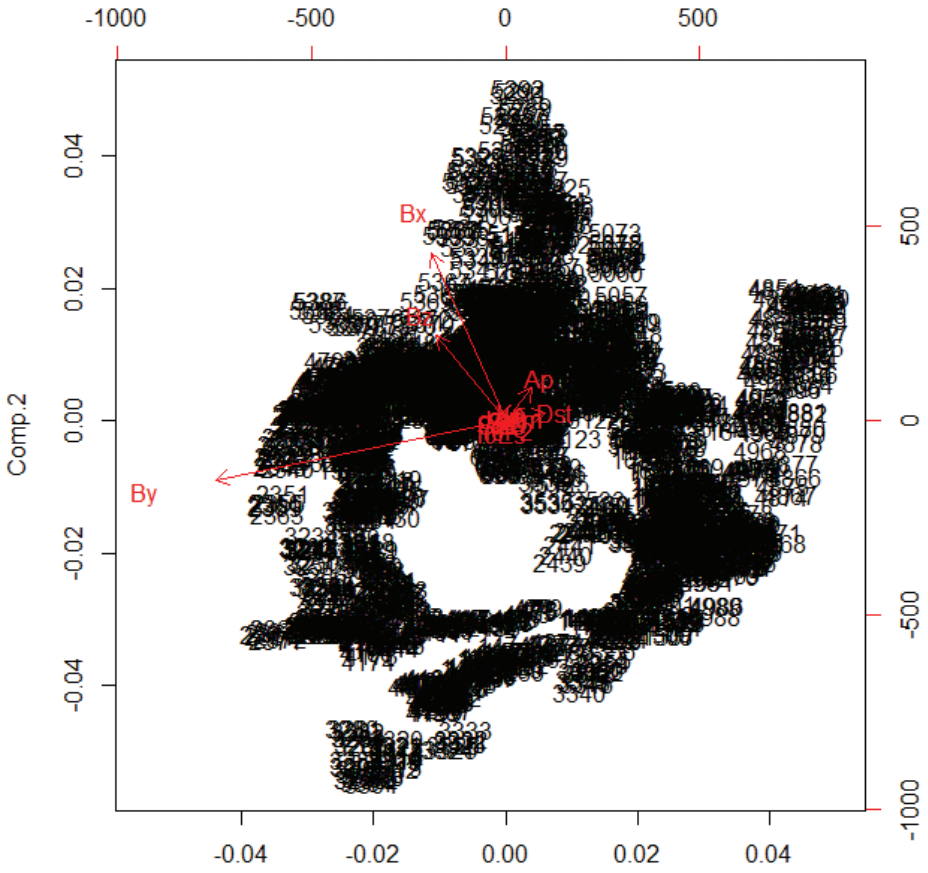

Figure 3. PC2-PC1 diagram outlining relation between the first two principal components

4 STUDY RESULTS

This research was conducted with the aim of identification of the principal components of the original ontology of data that would absorb most of the variance of the observed dynamics, and thus serve further in development of the Space Weather-GNSS Positioning Performance model. The scenario under scrutiny addressed a case of quiet space weather conditions. PCA was conducted on the 13 variables-data set with 3772 observations in total. Exploratory statistical analysis was conducted to assess the nature of related indices, including the correlation analysis. The correlation matrix obtained is depicted in Figure 2.

Correlation matrix reveals considerable (negative) correlation between By index and the geomagnetic (Kp, Ap) and ionospheric (Dst, and, to a lesser extent, SID) indices. However, a considerable negative correlation was identified between By geomagnetic index and the northing GPS positioning error.

The PCA method was applied on the data set under consideration, returning the results that again emphasise the role of geomagnetic indices in the SW-GNSS model definition, as shown in Figure 3. The PCA analysis was conducted using R environment for statistical computing (Williams, 2016).

Further PCA results analysis shows that the first three principal components account for 88.77% of variance. Two additional should be considered to cover 98.29% of the over-all variability. This emphasises the complexity of the process modelled, and interrelationship between measured indices.

Vector representation of variables in PC1 – PC2 diagram indicates the extent to which the variables contribute to two Principal Components with the largest variance. Contribution of By and Bx has been identified, that indicates relationship with related space weather indices. The preliminary results presented demonstrate applicability of the procedure to wider data sets, encompassing even larger list potentially relevant space weather indices (TEC).

5 CONCLUSION

This manuscript presents results of a study of GPS positioning performance in quiet space weather conditions, with the aim of establishing the process understanding for the later development of the space weather-GNSS positioning performance model.

Here we address the quest of identification of principal components established on linear combination of related indices from developed input data ontology, accounting for most of the over-all process variance.

Principal component analysis was applied on the relatively small database of space weather and GNSS positioning performance indices, with a goal of identification of the most influential space weather indices and their linear components.

Preliminary results show the importance of geomagnetic environment By and Bx indices, that couple space weather ones with those indicating the GPS positioning performance.

Further research will extend to consider massive data sets, comprising various space weather condition scenarios, and the PCA application on the extended data set (inclusion of additional space weather indices, such as TEC).

References

Abdi, H and Williams, L J. (2010). Principal component analysis. *WIREs Comp Stat*, 2, 433–459.

Cadavid, A C, Lawrence, J K, and Ruzmaikin, A. (2017). Principal Components and Independent Component Analysis of Solar and Space Data. arXiv.org pre-print archive. Available at: http://bit.ly/2q9OKGQ, accessed on 2 May, 2017.

Cannon, P *et al*. (2013). Extreme space weather: impacts on engineered systems and infrastructure. Royal Academy of Engineering. London, UK. Available at: http://bit.ly/11OdBNN. accessed on 4th November, 2017.

Efron, B and Hastie, T (2016). Computer Age Statistical Inference: Algorithms, Evidence, and Data Science. Cambridge University Press. Cambridge, UK.

Filić, M, Filjar, R, and Ruotsalainen, L. (2016). An SDR-based Study of Multi-GNSS Positioning Performance During Fast-developing Space Weather Storm. *TransNav*, 10, 395–400. doi: 10.12716/1001.10.03.03

IGS. (2017). International GNSS Service archive and products. Available at: http://www.igs.org, accessed on: 4 April, 2017.

INTERMAGNET. (2017). Internet database of geomagnetic indices observations. Available at: http://www.intermagnet.org/data-donnee/data-eng.php, accessed on 2 November, 2017.

James, G *et al*. (2015). An Introduction to Statistical Learning (6th printing). Springer Verlag. New York, NY.

Jolliffe, I T, and Cadima, J. (2016). Principal component analysis: a review and recent developments. *Phil Trans R Soc A*, 374, 20150202. http://dx.doi.org/10.1098/rsta.2015.0202.

Kyoto University. (2017). Internet database of geomagnetic equatorial Dst index. Available at: http://wdc.kugi.kyoto-u.ac.jp/dstdir/, accessed on 2 November, 2017.

NOAA Space Weather Prediction Center (SWPC). (2017). Internet database of space weather indices observations. Available at: http://www.swpc.noaa.gov, accessed on 2 November, 2017.

Pearson, K. (1901). On lines and planes of closest fit to systems of points in space. *Philosophical Magazine* 2, 559–572.

Williams, G *et al*. (2016). Rattle: Graphical User Interface for Data Mining in R. Available at: https://cran.r-project.org/web/packages/rattle/index.html, accessed on 4 April, 2017.

Sveučilište u Rijeci
POMORSKI FAKULTET U RIJECI
FACULTY OF MARITIME STUDIES RIJEKA
University of Rijeka

University of Zagreb
Faculty of Transport
and Traffic Sciences

Royal Institute of Navigation
Science Technology Practice

11th
Annual
Baška GNSS
Conference

SPATIAL ASSESSMENT OF GPS IONOSPHERIC DELAY MODEL DURING ST. PATRICK'S GEOMAGNETIC STORM

Barbara Pongračić[1], **Serdjo Kos**[2], **David Brčić**[2]

[1] Beihang University, Beijing, China

[2] University of Rijeka, Faculty of Maritime Studies Rijeka, Croatia
E-mail: brcic@pfri.hr (Corresponding author)

ABSTRACT

The proposed study represents a continuation of the research regarding standard GPS ionospheric delay mitigation. Globally distributed locations were elaborated in terms of positioning solutions, with analyses of the horizontal component of positioning error. The ionospheric delay was calculated on the basis of raw pseudoranges and compared with modelled values. The horizontal GPS positioning error was observed in three main ionospheric regions during the geomagnetic storm which took place in March 2015. Residuals between real and modelled values suggest different behaviour of positioning patterns depending on location. Increase in residual values appears notably after the commencement of the disturbance. The conducted study and noted observations open further possibilities for research in this domain of satellite positioning error mitigation.

Key words: *satellite positioning, horizontal positioning error, standard ionospheric delay model, geomagnetic storm*

1 INTRODUCTION AND BACKGROUND

GNSS receiver determines its position by measuring the propagation time of signals transmitted from the satellite's to the receiver's antenna. A pseudorange determined from the time measurement can be estimated as follows:

$$R_p = \rho + c\,(dt_r + dt^s) + T + I + K_{p,r} + K_p^s + M_p + \varepsilon_p \quad (1)$$

where:

R_p – code measured pseudorange, ρ – geometric range between the satellite and receiver, c – speed of light, dt_r, dt^s – receiver and satellite clock offsets, respectively, T – tropospheric delay, I – ionospheric delay, $K_{p,r}$, K_p^s – receiver and satellite instrumental delays, M_p – multipath and ε_p – unmodelled error.

Ionospheric delay is considered as the main particular source of error regarding single-frequency receivers (Parkinson *et al*, 1996). Standalone single-frequency receivers use different models to mitigate this effect. GPS system uses standard ionospheric (Klobuchar) model. It is considered that it reduces 50% of the error on a global basis (Klobuchar, 1987). However, due to its global nature and under specific circumstances, the model shows certain deficiencies regarding response delay, contributions to undesirable positioning error, unnecessary prolongation of response, as well as inability to describe local ionospheric delay patterns (Filjar, 2008, Filjar *et al*, 2011).

Ionospheric delay is related to geomagnetic disturbances, which influence ionospheric layers height and frequency oscillations and Total Electron Content (TEC) behaviour (Booker, 1954, Berkner and Seaton, 1940). Indeed, (Booker, 1954) states that if we analyse ionospheric disturbances, we also have to consider geomagnetic storms, since their origin is the same. Ionospheric delay can be expressed as follows:

$$\Delta\rho = \frac{40.3}{f^2} TEC \quad (2)$$

where:

f – system operating frequency, in this case being 1575.42 MHz and TEC – number of electrons on the signal ray-path in a cross-section of 1 m^2.

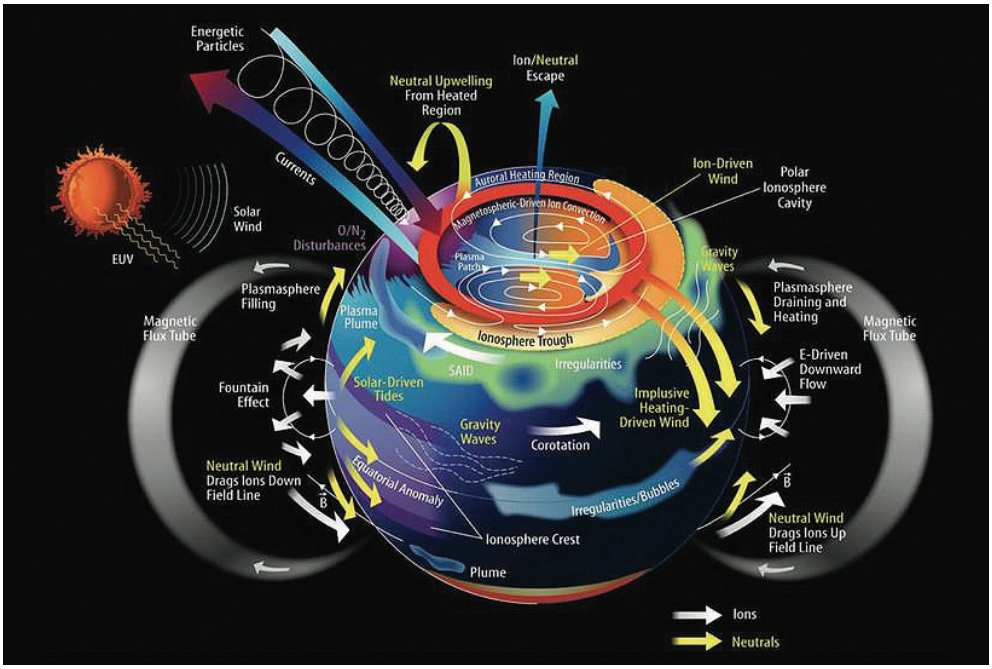

Figure 1. The Earth's ionosphere and corresponding processes (after Grebowsky and Aikin, 2009)

Depending on user's position, the ionosphere can be divided into high (latitude N/S 60° – 90°), middle (latitude N/S 20° – 60°) and low (latitude N/S 0° – 20°) regions, each characterised with its own features and typical processes (Figure 1). Mid-ionosphere is characterised by UV and X solar radiation (production) and chemical recombination (loss). Neutral winds are moving the ionisation along geomagnetic field lines towards higher and lower latitudes (Hunsucker and Hargreaves, 2003). Low-ionosphere is marked with Equatorial Electrojet (EE) and Equatorial Ionization Anomaly (EIA), resulting as consequence of horizontal geomagnetic field component and vertical ionospheric drifts (Zolesi and Cander, 2014). High-ionosphere is connected with the outer magnetosphere, and it is directly affected by the influence of the solar wind and interplanetary magnetic field (Schunk and Nagy, 2009).

Middle latitudes ionosphere is the least sensitive to external influences, also being the most studied one. In low and high regions, additional processes occur, regardless of the state of geomagnetic and solar activity.

Global scale ionospheric disturbances are characterised as storms, with Traveling Ionospheric Disturbances (TID) being smaller in scale and severity (Schunk and Sojka, 1996). Storms begin with a Sudden Storm Commencement (SSC), followed by growth, main storm phase, and finally the recovering. When considering GNSS, storms are discussed in terms of change in TEC and its behaviour. Characteristic of the storms and their influence on TEC have been investigated and elaborated thoroughly in (Schunk and Sojka, 1996, Mendillo, 2006, Buonsanto, 1999), while challenges in forecasting and modelling TEC are presented in (Borries *et al*, 2015). Variability of the ionospheric disturbances makes GNSS mitigation models even less successful which can lead to positioning deterioration.

2 PREVIOUS RESEARCH AND MOTIVATION

> *'Storms do not create new processes but rather intensify known processes to extents that are not fully known.' – Mendillo, 2006.*

In previous papers (Filjar *et al*, 2013, Kos *et al*, 2015) ionospheric delay patterns were elaborated regarding TEC behaviour as well as the cause of positioning degradation. The standard ionospheric model has been evaluated during three consecutive years, each characterised by different geomagnetic and ionospheric activity (Brčić *et al*, 2016).

It has been observed that during quiet and moderate periods, latitude and longitude residuals (differences between modelled and un-modelled values) followed similar patterns, with latitude tending to negative values and longitude to positive ones. However, during the storm period highly negative residual pattern was present in both coordinates observed at IGS station BZRG, as shown on Figure 2.

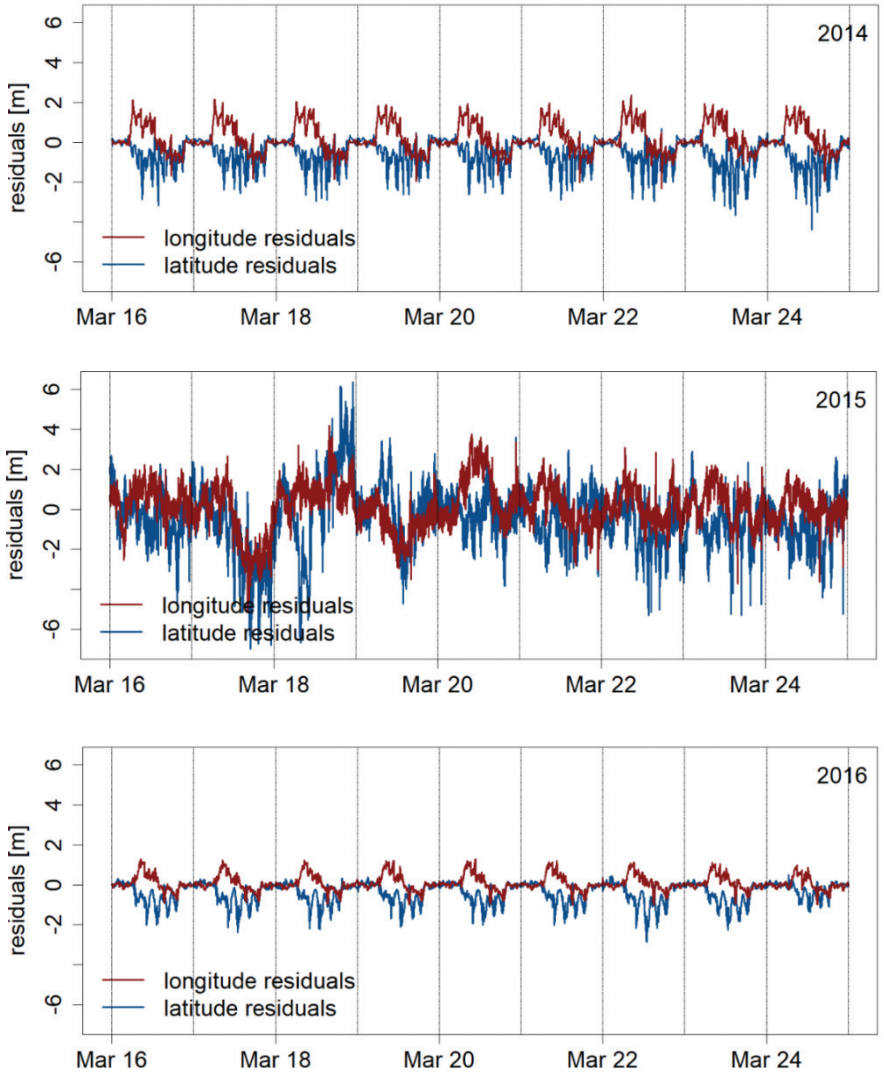

Figure 2. Nine-day (DOY 75 - 83) period of quiet (top image), storm (middle image) and moderate (bottom image) geomagnetic activity showing 30s-resolution latitude and longitude residuals

The most interesting patterns occurred in 2015 during the St. Patrick's geomagnetic storm. It caused sudden coordinate pattern deviations. Since the storm period was analysed in one specific region, a need for more spatially distributed stations appeared, to gain a detailed insight into positioning deviation

patterns. This was the motivation for the research presented here. Preliminary results showed unanticipated results, an example of which is shown on Figure 3, presenting coordinate residuals as observed in middle latitude region – the same region elaborated in (Brčić *et al*, 2016).

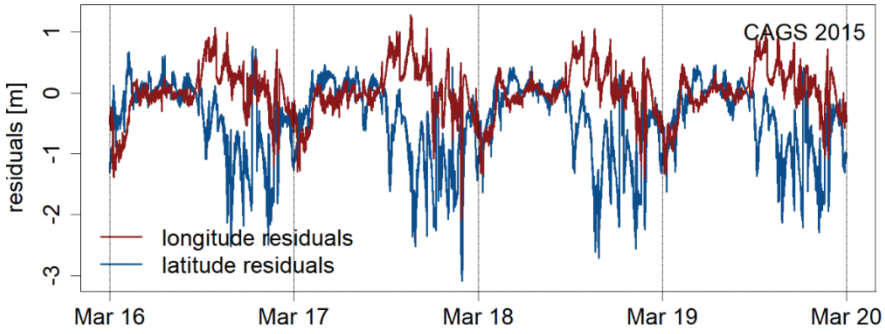

Figure 3. Latitude and longitude residuals during storm period as observed on CAGS IGS middle latitude region station

This study is an attempt to gain a further understanding the extent GPS coordinates behave during disturbances caused by geomagnetic storms. Or, more precisely how positioning disturbances act at different regions, implying main known features of high, mid and low latitudes and respective ionospheres. The successfulness of the standard ionospheric model employed in GPS receivers was analysed by obtaining modelled and unmodeled positioning solutions. Positioning deviations were concerned regarding error reduction by the employment of the Klobuchar model.

3 THE ST. PATRICK'S STORM EVENT AND METHODOLOGY

According to Dst and Kp indices (Figure 4), the storm commenced around 05 hrs UTC on March 17th, with a sudden increase in solar wind velocity of 400 – 500 km/s (USGS, 2015). This was the strongest geomagnetic storm during the solar cycle 25. *Dst* index was low as –223 nT, with Kp reaching its maximum of 9 (WDC, 2017, NASA, 2017).

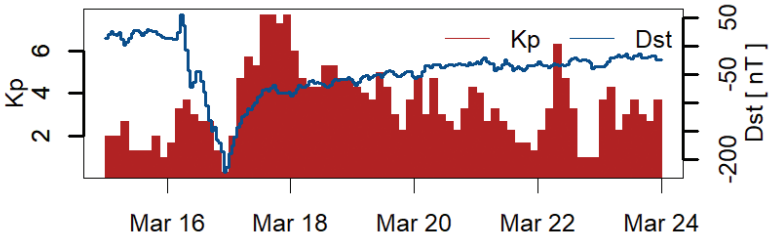

Figure 4. Dst and Kp values during the geomagnetic storm period

The severity of the storm's impact has been studied in terms of ionospheric disturbances (Cherniak and Zakharenkova, 2016, Fagundes *et al*, 2016) and as an additional cause of the error on PPP and RTK positioning (Jacobsen and Andalsvik, 2016). To assess positioning error under disturbed space weather conditions for standalone single frequency GPS users, we used ground-based International GNSS Service (IGS) network stations (Table 1).

Table 1. Locations of employed IGS observatories

ST_ID	latitude [°]	longitude [°]	height [m]	Δ UTC [h]
SYOG	69.0069444 N	039.5836111 E	50.09	+ 3
NYA1	78.9294444 N	011.8652778 E	84.00	+ 1
NURK	01.9444444 S	030.0897222 E	1485.30	+ 2
MCM4	77.8383333 S	166.6691667 E	98.02	+ 11
NAUR	00.5516667 S	166.9252778 E	46.30	+ 11
TIXI	71.6344444 N	128.8663889 E	46.98	+ 9
CZTG	46.4316667 S	051.8552778 E	202.80	+ 3
CAGS	45.5850000 N	075.8072222 W	235.00	− 5
ALRT	82.4941667 N	062.3402778 W	78.11	− 4
BZRG	46.4988889 N	011.3366667 E	328.80	+ 1
GRAZ	47.0669444 N	015.4933333 E	538.30	+ 1

Among other GNSS data observables and products, the network provides navigation and observation files (Dow *et al*, 2009) necessary for obtaining positioning solutions (Figure 5).

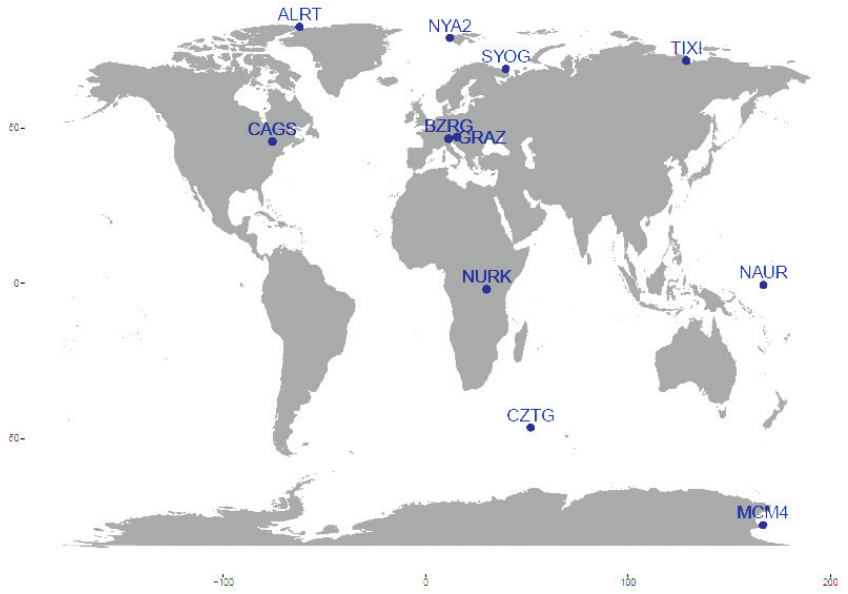

Figure 5. Spatial distribution of employed IGS stations

3.1 Calculation of Klobuchar model values. Standard ionospheric correction model coefficients are transmitted in the navigation message and estimated depending on the receiver's position, local time and satellite elevation. This is a composite model consisting of the nigh-time constant value of 5 ns of delay (22 – 06 h) and day-time value modelled as cosine function with the maximum value at 14 h LT (Klobuchar, 1987). According to the model, slant factor is calculated as:

$$F = 1 + 16(0.53 - E)^3 \tag{3}$$

where:

F – slant factor and E – satellite elevation.

Regarding local time and receiver position, modelled values (d_{in} or d_{id}) are calculated based on the modelling parameter X:

$$X = \frac{2\pi(t - 50400)}{\sum_{n=0}^{3} \beta_n \phi_m} \tag{4}$$

where:

X – modelling parameter, α_n, β_n – coefficients, ϕ_m – user's geomagnetic latitude and t – time of a signal transmission [s].

Finally, the estimated ionospheric delay is expressed as follows:

$$delay = \begin{cases} |X| \geq 1.57, & d_{in} = cF \cdot 5 \cdot 10^{-9} \\ |X| < 1.57, & d_{id} = cF\left[5 \cdot 10^{-9} + \left(\sum_{n=0}^{3} \alpha_n \phi_m^n\right)\left(1 - \frac{X^2}{2} + \frac{X^4}{24}\right)\right] \end{cases} \tag{5}$$

where:

α_n, β_n – model coefficients, ϕ_m – user's geomagnetic latitude, t – time of the signal transmission, d_{in} – uniform ionospheric delay [m], d_{id} – cosine ionospheric delay [m] and c – speed of light [m/s].

3.2 Residuals' determination. In (Brčić *et al*, 2016), residuals were calculated as the difference between modelled and unmodeled coordinates. Residuals calculated this way present direction and amount of deviation of coordinates due to Klobuchar model, concerning the unmodeled value. The modelled coordinate's solution moved southward or westward when residual is negative. This type of residuals can be used in directional coordinate's analysis, but it can't provide analysis of Klobuchar model successfulness on the positioning solutions. Thus, residuals were analysed in a horizontal plane, with the formulation which provides the assessment of actual mitigation of ionospheric delay.

Daily positioning solutions were calculated using *RTKLIB* open source software (RTKLIB, 2017).Two positioning datasets were created for each day and each station: with and without employment of ionospheric modelling. Latitude and longitude deviations from a median position with employed Klobuchar model on the DOY 75 for each station were calculated. Geomagnetic conditions during this

day were characterised as quiet, with small positioning deviations. Positioning error was assessed regarding the horizontal plane error as:

$$HE = \sqrt{d_{lat}^2 + d_{lon}^2} \tag{6}$$

where:

HE – horizontal plane error [m], d_{lat} – latitude deviation from median position and d_{lon} – longitude deviation from median position.

After the horizontal error has been determined for each station, we calculated residuals between modelled and unmodeled horizontal errors as:

$$res = \begin{cases} -|HE_{on}|, & |HE_{on}| < |HE_{off}| \text{ and } HE_{on} \cdot HE_{off} < 0 \\ \dfrac{HE_{on}^2 - HE_{off}^2}{|HE_{on} + HE_{off}|}, & else \end{cases} \tag{7}$$

where:

res – residual [m] and HE_{on}, HE_{off} – horizontal error with and without Klobuchar model, respectively.

This expression allowed residuals' analyses regarding model effectiveness, with negative results when Klobuchar model decreased horizontal plane error as compared to the unmodelled value. Successfulness of the model was calculated as the ratio of the total number of negative values over a total number of observations. Let $RES = \{res_i, i = 1, \ldots I\}$ be residuals set of I observations, and $K = \{x_n : x_n = res_i < 0$, and $n = 1, \ldots, N\}$ be a set of negative residuals of a length N, then:

$$C = \frac{|K|}{|RES|} \tag{8}$$

where *MSC* represents Modelling Success Coefficient.

4 RESULTS

Data were analysed according to main ionospheric regions. On Figure 6, horizontal error (HE) residuals calculated at high latitude stations are presented. The red line represents storm time (Dst) commencement. In Table 2, Modelling Success Coefficient as calculated for high latitudes is presented.

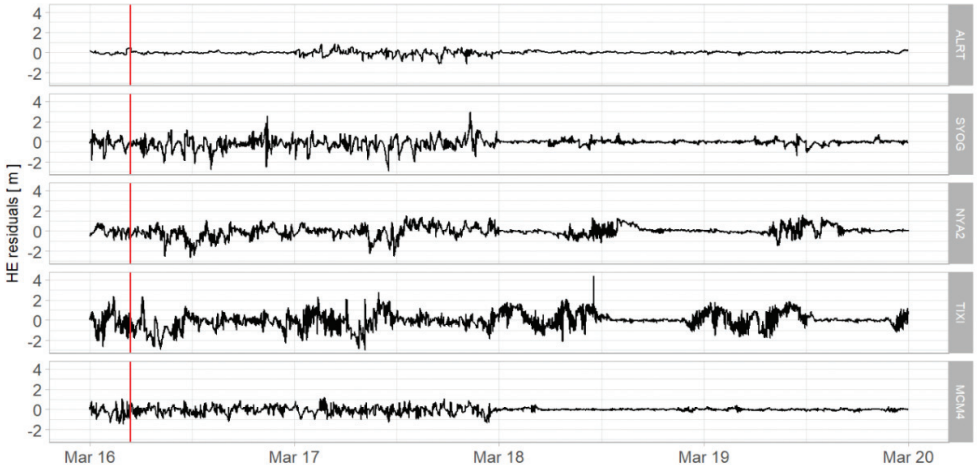

Figure 6. Horizontal error residuals observed at high latitude stations

Horizontal error residuals on high latitudes were in the range of ±2.9 m, except in the case of TIXI station with a maximum value of 4.4 m. On station ALRT, increased oscillations in residuals have been noticed on the day of the storm. After March 18th, smaller deviations in residuals have been noticed on all stations. Increase in deviations is noticed around mid-day.

Table 2. MSC for high latitude locations as calculated during the storm period

Station	ALRT	SYOG	NYA2	TIXI	MCM4
MSC	0.545	0.592	0.51	0.514	0.557

At middle latitudes (Figure 7) HE residuals showed a similar pattern, however with higher range (from −4.3 to + 3.2m) when compared to high latitude positioning solutions. In Table 3, MSC is presented for the respective stations.

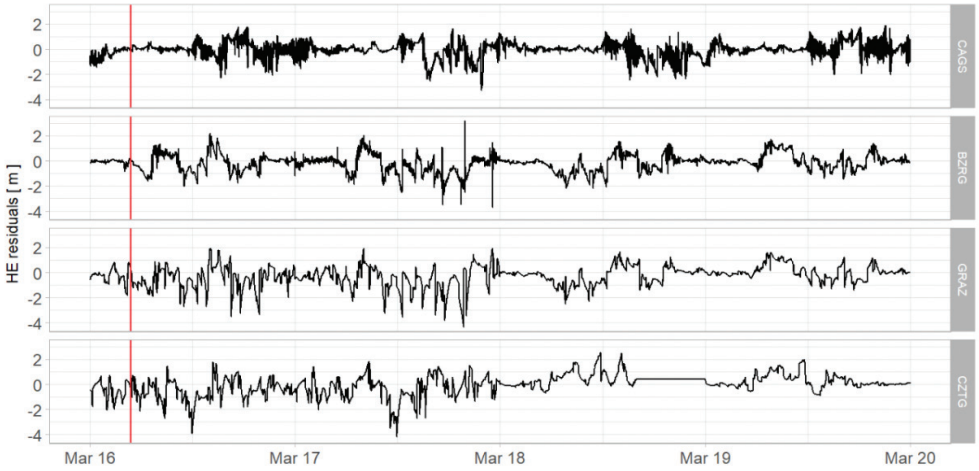

Figure 7. Horizontal error residuals observed at middle latitude stations

MSC was high for BZRG and GRAZ stations, while at CZTG station was 0.468. It means that employment of Klobuchar model reduced horizontal error accuracy.

Table 3. MSC for middle latitude locations as calculated during the storm period

Station	CAGS	BZRG	GRAZ	CZTG
MSC	0.508	0.59	0.625	0.468

As for low latitudes, horizontal error residuals were the smallest, reaching values of − 2 m to 2.5 meters, respectively (Figure 8). The greatest value of 3.4 m was observed at NURK station on March 16th.

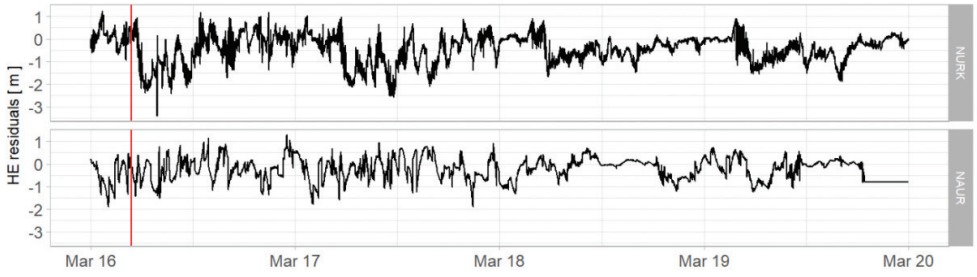

Figure 8. Horizontal error residuals observed at low latitude stations

Table 4. MSC for low latitude locations as calculated during the storm period

Station	NURK	NAUR
MSC	0.752	0.646

MSC calculation (Table 4) showed that values were mostly negative. Thus the model performed better in this region.

5 DISCUSSION

On Figure 9, distribution of residual values at all stations is presented. Data comprise the whole storm period.

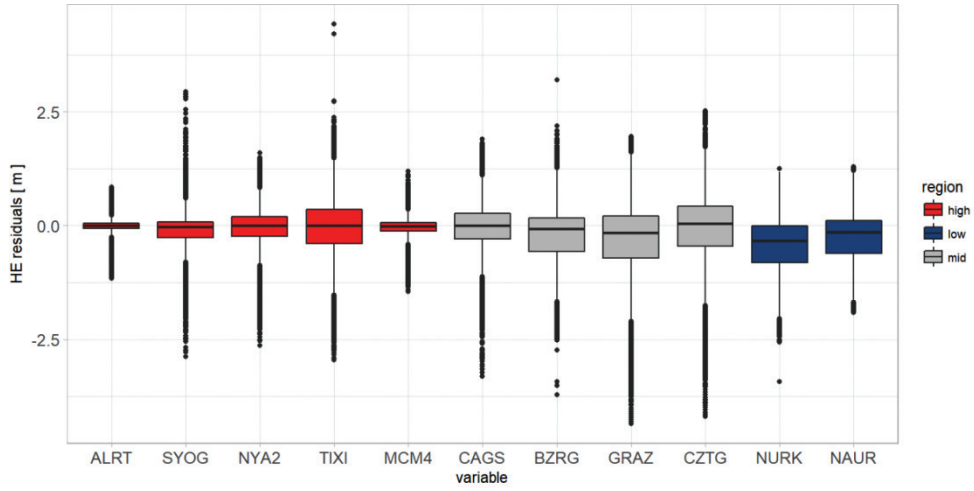

Figure 9. Distribution of residuals as calculated for each IGS station during the storm period. The distribution shows central 50% of data (boxes), medians (horizontal lines in boxes), upper and lower quartile of data (vertical lines) and outliers

High and low residual values (*outliers*) are more pronounced at high and middle latitudes, what can be interpreted in a way that in mentioned areas more extreme deviations from modelled and un-modelled values were present. On several occasions, most pronounced disturbances were noticed at the end of the storm period. Disturbances emerged in relatively short time delay. The model showed its best performance at low latitudes.

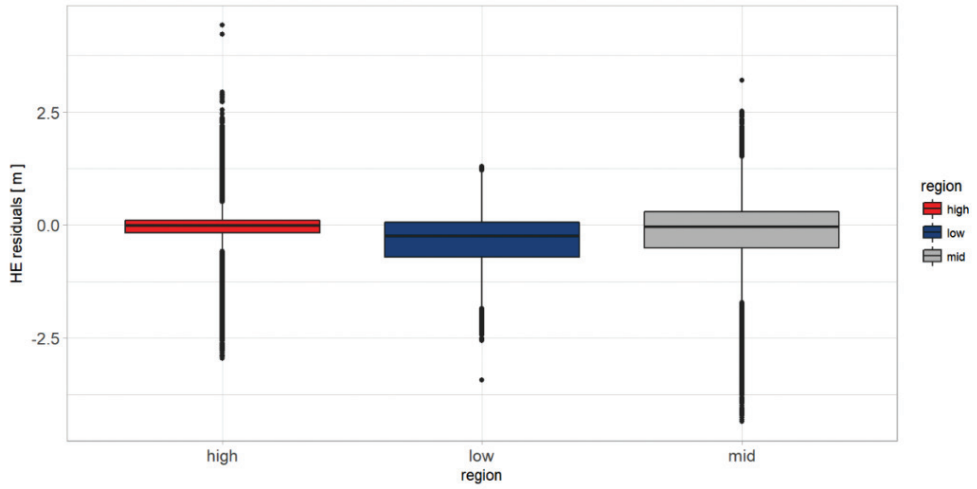

Figure 10. Distribution of residual values during storm period at high (red box), low (blue box) and middle (grey box) latitudes

At low latitudes, residual values were mostly negative, while they were zero-centred at other regions. On the other side, unlikely at low latitudes, normal distribution was present at middle and high regions. Regarding ionospheric regions, we can conclude following (Figure 10):

– During the storm, high latitudes experienced the most extreme residual values,
– The central dataset at middle latitudes was larger, as well as the range of residual values. However, extreme values are still present, reaching even greater (negative) values,
– Low latitudes experienced the smallest number of extreme values,
– A significant difference in model successfulness is noted at middle latitudes when comparing quiet and disturbed geomagnetic activity.
– Although middle latitudes represent an area of most common GPS usage, this study showed that during disturbed ionosphere model performed better in low regions.
– To confirm proposed findings derived inherences, further research is needed regarding spatial and time analyses of positioning solutions at the Earth's surface.

Analysis of horizontal errors and residuals could contribute to the identification of areas and circumstances under which existing models cause an additional error. Identification and eventual modelling of such cases should be used for further improvement of positioning and awareness of its faults.

6 TENDENCIES AND FURTHER WORK

We analysed horizontal error residuals' time-series in different ionospheric regions during specific storm period to assess the usefulness of the standard GPS ionospheric model. After positions were estimated both with and without ionospheric correction, we calculated horizontal errors and their differences, introducing equation which described successfulness of the model.

The paper presents an opportunity for regional or local modelling of the positioning deviations since similar horizontal error residuals were noticed on the stations near to each other (e.g. *bzrg* and *graz*). Stations which are near, experience similar ionospheric conditions and the other influential factors (e.g. dilution of precision) as well. Global modelling would have to take into consideration additional aspects, such as local time, spreading of disturbances, etc. As for disturbance propagation exploration, a denser global sample of stations providing positioning solutions are needed, which presents a further continuation of the presented research.

Acknowledgments

Research activities presented in this paper were conducted under the research project *Research into the correlation of maritime-transport elements in marine traffic: Satellite navigation segment*, supported by the University of Rijeka, Croatia. Authors appreciate, compliment and support the access to open software packages and tools used in the presented research: *R*, *R Studio*, *RTKLIB* and *Rinex-GPS-TEC*.

References

Berkner, L. W. & Seaton, S. L. 1940. Ionospheric changes associated with the magnetic storm of March 24, 1940. *Terrestrial Magnetism and Atmospheric Electricity,* 45, 393–418.

Booker, H. G. Morphology of Ionospheric Storms. Proceedings of the National Academy of Science of the United States of America, 1954 Washington, DC. PNAS, 931–943.

Borries, C., Berdermann, J., Jakowski, N. & Wilken, V. 2015. Ionospheric storms—A challenge for empirical forecast of the total electron content. *Journal of Geophysical Research: Space Physics,* 120, 3175–3186.

Brčić, D., Pongračić, B. & Kos, S. Vernal equinox storm time and quiet space weather TEC behaviour in correlation with GPS coordinate deviations. Proceedings of the 10th Annual Baška GNSS Conference., 8-10. 5. 2016. 2016 Baška, Croatia. The Royal Institute of Navigation, London & University of Rijeka, Faculty of Maritime Studies.

Buonsanto, M. J. 1999. Ionospheric Storms — A Review. *Space Science Reviews,* 88, 563–601.

Cherniak, I. & Zakharenkova, I. 2016. High-latitude ionospheric irregularities: differences between ground- and space-based GPS measurements during the 2015 St. Patrick's Day storm. *Earth, Planets and Space,* 68.

Data Analysis Center For Geomagnetism And Space Magnetism (WDC), Kyoto University. 2017. Available: http://wdc.kugi.kyoto-u.ac.jp/dstae/index.html [Accessed 15th March 2017].

Dow, J. M., Neilan, R. E. & Rizos, C. 2009. The International GNSS Service in a changing landscape of Global Navigation Satellite Systems. *Journal of Geodesy*.

Fagundes, P. R., Cardoso, F. A., Fejer, B. G., Venkatesh, K., Ribeiro, B. A. G. & Pillat, V. G. 2016. Positive and negative GPS-TEC ionospheric storm effects during the extreme space weather event of March 2015 over the Brazilian sector. *Journal of Geophysical Research: Space Physics,* 121, 5613–5625.

Filjar, R. 2008. A study of Direct Severe Space Weather Effects On GPS Ionospheric Delay. *The Journal of Navigation,* 61, 115–128.

Filjar, R., Brčić, D. & Kos, S. 2013. Single-frequency Horizontal GPS Positioning Error response to a moderate Ionospheric storm over Northern Adriatic. *In:* WEINTRIT, A. (ed.) *Advances in Marine Navigation.* London: Taylor & Francis Group.

Filjar, R., Kos, S. & Brčić, D. Local model of quiet space weather GPS ionospheric delay for the area of Northern Adriatic. Proceedings of the 5th Global Navigation Satellite Systems Vulnerabilities and Solutions Conference, 23.–25.5.2011. 2011 Baška, Croatia. London: The Royal Institute of Navigation.

Grebowsky, J. M. & Aikin, A. C. Planetary ionospheres – sources and dynamic drivers. Proceedings IAU Symposium No. 257, 2009 Cambridge. Cambridge University Press, 499–509.

Hunsucker, R. D. & Hargreaves, J. K. 2003. *The high-latitude ionosphere and its effects on radio propagation,* Cambridge, Cambridge University Press.

Jacobsen, K. S. & Andalsvik, Y. L. 2016. Overview of the 2015 St. Patrick's day storm and its consequences for RTK and PPP positioning in Norway. *Journal of Space Weather and Space Climate,* 6, A9.

Klobuchar, J. A. 1987. Ionospheric Time-Delay Algorithm for Single-Frequency GPS Users. *IEEE Transactions on Aerospace and Electronic Systems*, 325–331.

Kos, S., Barić, M. & Brčić, D. Discrepancies between predicted and final IGS ionospheric maps in the Northern Adriatic region. Proceedings of the 9th Annual Baška GNSS Conference, 10-12. 5. 2015. 2015 Baška, Croatia. The Royal Institute of Navigation, London & University of Rijeka, Faculty of Maritime Studies.

Mendillo, M. 2006. Storms in the ionosphere: Patterns and processes for total electron content. *Reviews of Geophysics,* 44, RG4001.

National Aeronautics and Space Administration (NASA), Goddard Space Flight Center. 2017. Available: https://omniweb.gsfc.nasa.gov/ [Accessed 15th March 2017].

Parkinson, B., Spilker, J. J., Axelrad, P. & Enge, P. 1996. *Global Positioning System: Theory and Applications,* Washington DC, American Institute of Aeronautics and Astronautics, In.

RTKLIB. 2017. *RTKLIB: An Open Source Program Package for GNSS Positioning* [Online]. Available: http://www.rtklib.com/rtklib_reference.htm [Accessed March 17th 2017.

Schunk, R. & Nagy, A. 2009. *Ionospheres: Physics, Plasma Physics and Chemistry,* Cambridge, Cambridge University Press.

Schunk, R. W. & Sojka, J. J. 1996. Ionosphere-thermosphere space weather issues. *Journal of Atmospheric and Terrestrial Physics,* 58, 1527–1574.

United States Geological Survey (USGS),2015. *National Geomagnetism Program: Geomagnetic storm 17 March 2015* [Online]. Available: https://geomag.usgs.gov/storm/storm22.php [Accessed 21 March 2017.

Zolesi, B. & Cander, L. R. 2014. *Ionospheric Prediction and Forecasting,* New York, Springer.

Sveučilište u Rijeci
POMORSKI FAKULTET U RIJECI
FACULTY OF MARITIME STUDIES RIJEKA
University of Rijeka

University of Zagreb
Faculty of Transport
and Traffic Sciences

Royal Institute of Navigation
Science Technology Practice

11th
Annual
Baška GNSS
Conference

DETECTION OF TEC ANOMALIES PRECEDING EARTHQUAKE OVER L'AQUILA REGION USING GROUND-BASED GNSS MEASUREMENTS

Barbara Pongračić, Falin Wu, Muhammad Abdul Alim Sikder

Beihang University, Beijing, China
E-mail: barbara.pong@gmail.com (Corresponding author)

ABSTRACT

*In recent years, numerous researches have been conducted to analyse the influence of earthquakes on the Earth's ionosphere. Earthquakes can cause anomalous variations in Total Electron Content (TEC) over the earthquake influential area. These ionospheric variations can be observed from few minutes to several days before the earthquake occurrence. Anomalous behaviour includes increase or decrease of TEC, or sometimes a notable change in daily distribution. This research aims to investigate TEC dynamics anomalies over the L'Aquila region in Italy, as an early indicator of earthquakes. We investigated TEC variations over this region during August 2016. An earthquake with M=6.2 occurred on August 24th, killing 299 people. Previous research in this area indicated an increase in TEC in a week preceding the earthquake which occurred in 2009. The region is seismically active, and more effort should be put into detecting earthquake precursors. Observations from eleven ground GNSS stations from Italian network RING (*Rete Integrata Nazionale GPS*) for 31 consecutive days (August of 2016) have been used. These stations are located in the vicinity of the earthquake epicentre. One additional station has been chosen as a reference station outside the earthquake influence area to detect possible TEC anomalies by cross-correlation with the stations near the earthquake epicentre. Daily TEC median values were calculated to observe daily variations of TEC. Indices of geomagnetic activity were used to specify space weather conditions. Time*

series of TEC of stations near the epicentre revealed significant increase on the 23rd August. Possible pre-earthquake induced increase in the TEC has been rejected as geomagnetic Dst *and* Kp *indices showed a disturbance in space weather conditions. Cross-correlation index between diurnal values of each individual station with the daily median values were low for three days preceding the earthquake. Cross-correlation with the values from the reference station revealed that two out of three days were successfully detected when using median values.*

Key words: *TEC, earthquake prediction, GNSS, ionosphere*

1 INTRODUCTION

For years, earthquake prediction has been the main subject of many researches. Recently, models of the Earth's crustal movement have been adjoined with the research on the changes in the atmosphere caused by earthquakes. Previous research has shown that there are atmospheric precursors occurring over the epicentre area. Changes in the atmosphere are possibly caused by crustal movement and release of gasses. Research on the ionospheric precursors is an interesting field of study among various researchers including variations in the height of ionospheric layers by measurement of critical frequencies, plasma densities, total electron content (TEC), electric current and ionospheric E-layer perturbations (Oikonomou *et al*, 2017a, Kelley *et al*, 2017, Chowdhury *et al*, 2017, Jin *et al*, 2015). TEC is the integrated electron density along the signal ray from the satellite to the receiver. It is measured in TEC units. GNSS has proven to be a powerful asset in ionospheric research by estimation of the TEC. There are numerous GNSS ground-based networks which provide free access to data. Space-based GNSS receivers have also been used as an additional data source using radio occultation (Hsiao *et al*, 2010, Karia *et al*, 2014).

The methodology includes monitoring long TEC time-series and investigation of the possible deviations from referenced daily distribution (mean or median). Another methodology suggests using cross-correlation technique for identification of anomalies. This technique is also used in forecasting of the earthquakes and requires a relatively high number of ground-based stations. Also, the technique proposed by Pulinets *et al*. (2004) requires additional station outside the earthquake preparation zone. Similar has been applied in research performed by Rhoades *et al*. (2015) in Australia. Instead of using the additional station, they used grid-points for creating TEC anomaly maps. This kind of

research is very well developed in Japan where they established dense ground-based GNSS network to investigate effects of earthquakes. In their studies, cross-correlation is performed based only on the satellites with high elevation angle regarding the epicentre with the aim of forecasting of the earthquakes' occurrence (Iwata and Umeno, 2017, Shalimov *et al*, 2017). Spectral analysis has also been proven useful (Oikonomou *et al*, 2017b).

Central Italy has been subject to many earthquakes. This area is tectonically active because of the movement of the Eurasian, African and Adria plates. In the recent years, the most devastating earthquakes occurred in L'Aquila region with magnitude M = 6.3 on the 6th April 2009, and M = 6.2 on the 24th August 2016. Studies of the ionospheric precursors over central Italy involved measuring TEC of stations surrounding the epicentre and using satellites with the greatest elevation angles to compute RMS error of the linear regression over the mean values of the particular satellite (De Agostino and Piras, 2011). Long-time TEC observations were statistically analysed by Mancini *et al*. (2015) in the period from the year 2005 to 2009 by creating regional TEC maps. TEC time-series analysis has been investigated for the 2009 earthquake (Masci *et al*, 2017).

Problems which arise from this type of research are mainly due to circumstantial nature of earthquakes. Insufficient data and ionospheric conditions which are regionally or locally driven, require the development of local models. Developed cross-correlation techniques assume either dense ground-based networks, reference stations outside earthquake preparation zone or both, which significantly narrows their application.

The last devastating earthquake was associated with huge infrastructure damages and tragic loss of lives induced by the strong ground motion at the epicentre. The epicentre was located near the village Accumoli (42.7°N, 13.2°E) and the hypocentre at a depth of approximately 4 km (European Commission, 2016, Piccardi *et al*, 2016). Shallow hypocentre increased the damage produced by the earthquake (European Commission, 2016). These earthquake phenomena have been investigated regarding the crustal movements and other physical properties (Piscini *et al*, 2017). In this paper, we analysed ionospheric precursors of the earthquake using ground-based GNSS TEC measurements by analysing time-series and cross-correlation coefficients. Main addressed constraints were the number of GNSS ground-based stations and availability of the reference station. We propose a cross-correlation technique which utilises only nearby stations to overcome the problem which can one face in need of the reference station.

2 DATA AND METHODOLOGY FOR DETECTION OF IONOSPHERIC ANOMALOUS BEHAVIOUR

This session deals with the methodology used for extracting TEC and investigation of ionospheric precursors. First, we estimated TEC from ground-based GNSS observations by code and phase observations creating geometry-free combinations. Further on, TEC has been detrended to analyse time-series. Finally, local cross-correlation index has been calculated for every day of the assessed period. The more detailed explanation is given below.

2.1 Ionospheric delay estimation from GNSS observations. A network of ground-based GNSS stations has significantly contributed to the investigation of ionospheric phenomena. The satellite signal is affected by the state of ionosphere causing ionospheric delay. By simultaneous receipt of signals on two or more frequencies, it is possible to estimate TEC values (Schaer, 1999). Code and phase observations are expressed as:

$$\phi_1^j = \rho^j - I^j + \lambda_1 N_1^j + \varepsilon_{L_1^j} \tag{1}$$

$$\phi_2^j = \rho^j - \mu I^j + \lambda_2 N_2^j + \varepsilon_{L_2^j} \tag{2}$$

$$P_1^j = \rho^j - I^j + (B_1 - B_1^j) + \varepsilon_{P_1^j} \tag{3}$$

$$P_2^j = \rho^j - \mu I^j + (B_2 - B_2^j) + \varepsilon_{P_2^j} \tag{4}$$

where:

ϕ_i^j – carrier-phase measurements of the satellite j on L_i band, where i = 1, 2,

P_i^j – code measurement of the satellite j on L_i band,

ρ^j – biased ionosphere-free pseudorange including receiver and satellite clock bias, and tropospheric delay,

I^j – ionospheric delay on L_1,

$\mu = (f_1/f_2)^2$ – scaling factor,

N_1^j – carrier-phase ambiguities,

B_i, B_i^j – receiver instrumental biases of code measurements, and

ε – unmodeled bias.

Geometry-free combinations are formed to eliminate measurements of the non-dispersive medium:

$$\phi_{GF}^{j} = \phi_1^j - \phi_2^j = (\mu - 1)I^j + \lambda_1 N_1^j - \lambda_2 N_2^j \quad (5)$$

$$P_{GF}^{j} = P_1^j - P_2^j = (\mu - 1)I^j + DCB \quad (6)$$

where:

ϕ_{GF}^{j}, P_{GF}^{j} – carrier-phase and code geometry free (GF) combinations, respectively, and

DCB – differential code bias.

Finally, the absolute value of ionospheric delay is obtained by removing instrumental biases by weighted levelling procedure:

$$\overline{\phi_{GF}^{j}} = \phi_{GF}^{j} - \frac{\sum w(\phi_{GF}^{j} - P_{GF}^{j})}{\sum w} \quad (7)$$

where:

$\overline{\phi_{GF}^{j}}$ – levelled observation, and

w – weight coefficient.

Levelled observations contain ionospheric correction which can be simply expressed in TECU. These observations are made on the line of sight from receiver to the satellite giving slant TEC values. For vertical values, the mapping function is required:

$$\cos z' = \frac{VTEC}{STEC} \quad (8)$$

where:

z' – satellite zenith distance at ionospheric pierce point [°],

VTEC – vertical TEC, and

STEC – slant TEC.

We used data from 12 ground-based stations which are part of RING (INGV RING) and EUREF network (Bruyninx *et al,* 2012) in RINEX format. The IDs and positions of the 12 ground-based stations are shown in Table 1.

Table 1. Ground-based stations

ID	Latitude [°]	Longitude [°]	Altitude [m]	Network
AQUI	42.36	13.50	713.00	RING
BARS	42.34	13.58	1158.06	RING
CAOC	42.29	13.48	970.28	RING
CONI	42.41	13.39	1239.10	RING
GNAL	42.58	13.52	1048.61	RING
LNSS	42.60	13.04	1150.88	RING
MTER	42.51	13.21	1142.83	RING
ROPI	42.33	13.34	991.87	RING
SGRE	42.34	13.50	808.42	RING
CESI	43.00	12.90	914.36	RING
GUMA	43.06	13.34	651.76	RING
NPAZ	43.13	20.51	549.50	EUREF

Stations from RING network are located near the epicentre to describe ionospheric conditions over the area affected by the earthquake. Station NPAZ is located further from the epicentre, outside the earthquake preparation zone. According to Dobrovolsky *et al.* (1977), earthquake preparation zone is:

$$R = 10^{0.43M} \approx 457 \text{ km} \tag{9}$$

where:

R – earthquake preparation zone [km], and

M – magnitude.

NPAZ station has been chosen because it is on the similar geomagnetic latitude as the epicentre and other RING network stations. Stations on the similar geomagnetic latitudes show alike ionospheric conditions, i.e. TEC values (Schaer, 1999). The distance between the earthquake epicentre and NPAZ station is 597.2 km, which is more than the estimated earthquake preparation zone. It has been the only station satisfying criteria of similar geomagnetic latitude, earthquake preparation zone and data availability. Choosing the station outside the earthquake preparation zone allows detection of local ionospheric anomalies (Pulinets *et al*, 2004). This station will be used for validation of the proposed cross-correlation technique. The position of the stations is shown in Figure 1.

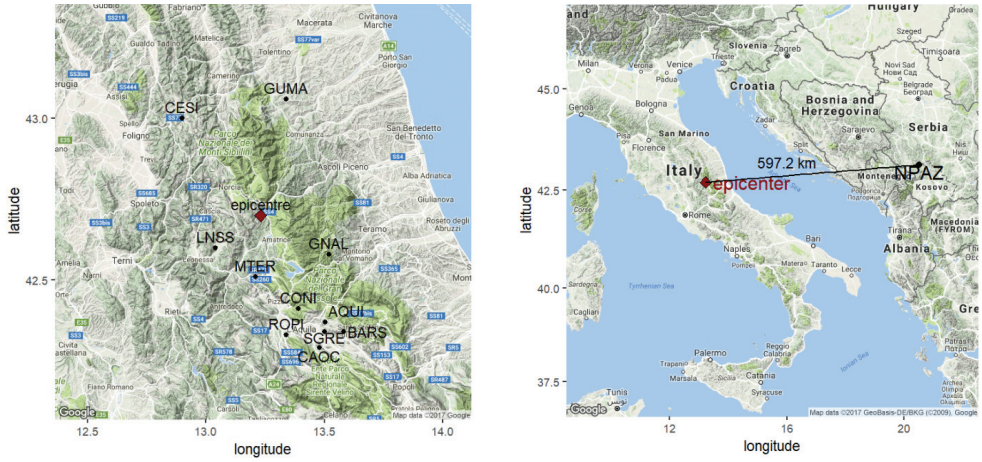

Figure 1. Position of ground-based GNSS stations

2.2 TEC time-series decomposition. TEC has been estimated for all stations near the epicentre from August 1st to August 31st. Data has been detrended by STL (Seasonal-Trend Decomposition Process Based on Loess) to reveal local fluctuations in TEC time-series.

Figure 2 shows TEC with its estimated trend and detrended values. Detrending of time-series is especially useful when analysing longer data periods since it removes the influence of the solar cycle oscillations.

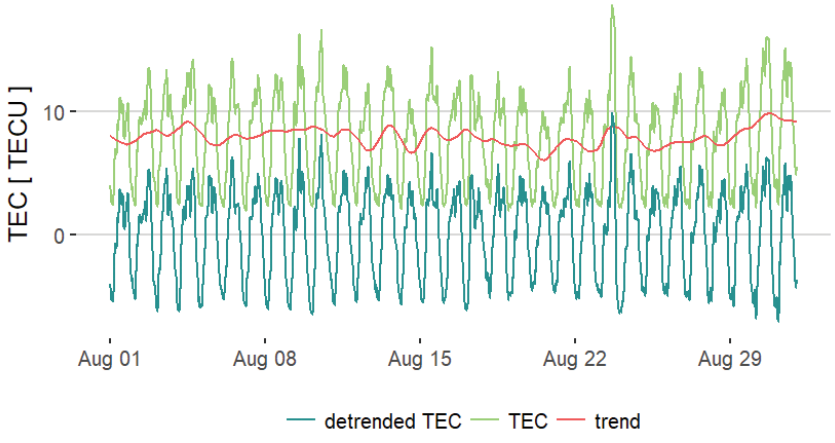

Figure 2. Time-series TEC trend decomposition

After data detrending, we analysed time-series to find days with obvious deviations from the mean TEC values. Cross-correlation has been performed afterwards.

2.3 Determination of Local Cross-Correlation Index (LCI). Calculation of cross-correlation coefficient has been introduced by Pulinets *et al*. (2004). Since that, the methodology has been modified based on the local conditions. Suggested methodology calculates cross-correlation between stations near the epicentre and the reference station outside the earthquake preparation zone. The reference station should satisfy certain criteria. Unavailability of the proper reference station makes application of the suggested methodology impossible. That's why we only used stations in the epicentre vicinity, and the reference station to verify our findings.

First, cross-correlation is calculated between daily values of each station and the corresponding mean value.

Let $\{x(i, j, k), i = 1, ..., I, j = 1, ..., J, k = 1, ..., K\}$ be TEC observations of K stations over I days, and J to be number of observations in a day. Summation of daily correlation indices over the number of stations forms local correlation index (LCI) as:

$$LCI(i) = \frac{\sum_{k=1}^{K} cor(x(i,j,k), \bar{x}(i,j))}{K} \tag{10}$$

where:

$LCI(i)$ – local correlation index,

$\bar{x}$ – daily median value of K stations for i-th day and j-th observation, and

$cor(x(i, j, k), \bar{x}(i, j)$ – Pearson's correlation.

This local correlation index follows methodology proposed by Pulinets *et al*. (2004) and Rhoades *et al*. (2015) but only utilises TEC values of stations near the earthquake epicentre.

Anomalous days should be classified as outliers. Here, we used Tukey's method which considers data points as outliers if outside of 1.5 interquartile ranges from the first or third quartile. The range is:

$$[Q_1 - k \cdot IQR, Q_3 + k \cdot IQR] \tag{11}$$

where:

Q_1 – first quartile,

Q_3 – third quartile,

k – coefficient, $k = 1.5$, and

IQR – Interquartile Range is:

$$IQR = Q_3 - Q_1 \tag{12}$$

This outlier method is more robust and more suitable for datasets with a small number of observations than the one considering mean values and standard deviations.

2.4 Space weather conditions. State of ionosphere and TEC depends on the solar activity and the state of the space-weather. To put observed TEC values, and possible anomalous behaviour, regarding space weather conditions, we used *Dst* and *Kp* geomagnetic indices.

Dst values were downloaded from the Kyoto observatory database (WDSC Kyoto). *Dst* index is used to describe decreasing of the geomagnetic field (Nose *et al*. 2015). Negative values of -20 nT and more denote geomagnetic storm (Cander and Mihajlovic, 1998). *Kp* index is accessible from NASA database (Goddard Space Flight Center). This index is used to assess the global geomagnetic activity and measured on 13 stations around the world on mid-latitudes. Maximum *Kp* value is 9, with $Kp \geq 4$ meaning disturbed geomagnetic conditions.

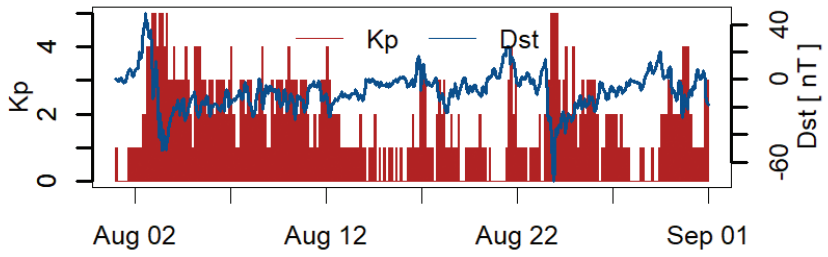

Figure 3. *Kp* and *Dst* indices

Figure 3 shows *Kp* and *Dst* indices for the assessed period.

Dst values were low during August 3rd, and again on August 23rd. Maximum *Kp* values were 5 during August 3rd and August 23rd, which corresponds with low values of *Dst* index. The whole period can be characterised as calm with two weak geomagnetic disturbances occurred on the August 3rd and August 23rd.

3 RESULTS

First, we calculated daily mean values of each station which were compared to the overall median value. TEC values are presented in Figure 4. The day of the earthquake has been marked with the red triangle. Values have been relatively low during all days without exceeding more than 18.69 TECU on August 23rd. Increase in TEC from monthly median values is the most noticeable during August 9th, August 10th and August 23rd. The lowest values preceding the earthquake have been noticed during August 21st.

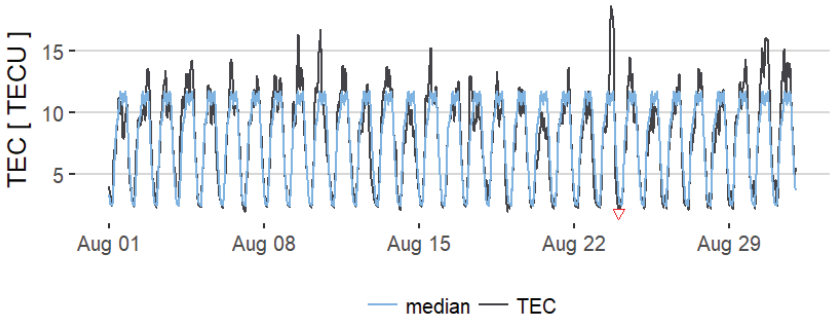

Figure 4. Daily mean and median TEC values

Some research showed that anomalous behaviour appears from one to five days (Pulinets, 2006), or even up to ten days before the earthquake (Papadopoulos *et al*, 2010). The obvious increase in TEC during August 23rd could imply it is induced by the earthquake.

Time-series of TEC values were used to detect anomalous changes in the ionosphere, but they are not sufficient for detection of ionospheric anomalies caused by earthquakes. We have further focused on the recognition of anomalous diurnal TEC pattern by calculating LCI for every day of the assessed period to isolate days with relatively different TEC distribution.

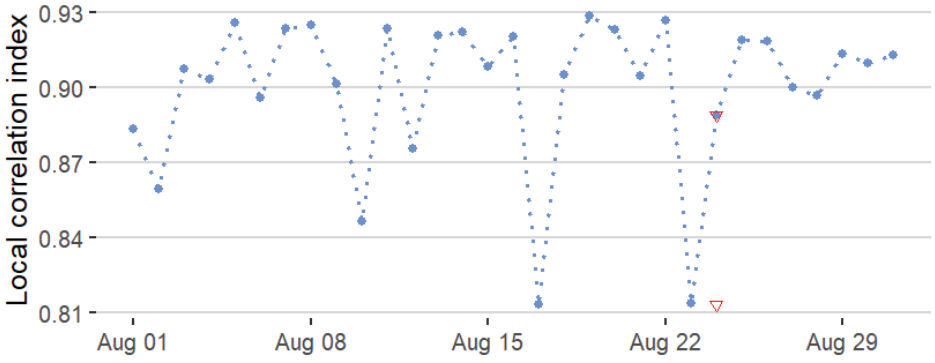

Figure 5. Local correlation index

Low LCI means that there have been disturbances in TEC values. Figure 5 shows lower coefficients during several days preceding the earthquake (August 10th, August 17th and August 23rd) with values of 0.841, 0.809, and 0.814, respectively. Again, the red triangle in Figure 5 shows the day of the earthquake.

During August 23rd, low correlation values were expected regarding the geomagnetic storm detected by *Dst* index. However, on August 17th, LCI was the lowest, even though there were no geomagnetic disturbances. During August 10th, space-weather conditions were calm although TEC values during this day significantly exceeded monthly median values.

From the time-series analysis and the LCI, several days (August 10th and August 23rd) have shown anomalous behaviour. Also, these days fit the time-window of the earthquake ionospheric precursors. To verify our findings, we compared our results to the cross-correlation performed with the reference station. With NPAZ station located outside the earthquake preparation zone, it is easy to detect anomalies. As it has been previously stated, this station is close enough to experience alike ionospheric conditions over the earthquake epicentre, and far away not to be influenced by the earthquake.

Figure 6 shows LCI computed regarding NPAZ station. The low value of 0.649 has been noticed on August 17th. Local correlation index of August 23rd is higher when compared to results obtained from the first LCI calculation, which confirms cancelling out this day as the potential ionospheric precursor of the earthquake. The most prominent peak is noticed on the August 17th, with the LCI of only 0.649.

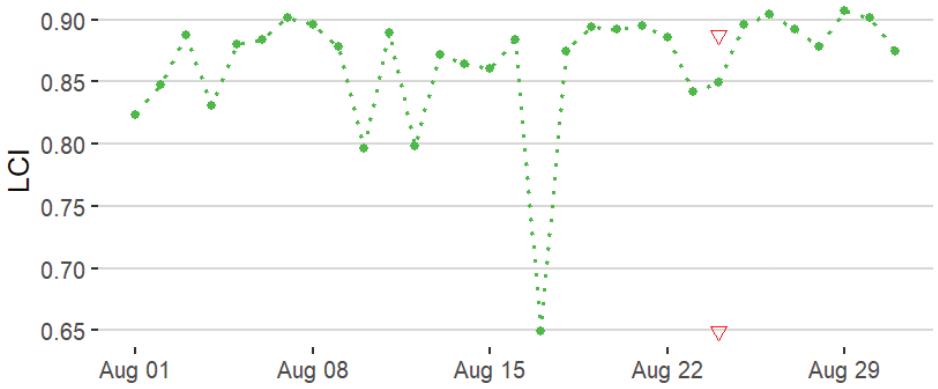

Figure 6. Local correlation index regarding NPAZ station

Calculated outliers are shown in Figure 7. Anomalies detected during these days could be the result of the earthquake.

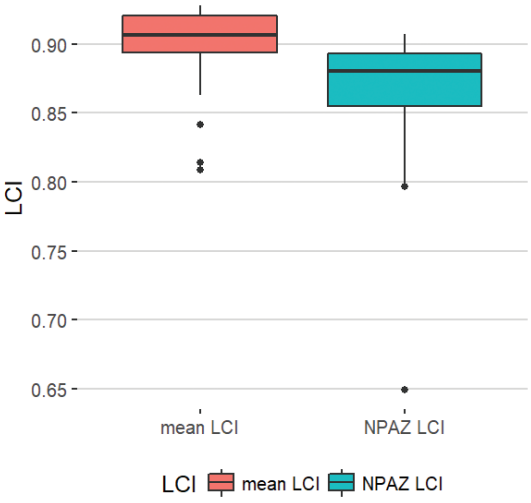

NPAZ LCI	
Date	LCI
Aug-10	0.796
Aug-17	0.649

Mean LCI	
Date	LCI
Aug-10	0.841
Aug-17	0.809
Aug-23	0.814

Figure 7. Boxplot of LCI with outliers' values

Boxplot reveals that LCI computed against the reference station had lower values. Also, outliers' analysis shows that there were only two anomalous days, not three as it was calculated from the LCI of the stations near the epicentre.

4 DISCUSSION OF RESULTS

We analysed TEC values estimated from the ground-based GNSS network as time-series, and with the cross-correlation. Time-series revealed some perturbations in TEC values. These changes can't be unambiguously related to the earthquake, as it has been shown on the August 23rd. From the sole time-series analysis, this day could be easily mistaken as the earthquake precursor. That's why TEC time-series should be analysed in the context of the space-weather conditions. When we observed space-weather conditions, we excluded that day as the potentially anomalous day. Since there were other days which could be assumed as anomalous, we performed a cross-correlation. Cross-correlation has been performed for all stations with the corresponding daily mean value. This way, we isolated three days which had the lowest LCI values, namely: August 10th, August 17th, and August 23rd. Since August 23rd has already been excluded, only the first two days were considered anomalous. This has been verified on the LCI with the reference station outside the earthquake preparation zone. Here, the lowest values were noticed during August 17th. During August 23rd, the daily median value was significantly different when compared to other days, but when compared to the NPAZ station it showed high LCI. This means that the disturbance in the TEC likely had a global origin which has been confirmed by analysis of the space-weather conditions.

When only using stations near the epicentre, LCI values are strongly affected by mean values showing higher values than compared to LCI calculated against the reference station. This could result in impossibility of detection of anomalous days.

5 CONCLUSION

This paper presented some of the ionospheric earthquake precursors over the affected area on the 24th August of 2016 in central Italy. It is shown that LCI, without using the reference station outside the earthquake area, can be used for the ionospheric earthquake precursor analysis, but one should be aware of its computational limits.

Since only one earthquake has been investigated, it can't be concluded that these variations are indeed caused by the earthquake itself. Future research should

involve investigation of other earthquakes in the area and consider utilisation of all available sources to densify spatial distribution of observations for detecting anomalies with the higher certainty.

Also, common properties of the earthquake precursors in this area should be investigated by including other severe earthquakes, more ground-based stations and longer analysis of the TEC time-series.

References

Bruyninx C. *et al.* (2012). *Enhancement of the EUREF Permanent Network Services and Products,* "Geodesy for Planet Earth", IAG Symposia Series, Vol. 136, pp. 27–35, doi: 10.1007/978-3-642-20338-1_4.

Cander, L. R. & Mihajlovic, S. J. (1998). Forecasting ionospheric structure during the great geomagnetic storms. *Journal of Geophysical Research: Space Physics (1978–2012),* 103, 391–398.

Chowdhury, S., Deb, A., Nurujjaman, M. & Barman, C. (2017). Identification of pre-seismic anomalies of soil radon-222 signal using Hilbert-Huang transform. *Natural Hazards,* 87, 1587–1606.

De Agostino, M. & Piras, M. (2011). Earthquake forecasting: a possible solution considering the GPS ionospheric delay. *Natural Hazards and Earth System Science,* 11, 3263–3273.

Dobrovolsky, I. P., Zubkov, S. I. & Miachkin, V. I. (1977). Estimation of the size of earthquake preparation zones. *Pure and applied geophysics,* 117, 1025–1044.

European Commission (2016). *Mw. 6.0 Earthquake in Italy (Situation Report)* [Online]. Available: http://portal.gdacs.org/GDACSDocuments/Situation%20Assessment%20Report-EQ%20Italy.pdf.

Goddard Space Flight Center, Space Physics Data Facility. Available: https://omniweb.gsfc.nasa.gov/.

Hsiao, C. C., Liu, J. Y., Oyama, K. I., Yen, N. L., Liou, Y. A., Chen, S. S. & Miau, J. J. (2010). Seismo-ionospheric precursor of the 2008 Mw7.9 Wenchuan earthquake observed by FORMOSAT-3/COSMIC. *Gps Solutions,* 14, 83–89.

INGV RING Working Group (2016), Rete Integrata Nazionale GPS, DOI: 10.13127/Ring, Available: http://ring.gm.ingv.it/.

Iwata, T. & Umeno, K. (2017). Preseismic ionospheric anomalies detected before the 2016 Kumamoto earthquake. *Journal of Geophysical Research-Space Physics,* 122, 3602–3616.

Jin, S. G., Occhipinti, G. & Jin, R. (2015). GNSS ionospheric seismology: Recent observation evidences and characteristics. *Earth-Science Reviews,* 147, 54–64.

Karia, S. P., Pathak, K. N., Yadav, K. S., Patel, N. C. (2014). Reception of over Horizon GPS propagation and Earthquake Precursors. *2014 Xxxith Ursi General Assembly and Scientific Symposium (Ursi Gass)*, 4.

Kelley, M. C., Swartz, W. E. & Heki, K. (2017). Apparent ionospheric total electron content variations prior to major earthquakes due to electric fields created by tectonic stresses. *Journal of Geophysical Research-Space Physics,* 122, 6689–6695.

Mancini, F., Galeandro, A., De Giglio, M. & Barbarella, M. (2015). Ionospheric activity and possible connection with seismicity: Contribution from the analysis of long time series of GNSS signals. *Physics and Chemistry of the Earth,* 85–86, 106–113.

Masci, F., Thomas, J. N. & Secan, J. A. (2017). On a reported effect in ionospheric TEC around the time of the 6 April 2009 L'Aquila earthquake. *Natural Hazards and Earth System Sciences,* 17, 1461–1468.

Nose, M., Iyemori, T., Sugiura, M. & T., K. (2015). Geomagnetic Dst index. *IAGA Bull.,* 40.

Oikonomou, C., Haralambous, H., Moldovan, I. A. & Greculeasa, R. (2017a). Investigation Of Pre-Earthquake Ionospheric Anomalies Using VLF/LF INFREP European And GNSS Global Networks. *Romanian Journal of Physics,* 62, 13.

Oikonomou, C., Haralambous, H. & Muslim, B. (2017b). Investigation of ionospheric precursors related to deep and intermediate earthquakes based on spectral and statistical analysis. *Advances in Space Research,* 59, 587–602.

Papadopoulos, G. A., Charalampakis, M., Fokaefs, A. & Minadakis, G. (2010). Strong foreshock signal preceding the L'Aquila (Italy) earthquake of 6 April 2009. *Nat. Hazards Earth Syst. Sci.,* 10, 19–24.

Piccardi, L., *et al*. (2016). *The August 24,2016,Amatrice earthquake (Mw 6.0): field evidence of on-fault effects – Preliminary report* [Online]. Available: http://www.isprambiente.gov.it/files/notizie-ispra/notizie-2016/sisma-italia-centrale/REPORT_Amatrice_en_2016_09_16.compressed.pdf.

Piscini, A., De Santis, A., Marchetti, D. & Cianchini, G. (2017). A Multi-parametric Climatological Approach to Study the 2016 Amatrice-Norcia (Central Italy) Earthquake Preparatory Phase. *Pure and Applied Geophysics,* 174, 3673–3688.

Pulinets, S. A. (2006). Space technologies for short-term earthquake warning. *Advances in Space Research,* 37, 643–652.

Pulinets, S. A., Gaivoronska, T. B., Leyva Contreras, A. & Ciraolo, L. (2004). Correlation analysis technique revealing ionospheric precursors of earthquakes. *Natural Hazards and Earth System Science,* 4, 697–702.

Rhoades, D. A., Mueller, C., Buxton, R. & Gerstenberger, M. C. (2015). Ionospheric Earthquake Precursors.

Schaer, S. (1999). Mapping and Predicting the Earth's Ionosphere Using the Global Positioning System. *Geodatisch-geophysikalische Arbeiten in der Schweiz.*

Shalimov, S. L., Nesterov, I. A. & Vorontsov, A. M. (2017). On the GPS-Based Ionospheric Perturbation after the Tohoku Earthquake of March 11, 2011. *Izvestiya-Physics of the Solid Earth,* 53, 262–273.

World Data Center for Geomagnetism, Kyoto, Data Analysis Center for Geomagnetism and Space Magnetism. Available: http://wdc.kugi.kyoto-u.ac.jp/dstdir/.

Sveučilište u Rijeci
POMORSKI FAKULTET U RIJECI
FACULTY OF MARITIME STUDIES RIJEKA
University of Rijeka

University of Zagreb
Faculty of Transport
and Traffic Sciences

Royal Institute of Navigation
Science Technology Practice

11th
Annual
Baška GNSS
Conference

SECURITY-ENHANCED SEARCH AND RESCUE SYSTEM BY USING LTE AND COSPAS SARSAT

Sanguk Lee[1], **I. C. Jeong**[1], **Jaehyun Kim**[1], **Woo-Geun Ahn**[2]

[1] Electronics Telecommunication Research Institute, Daejeon, Korea
E-mail: slee@etri.re.kr (Corresponding author)

[2] Agency for Defense Development, Daejeon, Korea

ABSTRACT

A security-enhanced search and rescue system is required for military or privacy required operations. In this paper, we propose utilization LTE as search and rescue communication link for helping out the limitation of the capacity of COSPAS SARSAT link in the sense of a number of users at the same time. Also, enhancement of security of the search and rescue system by COSPAS SARSAT and LTE made by using encryption mechanism. We employed encryption algorithm as AES/CFB (Cipher FeedBack) 256bit for COSPAS SARSAT with mode and IV (Initialization Vector) key management by return link message. AES 256 bits for LTE was used for an encryption algorithm with IPSec protocol. Some simulation results from Modeling & Simulation Platform for COSPAS SARSAT with LTE Modem were presented in this paper.

Key words: *Search and Rescue, COSPAS SARSAT, LTE*

1 INTRODUCTION

In war or peace, if a soldier, aircraft, and warship are in distress, exposure of the information about distress situation to an enemy or others who may use it maliciously may cause serious results. Also, if the search and rescue system is disturbed purposely, it may not rescue distressed people timely, or waste human resources. Encryption/decryption techniques are required to mitigate the situation for transmission of the distress signal and reception of return link message.

Cosmitscheskaja Sistema Poiska Awarinitsch Sudow (Russian: space system for the search of vessels in distress) Search and Rescue Satellite-Aided Tracking (COSPAS SARSAT) system allows utilization of national use field for each member states as described in COSPAS SARSAT (2017). But it can process a limited number of distress signal simultaneously due to a number of channel allocation and frequency bands. The burden due to the restriction may be mitigated by additional encrypted satellite link and/or terrestrial link.

We considered the interoperability of satellite links such as Orbital Communications (Orbcomm), International Maritime Satellite (Inmarsat), Thuraya, and interoperability of terrestrial links such as Long Term Evolution (LTE), Wireless Broadband (WiBro), and Trunked Radio System (TRS) with COSPAS SARSAT. It was for the reduction of the burden on the COSPAS SARSAT system, costs and complexity of the system. As a result of various analyses, combining of the COSPAS SARSAT system using encrypted national use field and the encrypted LTE were selected and studied as the military search and rescue system in this paper.

2 COSPAS SARSAT PROTOCOL DESIGN

COSPAS SARSAT is the search and rescue program and system founded by Canada, United States of America (USA), France and old Union of Soviet Socialist Republics (USSR) in 1979. Currently, it is used as worldwide search and rescue system for terrestrial, maritime and aviation areas such as Personal Locator Beacon (PLB), Emergency Position-Indicating Radio Beacon (EPIRB), and Emergency Locator Transmitters (ELT) and it has rescued tens of thousands of people from distress. Three major Global Navigation Satellite System (GNSS) like Global Positioning System (GPS), GLObal Navigation Satellite System (GLONASS), and Galileo will equip search and rescue payload for their system for the international community.

Especially, Galileo provides search and rescue service including return link service which is very helpful for mitigation of critical false alerts and for efficient utilization. Global navigation Satellite system Agency (GSA) announced Galileo/SAR is operational on the 6th day of April in 2017 and the date meant COSPAS SARSAT frequency band, 406 MHz. Galileo. SAR will make the breakthrough for worldwide search and rescue without limitation like coverage, independent localization of distress people, false alerts and so on. We are considering utilization of COSPAS SARSAT for military search and rescue system by using national user field as other countries do.

In this paper, we introduced an improved method to protect the search and rescue signal of COSPAS-SARSAT system and a protocol that can maintain a stable security system between the people in distress and the rescue organization using the Galileo search system return link. The message of COSPAS SARSAT has 112 bits short and 144 bits long message formats. Long message format was used for better precision position information for the people in distress and increased security capability. Encryption was applied to data for national use area bits including encryption key information as shown in Figures 1&2 as follows, national use areas ,40~85 bits and 107 ~ 132, are merged as one message; merged message is encrypted with the algorithm; and then split into two pieces as the original sizes; placed original location as shown in Figure 1.

	Bit Synchronization	Frame Synchronization	PDF–1					BCH–1	PDF–2	BCH–1
Unmodulated Carrier (160 ms)	Bit Synchronization Pattern	Frame Synchronization Pattern	Format Flag	Protocol Flag	Country Code	Protocol Code	National Use	21–Bit BCH Code	National Use	21–Bit BCH Code
Bit No.	1–15	16–24	25	26	27–36	37–39	40–85	86–106	107–132	133–144
Value	···	...	F	1	...	1 0 0	...			

Bit#	1 24	25 26	27 36	37 39	40	41 58	59 85						86 106	107 120						121 132	133 144
Field Desc.	[24] Bit & Frame Sync Patterns	[2] Fmt Prot.	[10] Country Code	[3] Prot. Code	[1] Data. Fmt	[18] Beacon Id	[27] Position Data						[21] BCH-1	[14] △ Position						[12] CTR	[12] BCH-2
							[13] Latitude			[14] Longitude				[7] △Latitude			[7] △Longitude				
Loc.		11		100	0		[1] N S	[7] Deg 0-90 (1deg)	[5] Min 0-58 (2m)	[1] E W	[8] Deg 0-180 (1deg)	[5] Min 0-58 (2m)		[1] Sign – +	[2] Min 0-3 (1m)	[4] Sec 0-56 (4s)	[1] Sign – +	[2] Min 0-3 (1m)	[4] Sec 0-56 (4s)		
							Encrypted							Encrypted							

Figure 1. National User Protocol message format and data fields

The Design based on (COSPAS SARSAT, 2012 A & B, 2013, and 2016) in this paper had been done with considerations such as protection of user location information, minimization of the impact when a user beacon is lost or stolen, and mitigation of security risks for long-term use of the device. Also, the backward compatibility of the existing COSPAS SARSAT and LTE as constraints has been taken into account.

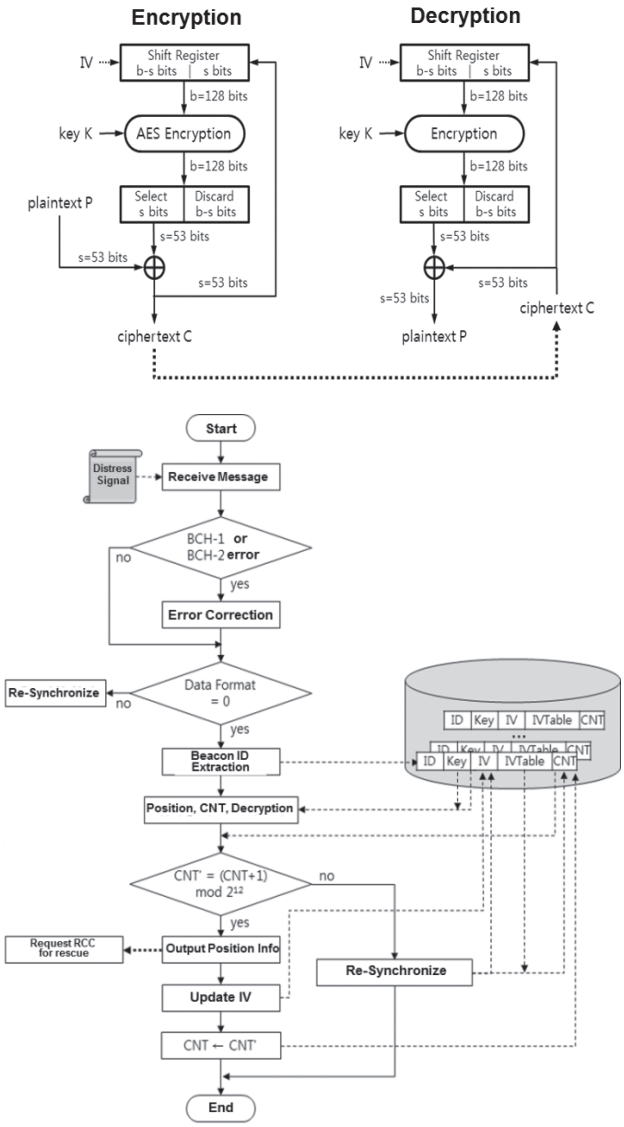

Figure 2. Encryption/Decryption by 128 bits AES/CFB & Key management

Encryption key management and beacon remote control from (FIPS, 2001, Menezes *et al*, 1996, IEEE, 2007, Stallings, 2011) was applied by using Galileo/SAR return link message with data encryption method as Advanced Encryption Standard/Cipher FeedBack (AES/CFB) stream as shown in Figure 2. The beacon and the MCC share the permanent key. Encryptions and decryptions are performed by Initial Vector (IV) counter and reset key command is made when keys between beacon and Mission Control Center (MCC) are difference through return link message (RLM).

Figure 3 shows return link message format and command service definition for Galileo/SAR. Acknowledgment, command, and encryption key reset (Re-synchronization) are implemented by 160 bits long return link message format to the conceptual study. Figure 3 shows that red dot line depicts how beacon control and encryption can be applied to the MSAR through return link message as acknowledgment and command services within COSPAS SARSAT modeling and simulation software.

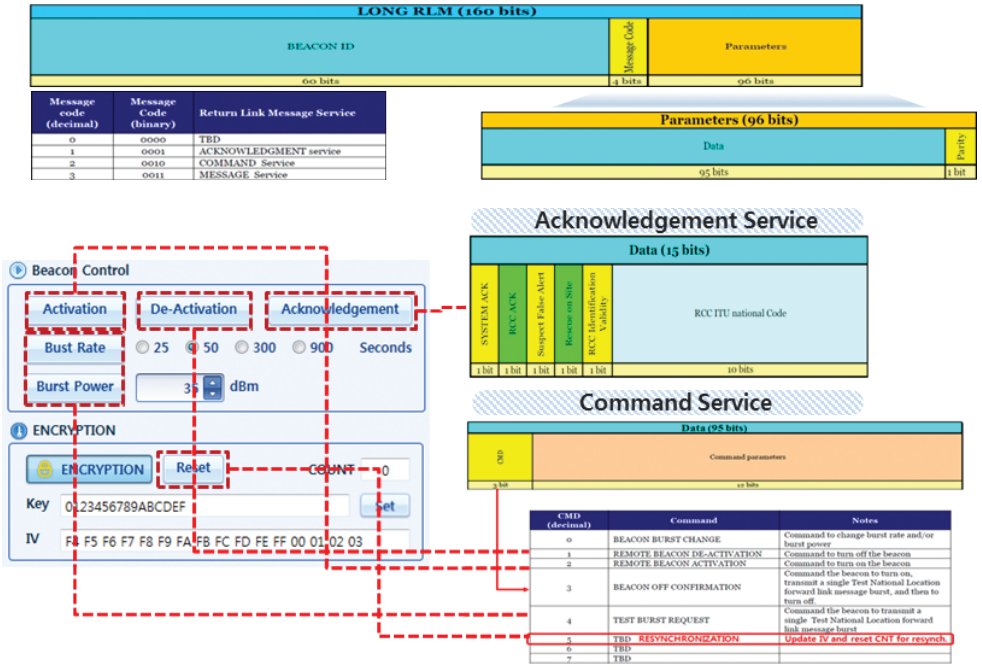

Figure 3. Return link message format and command service for Galileo/SAR

3 LTE PROTOCOL

Despite EU and other GNSS contributor's efforts, maximum numbers of operational beacons are limited due to limited frequency band allocation for the COSPAS SARSAT service. Therefore, we include LTE link as terrestrial search and rescue link with encryption/decryption in order to resolve the restriction and mitigate the burden of the COSPAS SARSAT.

The LTE network is a rapidly expanding communication network and provides a high data rate of about 100Mbps. LTE entity consists of UE (User Equipment) that is user terminal and has a wireless interface with eNB (evolved NodeB) and eNB that is the base station and provides wireless interface and radio resource management function. Figure 4 shows the configuration and architecture of LTE (Basic, 2013).

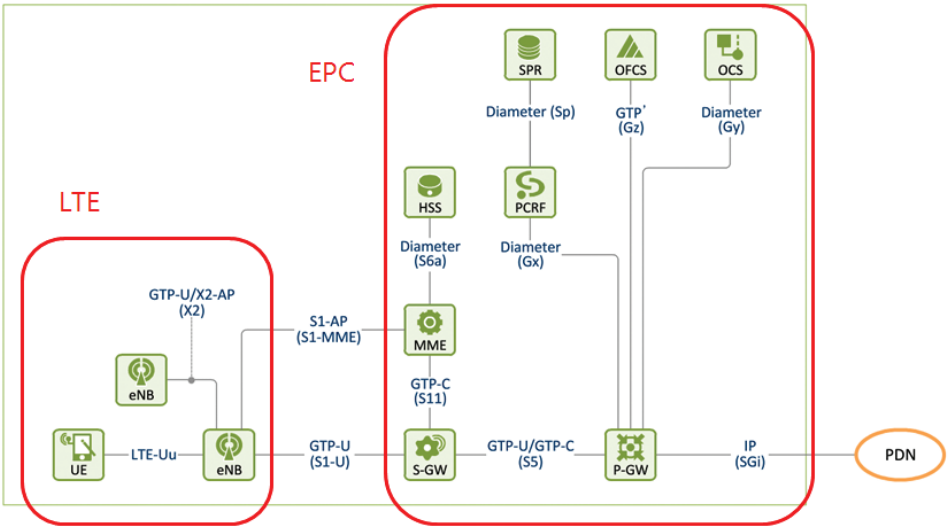

Figure 4. Configuration and architecture of LTE

Scheme and design of Encryption. LTE networks have a very complicated network structure and provide their security mechanisms. We used AES 256 bits with IPSec protocol for LTE to have an additional security mechanism. This security mechanism is for user terminal control, MCC encryption message processing, and encryption key management through return link with encryption. The attack scenario for an LTE network assumes that an attacker is not

monitoring an unspecified number of terminals, but instead analyzes the signal transmitted to the MCC and tracks the location of the terminal sending the search and rescue signal.

4 IMPLEMENTATIONS

MSAR (Military Search and Rescue) M&S (Modeling and Simulation) tool consists of modeling and simulation software of COSPAS SARSAT and LTE with Ethernet of LTE modem for search and rescue links as shown in Figure 5, respectively.

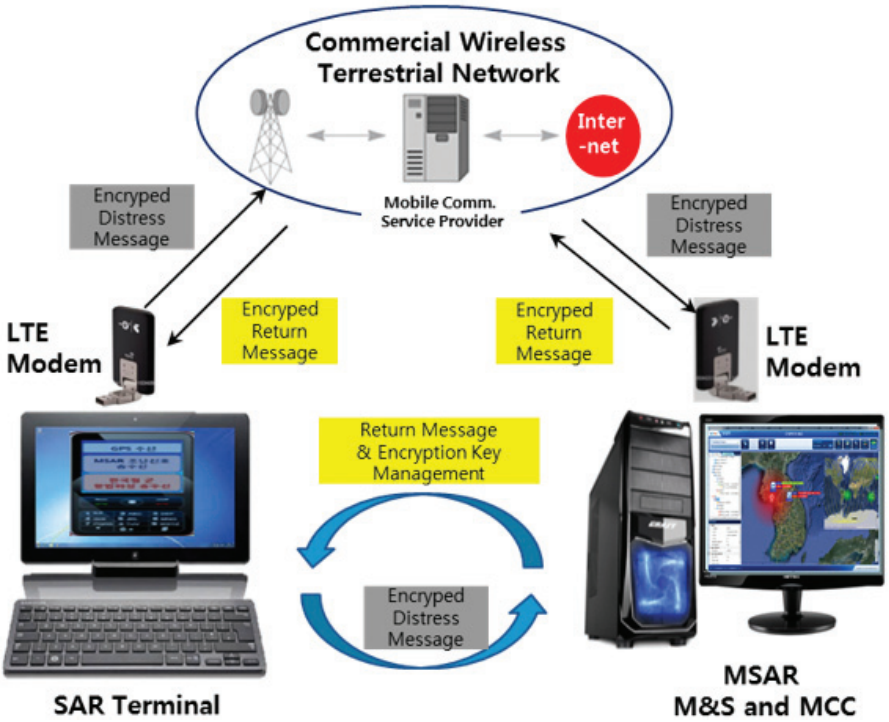

Figure 5. Simulation Window for Distress Signal in MSAR M&S

Figure 6 show user interface window that MCC provides beacon selection for location, communication link selection for COSPAS SARSAT, and LTE, beacon control, encryption and decryption including crucial reset, received beacon information, and finally, data log for the simulation.

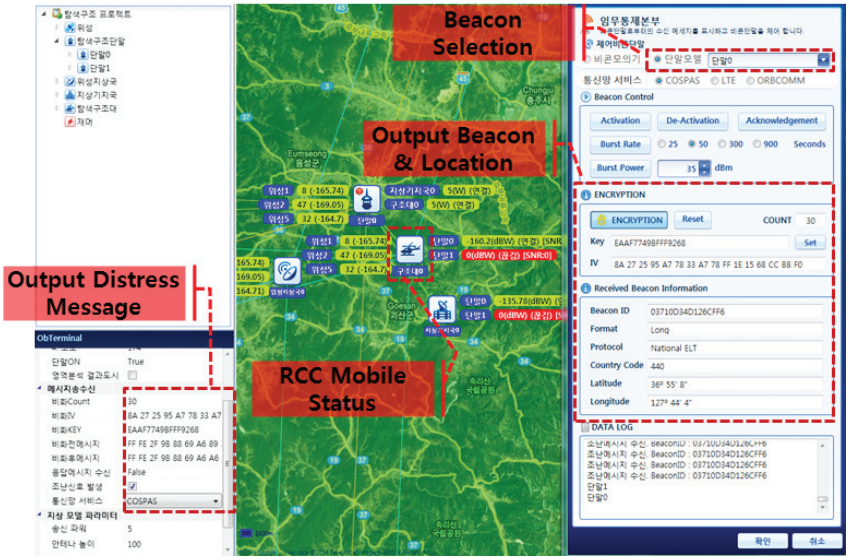

Figure 6. Simulation Window for Distress Signal in MSAR M&S

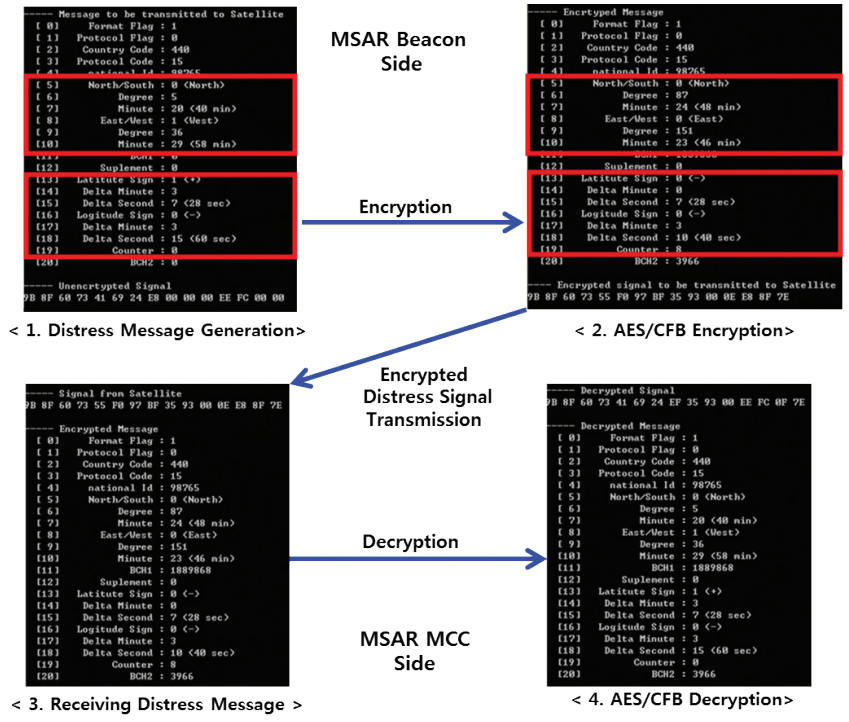

Figure 7. Verification of Encryption and decryption process

Figure 7 shows that the encryption and decryption flow for security-enhanced search and rescue by COSPAS SARSAT and the AES/CFB decrypted distress message by MCC side is identical with distress message generated by beacon side. This the procedure through LTE link showed the same test result with COSPAS SARSAT link.

5 OPERATION OF MSAR

Operation concept for Military Search And Rescue (MSAR) is proposed as shown in Figure 8. It reflects threat level, a burden to COSPAS SARSAT in the sense of limitation on channel allocation and assigned frequency band. For operation in peace, the MSAR may use terrestrial LTE network as the primary link for distress signal and its return link and will use COSPAS SARSAT link when terrestrial LTE link is not available like shadow area of LTE after several times watch-dog timer like trials without any acknowledgment from MCC. For the operation in war, COSPAS SARSAT link may be the primary link and its return link and terrestrial LTE link will be the secondary link and will be its return link when return link does not provide acknowledgment from MCC.

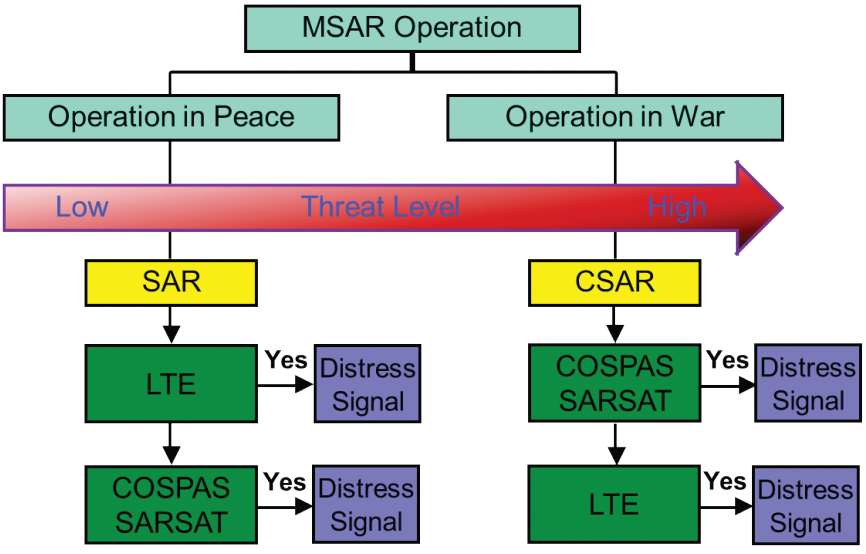

Figure 8. Operation Concept for MSAR

6 CONCLUSIONS

Security-enhanced COSPAS SARSAT system was proposed by national user protocol using encryption. In order to reduce a burden to COSPAS SARSAT, AES 256 bits for LTE was used for the encryption algorithm with IPSec protocol. Return link message format was utilized for implementation of acknowledgment, command and encryption key reset (Re-synchronization) for the both COSPAS SARSAT and LTE protocols. Security-enhanced military search and rescue system by COSPAS SARSAT and LTE with encryption was designed and implemented. Its functioning demonstrated through software Modeling & Simulation (M&S) MSAR SW with LTE modem and Ethernet link and verified. If it is realized as a real system, burden to COSPAS SARSAT under over-crowded beacons can be mitigated. The security-enhanced COSPAS SARSAT will be studied using Universal Software Radio Peripheral (USRP) by considering new Code Division Multiple Access (CDMA) signal for future work for more realistic implementation.

Acknowledgment

This work has been supported by National GNSS Research Center program of Defense Acquisition Program Administration and Agency for Defense Development.

References

International Satellite System for Search and Rescue (COSPAS SARSAT) (2017). Available at: https://www.cospas-sarsat.int/en/system-overview/cospas-sarsat-system

International Satellite System for Search and Rescue (COSPAS SARSAT) (2016). Specification for COSPAS-SARSAT 406 MHz Distress Beacons, C/S T.001 Issue 4. Montreal, Canada: COSPAS-SARSAT.

International Satellite System for Search and Rescue (COSPAS SARSAT) (2012a). SAR/GALILEO Return Link System Message Specification, JC-26/Inf.27. Montreal, Canada: COSPAS-SARSAT.

International Satellite System for Search and Rescue (COSPAS SARSAT) (2012b). RLS Type-1 Message Definition and Standardization., JC-26. Montreal, Canada: COSPAS-SARSAT.

International Satellite System for Search and Rescue (COSPAS SARSAT) (2013). Return Link Service of Type-2, JC-26/Inf.27. Montreal, Canada: COSPAS-SARSAT.

Federal Information Processing Standards (FIPS) (2001) Announcing the Advanced Encryption Standard (AES). Publication 197. Gaithersburg, Maryland: FIPS.

Menezes, A. J., van Oorschot, P. C. and Vanston, S. A. (1996). *Handbook of Applied Cryptography*. 5th Ed. London: CRC Press.

Institute of Electrical and Electronics Engineers (IEEE). (2007). Standard for cryptographic protection of data on block-oriented storage services. P1619/D16. Piscataway, New Jersey: IEEE.

Stallings, W. (2011), Cryptography and Network Security, 5th Ed. Pearson. Upper Saddle River, New Jersey: Pearson Education Inc.

NETMANIAS (2013). LTE Network Architecture: Basic. Available at: http://www.netmanias.com/en/?m=view&id=techdocs&no=5904.

Sveučilište u Rijeci
POMORSKI FAKULTET U RIJECI
FACULTY OF MARITIME STUDIES RIJEKA
University of Rijeka

University of Zagreb
Faculty of Transport
and Traffic Sciences

Royal Institute of Navigation
Science Technology Practice

11th
Annual
Baška GNSS
Conference

TRUNCATED LEAST SQUARES: HOW GOOD IS THE APPROXIMATION?

Željko Jeričević[1,2], **Ivica Kožar**[3]

[1] KMS Technologies, Houston, TX, USA
E-mail: zjericevic52@gmail.com (Corresponding author)

[2] Formerly Department of Computer Engineering,
Engineering Faculty & Medical School

[3] Civil Engineering School, University of Rijeka, Croatia

ABSTRACT

The solution of linear least squares system requires the solution of over-determined system of equations. For large dense systems that requires prohibitive number of operations. We developed a novel numerical approach for finding an approximate solution of this problem for the problems when system matrix is of a dense type. The method is based on Fourier or Hartley transform although any unitary, orthogonal transform which concentrates power in a small number of coefficients can be used. This is the strategy borrowed from digital signal processing where pruning off the redundant information from spectra or filtering of selected information in frequency domain is the usual practice.

Key words: *algorithm, modeling, numerical Simulation*

1 INTRODUCTION

The solution of a system of linear equations is one of the most widely used methods in scientific computing. In the case of dense systems the order of magnitude N^3 multiplications is required (N is dimension of a square matrix). The linear least squares method requires solution of overdetermined system of equations through some of decomposition methods. Because the least squres is one of the most used methods in data processing and data sets are becoming progressively bigger, it is of interest to speed up the calculations.

This paper extends the previous work (Jeričević and Kožar, 2005) and (Jeričević and Kožar, 2015) in which we developed a framework for efficient linear least squares problems. We also supplement previous analysis with illustrative example with various levels of approximation. Some equations developed previously (Jeričević and Kožar, 2013) are briefly repeated here as final results without the details. The basic idea of constructing the approximate solutions for large, dense systems using the Fourier or Hartley space representation remains the same.

2 COMPUTATIONAL FRAMEWORK

The Fourier transform of data matrix A is formally done by premultiplication with the Fourier matrix. However, in actual computations FFT is used whenever possible.

$$b = Ac \tag{1}$$

For overdetermined system, the Fourier transform is applied on column vector b and columns of matrix A representing a system of linear equations Equation (1). Prior to applying the transform, the vector b and matrix A have to be rearranged (obeying the rules of linear algebra) in such a way that transform has as compact representation as possible. That would concentrate the energy in the Fourier transform in smallest number of frequencies.

$$Fb = FAc \tag{2}$$

To avoid computations with complex numbers in the case of real systems the Hartley transform (Bracewell, 1986) is used. After the transformation the system (2) is of the same size as original system but it could be pruned down by deleting rows containing “insignificant” information, yielding the smaller system.

The information is termed insignificant in the signal processing sense: the frequencies in vector b whose magnitude is a smallest percentage of total magnitude are discarded, as well as the corresponding rows in the transformed matrix A. The selection of significant frequencies is accomplished by computing the magnitudes for frequencies in vector b and sorting them in decreasing order. For columns, the sum of frequencies for each column is used for that purpose. Using that information, the transforms of vector b and matrix A can be shortened into significant parts to be retained and insignificant parts to be discarded. The solution of pruned system (denoted with subscript p in equations) will be approximation of solution vector c. This approach decreases the size of the system and represents the filtering out of non significant frequencies in order to build a smaller model system with a smaller number of equations and the same number of unknowns as the original system (Jeričević, 2005). In this respect our approach is different from Beylkin's, (Beylkin *et al*, 1991) whose idea was to use wavelet transform in order to increase the sparsity of the system matrix. Using residual matrix R and Taylor order expansion (Jeričević and Kožar, 2013) it was shown that approximate inverse for system converges faster to exact equations inverse the smaller eigenvalues (λ) for (I-R) matrix are (R is residual matrix).

$$
\begin{aligned}
& y = Bc \qquad \left(y = Fb \quad B = \left[FA \right]^T \left[FA \right] \right) \\
& B_p^{-1} \approx B^{-1} \qquad \left(B_p = \left[FA \right]_p^{\mathrm{T}} \left[FA \right]_p \right) \\
& R \equiv I - B_p^{-1} B \Rightarrow B_p^{-1} B = I - R \\
& B = B_p \left(I - R \right) \\
& B^{-1} = \left(I - R \right)^{-1} B_p^{-1} \\
& \delta c = \left(I - R \right)^{-1} B_p^{-1} \delta y \\
& \left(I - R \right)^{-1} = \left(Q Q^{-1} - Q \Lambda Q^{-1} \right)^{-1} \\
& \qquad = \left[Q \left(I - \Lambda \right) Q^{-1} \right]^{-1} = Q \left(I - \Lambda \right)^{-1} Q^{-1} \\
& \lim_{\lambda \to 0} \left[Q \; diag \left(\frac{1}{1 - \lambda_i} \right)_{i=1,\ldots,n} Q^{-1} \right] \to I \\
& \left(I - R \right)^{-1} = I + R + R^2 + R^3 + \ldots \\
& B_n^{-1} \equiv \left(I + R + \ldots + R^n \right) B_p^{-1} \\
& B_\infty^{-1} \to B^{-1}
\end{aligned}
\tag{3}
$$

The convergence proof is done using normal equations formalism (premultiplying the system of equations with the transpose of matrix A). Matrix B_p is pruned approximation of B based on the most significant frequencies. Solving the model system will yield the approximate solution of original system Equation (1). The approximate solution $(c+\delta c)$ is different from true solution c for difference vector δc. It is important to show how difference vector behaves depending on truncation of matrix B_p. The equation (3) shows that requirement for convergence on R is that it should be a contraction mapping: its eigenvalues λ_i should all be non-negative, and smaller than one. Smaller the eigenvalues are, closer $(I-R)^{-1}$ is to identity matrix as can be seen from the limit equation (3) and consequently closer B_p^{-1} is to B^{-1}. The matrix Q contains eigenvectors of matrix R.

3 COMPUTATIONAL EXAMPLE

The synthetic data with superimposed random, Gaussian distributed noise using levels 0%, 1%, 5%, 10% and 20% absolute error was used in testing the algorithm. The problem was determination of polynomial coefficients from series of points containing pairs of values for independent (x) and dependent $f(x)$ variable. The data are shown in Figure 1 and its frequency domain information in Figure 2.

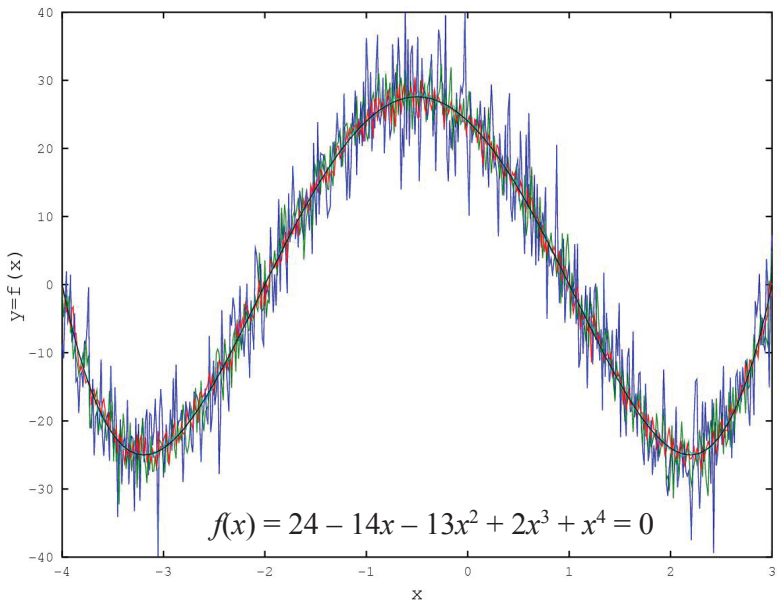

Figure 1. Polynomial data with superimposed noise

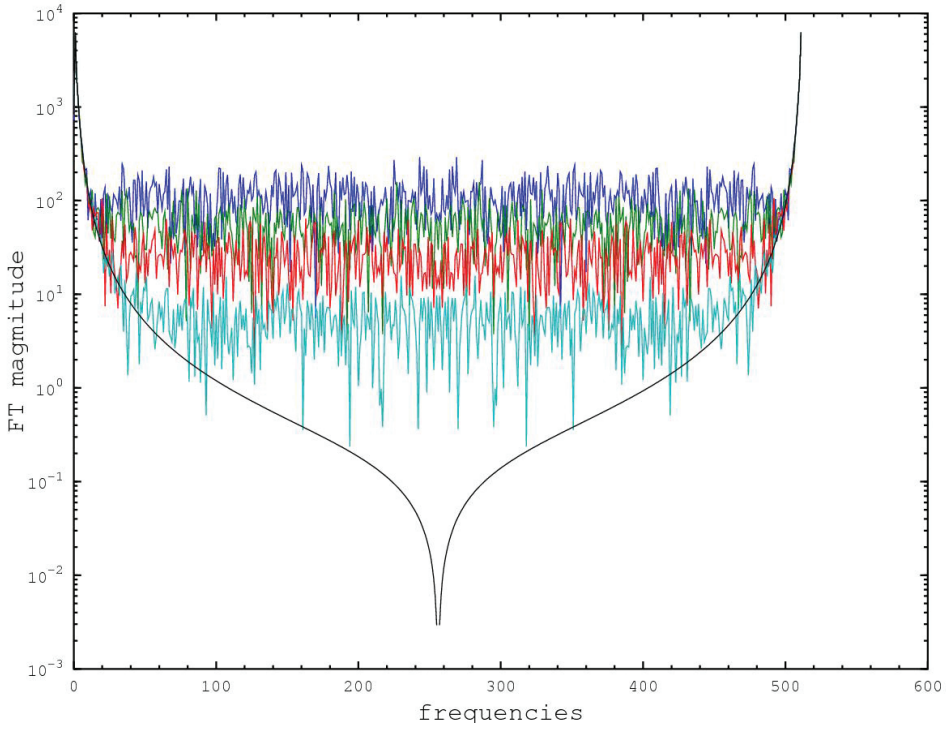

Figure 2. Polynomial data with superimposed noise shown in frequency domain. Note the domination of high frequencies by noise while lower frequencies (more intensive) are stable. Nyquist frequency is in the middle of the plot. The curves from bottom up are: no error, 1%, 5%, 10% and 20% error.

Some interesting conclusions can be concluded from the Figure 3. The accuracy of solution vector *c* and restoration of vector *b* is fairly good even for the worst of computed solutions. Consequently, the backward error analysis is too optimistic.

The results of forward error analysis are more realistic, but are not easy to compute, requiring the correct answer to evaluate an approximate one (O'Leary, 2009).

Approach with eigenvalues shown in equation (3) seems overly expensive, but to evaluate the convergence, only the highest eigenvalue is required. If it is less than 1, the iterative improvement will converge.

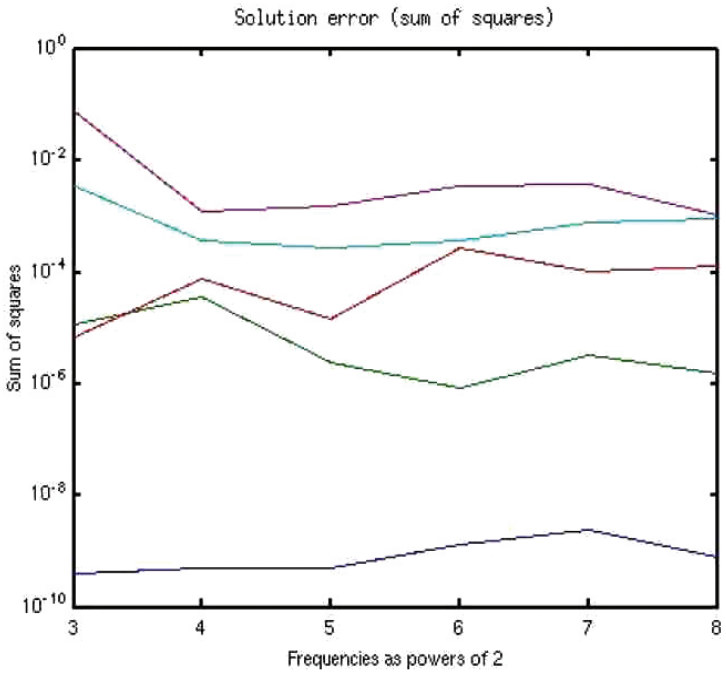

Figure 3. Error in the solution of polynomial coefficients for various noise levels and different truncation lengths

Showing the sum of squared errors in solution vector as function of the number of frequencies used to compute the approximate solution. The curves from bottom up are: no error, 1%, 5%, 10% and 20% error. Solution computed using all frequencies is used as correct solution. The results clearly indicate that truncation has much smaller effect on accuracy of solution then the overall noise levels. The error curves are fairly flat and well separated, with only one crossover.

The above simple example illustrates the power of the truncated least squares approach. A simple navigation example would be the point positioning problem using overdetermined system of linearized pseudorange observation equations. The overdetermined system is the consequence of using more then four satellites in order to improve positional accuracy.

4 CONCLUSION

The approximate method for a fast solution of linear least squares problems has been proposed. The quality of the approximation can be tested and controlled. We developed the equation which shows how the eigenvalues of residual matrix determine quality of solution and extent of corrections to be applied in order to approach the true solution. The proposed method offers more detailed assessment for the quality of solution then classical forward and backward error analysis. The quality of approximate solution is compared against full system solution and differences are found to be on the level of numerical noise. Numerical experiments illustrating feasibility of the method and quality of the approximation are presented.

Acknowledgements

The paper was presented at 11th ANNUAL BAŠKA GNSS CONFERENCE, May 2017. The authors thank the organizers for the opportunity to present their work. The part of this work was done while the first author was affiliated with the University of Rijeka.

References

Beylkin, G., Coifman, R. and Rokhlin, V. (1991). Fast Wavelet Transforms and Numerical Algorithms. *Com. Pure App Math*. Vol. 44. pp. 141–183.

Bracewell, R. N. (1986). *The Hartley Transform*. New York: Oxford University Press. p. 160.

Jeričević, Ž. (2005) Approximate Solution of Linear Systems. *Croatica Chemica Acta*. Vol. 78. pp. 601–615.

Jeričević Ž. and Kožar I. (2013). Faster Solution of Large, Over-Determined, Dense Linear Systems. *Proceedings of 36th Conference on Distributed Computing and Visualization (DC VIS MIPRO)*. Opatija, Croatia, March 20th–24th 2013. pp. 228–231.

Jeričević Ž. and Kožar I. (2015). Theoretical and statistical evaluation for approximate solution of large, over-determined, dense linear systems. *Proceedings of 38th Conference on Distributed Computing and Visualization (DC VIS MIPRO)*. Opatija, Croatia, May 28th–29th 2015. pp. 227–229.

O'Leary, D.P. (2009). *Scientific Computing With Case Studies*. Philadelphia: SIAM.

Sveučilište u Rijeci
POMORSKI FAKULTET U RIJECI
FACULTY OF MARITIME STUDIES RIJEKA
University of Rijeka

University of Zagreb
Faculty of Transport
and Traffic Sciences

Royal Institute of Navigation
Science Technology Practice

11th
Annual
Baška GNSS
Conference

GNSS PROTECTION AND ENHANCEMENT OF PERFORMANCE AND RELIABILITY THROUGH E-LORAN INTEGRATION

Gene H. McCall, AFRIN

Los Alamos National Laboratory, NM, USA
E-mail: ghm7723@gmail.com

ABSTRACT

The use of satellite systems to provide accurate Positioning, Navigation, and Timing (PNT) has become an essential part of life throughout the world. The systems have, however, vulnerabilities that can cause them to fail without notice. Rather than completely replacing these systems, or providing a complete backup system for them, it is shown that a combination of systems, in this case GNSS and e-Loran, can provide adequate protection against loss of capabilities, and can, even, provide PNT performance better than either system, alone.

Key words: *GNSS, e-Loran, signal protection*

INTRODUCTION

The use of satellite systems to provide accurate positioning and timing services on, and above, the surface of the earth has become a common feature of modern life. Coupled with a properly designed receiver and digital maps, precision navigation is possible. Many people use these capabilities for tasks as simple as driving an automobile from one place to another. The use of the timing feature of GNSS systems is, perhaps, less well-known among the general public, but it is as important to modern life as is the positioning capability. Communication systems, such as cell phones, depend on it for synchronization of signals, stock exchanges depend upon it for establishing trading priorities, power grids depend upon it to enable proper phasing of components and automated teller machines use it to assist in cash withdrawals. Many other uses, too many to enumerate here, are important, a well. Although current standards usually specify accuracy to within a few nanoseconds, or, even, microseconds, many important scientific experiments require accuracy of one nanosecond, or better. Therefore, one should be careful when stating *requirements* for timing. Today's requirements should be taken as, only, minimum standards.

Because of the author's experience, the points made in this paper will apply most directly to the United States GNSS system, the *Global Positioning System* (GPS), and GPS will be used instead of the more generic abbreviation, GNSS. The GPS has been described in detail in many places. See, for example (Misra and Enge, 2010). If detailed descriptions are needed, one should see (Parkinson *et al*, 2001). It is believed, though, that the methods described here will apply to all GNSS systems. The e-Loran system has its roots in the Loran system of World War II. The United States Department of Homeland Security defines sixteen *Critical Infrastructure sectors* deemed to be essential to American life (DHS, 2017). For some obscure reason, GPS, or, even, PNT capability, is not defined as critical even though almost all of the identified sectors depend, strongly, on this capability. I suppose, one simply dismisses the issue as a bureaucratic aberration, of which there are many throughout all governments.

REQUIREMENTS CONSIDERATIONS

Specifying requirements for the accuracy of PNT using GPS has not been very useful. The system satellites have always been built to the limit of the available timing and ranging technologies, and the result has been that the requirements

have always represented a worst-case specification. A historical summary of position accuracy of the civil signal is shown in Figure 1. It can be seen that the 2008 requirement for SPS positioning accuracy for the worst satellite 95 percent of the time is 7.8 meters with an equivalent *rms* value of 4 meters. The actual value achieved in 2008 was 1 meter and that error had been reduced to 0.7 meters by 2014. It is, also, likely that there are important applications that are not widely known, particularly those related to classified programs.

An example from a 1991 paper by Ralph Partridge, of Los Alamos (Partridge, 1991) is shown on Figure 2. The system used timing from a GPS satellite to fire an underground nuclear test at the Nevada Test site and to synchronize test diagnostic measurements. The time was also used to calibrate seismometers in the worldwide nuclear test detection network. It is interesting that the system was being used in 1988, well before the GPS was declared operational in 1995. Tests were scheduled at times when at least one satellite was in view at critical places.

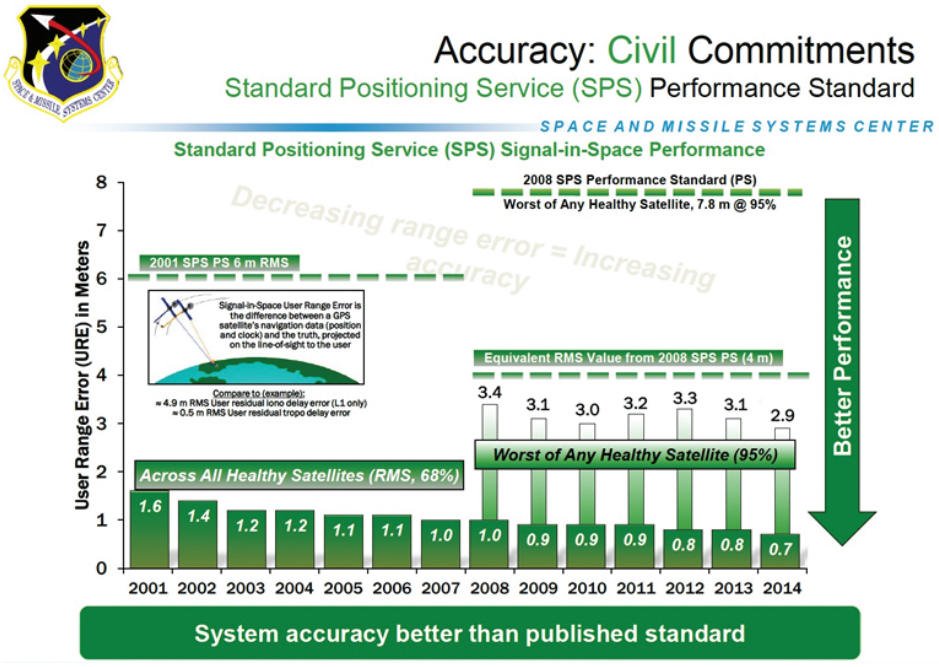

Figure 1. The history of position accuracy for the Global Positioning System

THE SIGNAL ISSUE

The GPS satellites orbit the earth at an altitude of 20,200 km. The transmitters broadcast a power of, approximately, 25.6 watts per navigation channel. The signal is distributed uniformly over the entire portion of the earth's surface visible from the satellite. The visible area corresponds to, approximately 38 percent of the earth's surface. Therefore, the signal received at the surface of the earth is very weak. For example, the L1 navigation channel has a typical received power of 1.41 × 10−6 watts, or, -158.5 dBW, which is below thermal noise. While the extreme importance of PNT may be not be completely recognized by the government bureaucracy, others are addressing the problem seriously. The United States Congress has held hearings to define the issues and to obtain suggestions for solutions (HASC, 2017). Technical and *backup* approaches have been suggested (Cameron, 2017), and the U. S. Navy has, even, reintroduced the teaching of the use of the sextant into navigation classes at the Naval Academy (Burke, 2016). Presumably, they will also reintroduce the chronometer, as well, and ships will carry windup chronometers. It was known for centuries, that the sextant provides only latitude information, and accurate time is needed to obtain longitude.

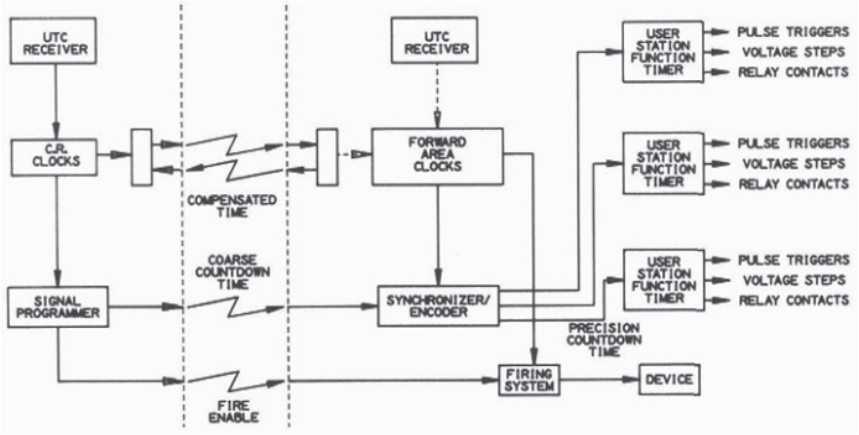

Figure 2. An application of GPS timing used before GPS was operational

Newer satellites, such as the Block IIF satellites broadcast slightly more power in the L1 navigation channel. More important, the IIF satellites broadcast a new navigation signal on an internationally protected *safety-of-life* channel at a frequency of 1176.45 MHz. It will be shown below that the ranging signal

broadcast on L5 has characteristics that are more important than the additional power. The satellite signals all occupy the same frequencies, and they are separated by standard spread spectrum methods (Ipatov, 2005). It is necessary for a receiver to receive usable signals from, at least, four satellites simultaneously to calculate an accurate position and time. Fortunately, the signal power is, effectively, increased substantially by the process of detecting it. This *processing gain* amounts to 43 dB for the L1 signal. The L5 signal has a chipping rate of 10 MHz, and the data rate is 100 symbols per second. The processing gain is, therefore, 50 dB. The factor of 6.3 resulting from the additional 8 dB processing gain is significant, as will be shown below.

SIGNAL PROTECTION

The signals considered, here, are those of GPS and e-Loran. Physical protection of the sources is straightforward, if, somewhat, expensive. The e-Loran signals are generated by terrestrial transmitter sites and a terrestrial control center. The sites may require individual physical security, fulltime, but it will be assumed that local law enforcement services will suffice.

The GPS, also, has a terrestrial component. The control centers are located on well-protected United States Air Force bases, but most of the communication antennas used to transmit control information to the satellites, are located outside the continental United States. Protection of these sites is more problematic, but local authorities may be capable of adequately protecting them. The GPS satellites are protected, first, by their orbital altitude, and, second, by their hardness to radiation. Even if nuclear weapons were used, one per satellite would be required. Antisatellite weapons could, in principle, be developed to destroy the satellites, one at a time, but the source of an attack would be identifiable, and it is likely that the United States would retaliate. Of course, satellites, themselves, could fail, but past experience is that the satellites operate, on average, a decade, or more, and several simultaneous failures would be necessary to cause system failure. It is safe to assume that satellite failure is not a serious issue.

Many governments have passed laws against jamming of PNT signals. The United States Federal Communication Commission (FCC) states on its website that use of a GPS jammer can result in fines of up to $100000 and, even, imprisonment. It seems, however, that such penalties have seldom been applied, and jammers are readily available on the internet.

INTERFERENCE AND JAMMING

Although the intent, here, is to integrate the GPS and e-Loran systems, it is useful to consider, first, the susceptibility of the individual systems to interference. Interference generated by humans with the intent of preventing the use of the system is, usually, identified as *jamming*. Although the effects may be similar, jamming is the process of most interest, here. Another form of interference, *spoofing*, which results in misdirecting the user, is also defeated by the system to be described, and a separate anti-spoofing signal will no longer be required. Even though governments advocate the development of backup, or substitute, systems for GNSS, and substantial funding has been provided for the development of such systems, little effort has been devoted to the enforcement of existing laws, an few convictions have resulted.

E-LORAN JAMMING

The e-Loran system operates at a low frequency of 100 kHz at high power. Studies have shown (Chadwick, 2006) that jamming of e-Loran signals is very difficult, and it is likely to require a large, and expensive, apparatus. It will be assumed, here, that, for practical purposes, e-Loran cannot be jammed. The signals are subject to atmospheric interference, but such interference is moderate, at worst, and will be ignored here.

GPS JAMMING

The received GPS signal is, as noted above, at a power level below thermal noise, and it is the processing gain that enables detection. Figure 3 was taken from a Defense Science Board report (DSB, 2005). The report recommended a jamming resistance of 90 dB. It is, perhaps, useful to recognize that the different navigation signals have different powers and different processing gains.

Here two versions of jammers will be considered. The first is assumed to project a random noise signal uniformly over the entire frequency band covered by GPS signals. The band ranges from, approximately, 1164 MHz to 1577 MHz, a range of 413 MHz. Each navigation channel will receive an amount of power proportional to its bandwidth.

A somewhat more dangerous form of jammer could radiate one-third of its power into each of the GPS bands, L1, L2, and L5. This form of jammer will be assumed as a *worst case*.

THE UNJAMMABLE RECEIVER

Of course, any device that depends on the reception of radio frequency signals is susceptible to jamming. To designate a device as *unjammable* must, therefore, involve practical considerations. Most jammers encountered at present are similar to those shown in Figure 4. Jammers of this type tend to radiate powers in the range of 0.1 to two watts. Prices range from, approximately, $100 to $500, depending on output power Figure 3 shows, however, that existing receivers can be affected at ranges as long as several kilometers.

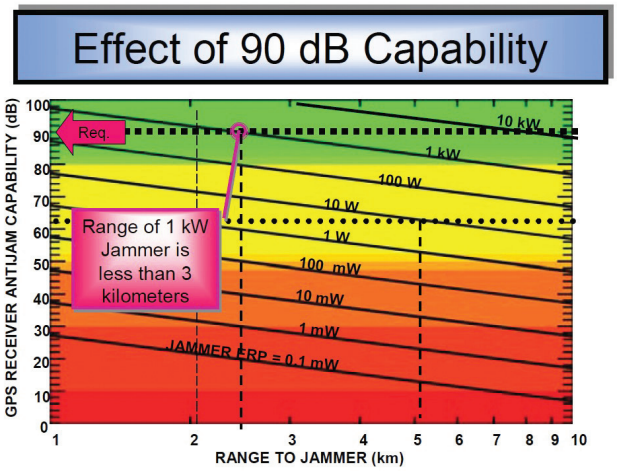

Figure 3. Required jamming resistance

Figure 4. GPS jammers available on the internet

It is not safe to assume, however, that jamming technology has reached its peak. In the near future, it is likely that jammers having powers in the 100 watt range will become common, and inexpensive. But, even at 100 watts, an L-band transmitter can take the form shown in Figure 5, a device which weighs 50-60 kg and has a panel over 60 cm wide.

Figure 5. A 100 watt L-band transmitter

Figure 6. A 250 watt GPS jammer sold on the internet (JFC, 2017)

Therefore it will be assumed that a practical jammer limit in the foreseeable future will be 1 kW. A receiver will be identified as unjammable if it can operate effectively at a distance of less than 3 kilometers from a 1 kilowatt jammer, as recommended by the DSB. A 250 watt jammer sold on the internet, apparently for a price around $13000, is rack-mounted, and it has a size consistent with the

unit of Figure 5. A photo is shown on Figure 6. It has been shown, though, that jamming of GPS receivers is not a completely generic process. Niekerk and Cambrinck (2013) measured the jamming threshold of several commercial receivers by placing a jammer at a distance of 2 km from the receiver and varying the jammer power. The results are shown in Figure 7, which was labeled as Table 1 in the original document.

TABLE 1: The ability of four GPS receivers to resist jamming at different signal strengths.

Signal strength (dBm)	GPS receiver			
	Garmin 60CSx	Garmin eTrex	Trimble ProXH	Topcon GB-1000
-3	P	P	P	P
0	P	P	P	NP
1	P	P	P	NP
4	P	P	P	NP
7	P	P	P	NP
9	P	P	P	NP
10	NP	P	P	NP
12	NP	P	P	NP
13	NP	NP	P	NP
15	NP	NP	P	NP
17	NP	NP	NP	NP

P, indicates the ability to determine a position; NP, indicates that a position could not be determined.

Figure 7. Sensitivity of various receivers to jamming from a jammer on the L1 band at 2 km. P indicates that the receiver gave an accurate position, and NP indicates that no position was given.

It is clear that different receivers respond differently to a jammer. For example, Figure 7 shows that the Topcon GB-1000 receiver is unable to operate properly in the presence of a 1 mW jammer at a distance of two kilometers, while a Trimble ProXH operates well with a 32 mWs jammer at the same range. The jamming resistance appears to have little to do with the quality of normal operation.

The jamming of GPS receivers is not just a possibility in the future. South Korean government officials have reported significant GPS jamming emanating from North Korea (KH, 2016), and the Russian newspaper, *Izvestia* has reported that the Russian government is installing thousands of jammers on cellphone towers throughout Russia (Izvestia, 2016). Within the United States, the Economist has reported five to ten minutes of GPS jamming every day at the New York Stock Exchange (The Economist, 2013), which is dependent on GPS for transaction

timing. This is consistent with measurements at 40 sites, mostly in Europe, that have detected 124,100 jamming events from 17,000 identified jammers (GSA, 2017), mostly in city centers. It is believed that the jammers are used by truckers to block their company's attempts to track them. In spite of possible legal penalties, the truckers' use of jamming is, essentially, a casual process.

REQUIRED JAMMING PROTECTION

Consider a jammer having power P_j operating at a distance R from a receiver and radiating uniformly. The jamming intensity at the receiver, I_j, is given by:

$$I_j = \frac{P_j}{4\pi R^2} \tag{1}$$

The received power in each channel can be calculated by multiplying the intensity at the receiver by the effective area of a 0 dB antenna:

$$A_{eff} = \frac{\lambda^2}{4\pi} \tag{2}$$

where λ is the channel wavelength. In terms of dB relative to one watt, dBW, the received jammer powers for channels, L1, L2, and L5, are -80.7, -78.5, and -78.2, respectively. Given that the received power in channels L1 and L2 are, approximately, -160 dBW, and in L5, -158 dBW, it appears that the ratio of jammer to signal power is, approximately, 80 dB, for all channels. Thus, it appears that a processing gain of 90 dB is required for all three channels to defeat the jammer described above. If one attempts to produce 90 dB of processing gain by increasing the correlation time, L1 and L2 would need a correlation time of 1000 seconds, and L5 would require 100 seconds. While times as long as these could be used to track a very slow moving receiver, such long times are not, in general, practical. At least, a complementary tracking method must be used during the correlation time.

Ohlmeyer (2006) has described an ultra-tightly coupled GPS/INS system that enhanced jamming resistance by 75 dB. No particular detail of the system indicated that it had reached its limit. The elapsed time for the test was, approximately 230 seconds, although the starting time was, about 80 seconds, giving a running time of 150 seconds. If the jamming resistance of 75 dB had been obtained solely by increasing the correlation time, the time required would

have been 3.16 seconds. Although the accuracy obtained was not high, the jamming resistance was useful.

Petovello *et al*. (2008) have demonstrated an increase in the effective signal strength of 30 dB in carrier phase measurements with short GPS correlation times. The carrier phase measurement is important for achieving the best possible accuracy.

Next, The effects of e-Loran will be considered.

e-LORAN

e-Loran is a low frequency navigation system operating at a carrier frequency of 100 kHz. The system is well known, and its detailed specifications will not be given here. For reference, accuracy specifications for GPS and e-Loran are given in table 1, where the e-Loran values are taken from (Helwig *et al*, 2011), and the GPS values are taken from (FAA, 2014).

It appears in Table 1 that the performance specifications would lead one to choose GPS over e-Loran. That is true if accuracy is the primary, or only, consideration, and if the values given represent the best possible obtainable. However, the importance of PNT capabilities to modern civilization is so high that better performance must be required, and a continuing technology upgrade path should exist.

Table 1. Comparison of GPS and e-Loran performance

Spec.	e-Loran	GPS
Position	20 m	4 m
Time	50 ns	8 ns
Jamming Sensitivity	low	high

In fact, neither system, alone, provides adequate resolution in either position, or timing, for the future. The best position (GPS) resolution shown in Table 1 is, for example, inadequate for the control of driverless automobiles. It is said that these automobiles are soon to appear on highways. The timing resolution of 8 ns is inadequate for the synchronization of high speed computer networks of the future and for cybersecurity applications.

CORRELATION TIME AND ANTI-JAM IMPROVEMENTS

It is well-known that the processing gain protects against noise jamming, and that the processing gain can be increased by increasing the correlation time. However, the increase occurs only if the receiver code is a true representation of the satellite code. The satellite navigation message is modulated onto the ranging code, and, therefore, the satellite pseudo-random noise (PRN) code will not match the receiver code, at least after the first navigation code bit. In the case of the C/A code, the bits can change every 20 ms. Thus, the correlation integration time is limited to 20 ms, which sets the correlation integration time to a value corresponding to the 50 Hz navigation message frequency. For an integration time, τ, and a chipping rate of f_c, the processing gain G, is given by:

$$G = \tau f_c \tag{3}$$

For the 1 MHz C/A code and an integration time of 20 ms, the gain is 43 dB. If the navigation message were known, the true satellite code could be constructed inside the receiver and, in principle, the correlation integration time could be extended indefinitely (Ward *et al*, 2006). In addition to the integration time extension, other advantages are incurred. The receiver also produces a replica carrier, which is locked to a local oscillator by a Phase Locked Loop (PLL). Since the navigation message is modulated onto the carrier, the presence of the message disturbs the carrier lock. If the message were removed, a pure PLL discriminator could be used, and the signal tracking threshold would be improved by up to 6 dB.

The standard way of stripping the data message is to detect, and extract, it first and, then, use the extracted bit train to construct the receiver code and carrier. Of course, this method will not work in areas where one is attempting acquisition and high power jammers exist. Therefore an independent method for obtaining the navigation message will be described. It will be shown that the method, also, provides significant additional advantages.

e-LORAN MESSAGING

From this point forward, it will be assumed that receivers of interest receive both GPS and e-Loran signals.

The e-Loran system has a data channel (Helwig *et al*, 2011), but it is designed to transmit messages at the low rate of 20-50 bps. However, that low rate has been shown not to be the limit of loran transmission possibilities. A transmission rate of 250 b/s using a hybrid modulation technique was used to transmit data required by the FAA Wide Area Augmentation System (WAAS) in flight trials in Alaska where the data signals from the WAAS satellites were not reliable (Lo and Enge, 2002). The method worked perfectly, and the authors commented that: The ability to carry communication on LORAN would be of immense use to navigation. This author agrees completely.

Liang and coworkers have extended the hybrid modulation scheme (Liang *et al*, 2012) to a point where they claim that a modulation rate of 2560 bps can be obtained. The rate depends on the number of Group Repetition Intervals (GRI) being, at least, 20 per second. The maximum rate will not be invoked below, but it will be assumed that a transmission of, at least, 1 kbps is possible.

Work at the U. S. Coast Guard Academy (Peterson, 2000), though, has shown that data rates as high as 4 kbps are possible.

The dual function GPS/e-Loran receiver will be designed, first, to receive GPS navigation data over the loran channel and use the data to construct navigation message-free PRN codes for all the GPS satellites. It will not be necessary to transmit a full navigation message for all satellites, separately, since much data, such as the almanac applies to all satellites. A transmission time of 1-2 seconds per satellite should be sufficient, given the system architecture described below. Given the work cited above, however, a time of 0.5 seconds per satellite is possible.

It should be noted that only the ninth pulse of the e-Loran system is involved in creating the integrated system. Therefore, if the entire GPS system failed, the e-Loran system would perform as now understood.

e-LORAN SYSTEM ARCHITECTURE

The e-Loran system will be self-contained for the process of constructing messages. Each will be equipped with a GPS receiver that can collect information from all GPS satellites in view. Whether the entire constellation is covered will depend on the number, and locations, of the participating e-Loran stations. The stations will, also, be equipped with a Two-Way Satellite Time

Transfer Terminal (TWSTTR). The range information and navigation message for each satellite in view will be transmitted to the e-Loran control center, time stamped with the TWSTTR data, which will be within one nanosecond of UTC.

The control center will calculate a real time ephemeris and clock offset for each satellite and uses it to prepare the second part of the data message.

The data message for each satellite will be in two parts. The first part of the message will permit the construction of the navigation data message and the preparation of data-free receiver codes and carriers. The second part of the message for each satellite will be a current ephemeris and clock offset. it should be possible to prepare the data so that the ephemeris and clock information are no more than three minutes old. It has been found that a network of stations as described, which produce a real time ephemeris, can produce position errors in the range of 2-6 centimeters and clock errors of 0.2 ns (Sun *et al,* 2016). Other studies using an ephemeris, approximately, 15 minutes old have observed position errors of less than one meter (Brown *et al*, 2008).

Therefore, it appears reasonable to characterize the system described as producing position errors of 10 cm and time error around one nanosecond. Identifying the integrated system as GLI, for GPS-Loran integrated, Table 1 becomes Table 2. If necessary, the ephemeris update time can be reduced to a value as small as one second. The useful characteristics of the integrated system are apparent.

Table 2. Comparison of GPS, e-Loran, and GLI

Spec.	e-Loran	GPS	GLI
Position	20 m	4 m	10 cm
Time	50 ns	8 ns	1 ns
Jamming Sensitivity	low	high	low

GLI JAMMING

It is clear that jamming sensitivity of the GLI system will be lower than for GPS because of the absence of the constructed navigation message in the receiver replica of code and carrier permitting longer correlation times, but other improvements should be possible, as well. It was noted above that ultra-tight coupling of GPS and INS systems improve jamming resistance (Ohlmeyer,

2006). It should be possible to construct an INS emulator using phase information from the e-Loran signal. Using the emulator to calculate INS-like corrections to the motion should give results similar to those of the ultra-tightly coupled system. Although absolute e-Loran position measurements depend strongly on variables, such as additional secondary factors (ASF), small differential phase measurements should be accurate replicas of receiver motion. These assertions remain rather speculative at present, but the possibilities make them deserving of study. If the e-Loran phase measurements fail to provide adequate accuracy, a MEMS inertial system can be inserted into the receiver.

COHERENT DETECTION

It has been shown that simultaneous tracking of all satellites in view effectively multiplies the signals by the number of channels tracked (Axelrad, 2011). Observation has, also, shown that on average 10 GPS satellites are in view at all times. Tracking an average of 4 channels per satellite will give an effective signal increase of 16 dB. Allowing 30 dB for ultra-tight-coupling, further protection of, approximately, 60 dB will render the GLI system, effectively, unjammable. As a conservative estimate, a further protection of 70 dB will be supplied. The additional protection can be obtained at the expense of increasing the correlation time by one second, assuming that the ranging code is chipping at a rate of 10 MHz, as is the case for the P, and L5 codes.

Thus, the total jamming protection is 116 dB, more than adequate to characterize the GLI system as *unjammable*.

SPOOFING

Spoofing requires that a GPS receiver lock to one, or more, false satellite signals that cause the vehicle being controlled by the receiver to divert from its intended course. Usually, the false signal delivers a false ephemeris to produce the diversion. The integrated system protects against spoofing in two ways. First, the ephemeris information will be received from the e-Loran message, not the satellite. When the message is used to construct a valid ranging code, it is unlikely that the code will agree with that transmitted by the false satellite. Second, the e-Loran signal is extremely difficult, even impossible, to replace with a false signal. Further, the GPS course and the e-Loran course must agree within system errors - again, an impossible task for the spoofer.

Therefore, it is suggested that the Y-codes be eliminated from the satellites and P-codes with a chipping rate of 10 MHz be provided to everyone. Thus, the expensive SAASM chip will no longer be needed in receivers, and overall jamming resistance will be improved.

SYSTEM IMPLICATIONS

If the integrated system can achieve its goals, the implications for future GPS developments are severe. It would seem that the route to pursue for future satellite development and launch would be optimum if future satellites were of the IIF type with the L1 signal replaced with a 10 MHz chipping rate signal similar to the L5 signals. Using the P codes will accomplish this. The GPS III satellites will provide little, if any, improvement, even though they will require much effort and will be extremely expensive. if the accuracy and reliability of the system can be verified, one can address the question as to whether continued use of augmentation systems, such as WAAS and EGNOS are necessary. Those systems provide position accuracies only in the 1-2 meter range. They are used for safety-of-life tasks, such as instrument landings, and they require high GNSS reliability, a need which is satisfied by the GLI system.

The e-Loran system will require development and construction, but those projects will be inexpensive compared to, say, GPS III satellites.

TIME TO FIRST FIX

A significant, if somewhat less important, feature is that the Time to First Fix (TTFF) will be reduced substantially for a receiver attempting a *cold start*. The receiver location will be known to within the e-Loran accuracy of 20 meters, and the ephemerides and clock offsets for all satellites in view will be known. Therefore the optimum set of satellites for the receiver to consider for first lock can be determined immediately, and no trials will be required.

INDOOR NAVIGATION

Another benefit of the integrated system is that, since it, effectively, increases signal power by a large factor, indoor navigation will be enabled. Accurate indoor navigation will have many important commercial and safety of life advantages.

INTERNATIONAL ISSUES

e-Loran is a system used by several nations, and there may be objections to the substantial changes to the system that will be required to produce the integrated system. It should be noted, however, that the changes to the signal are only in the ninth pulse, and e-Loran receivers will perform in the normal way.

It may seem that the modified system will enhance GPS, alone. That objection is, however, is not valid. More, and more, receivers are being designed to accommodate more than one GNSS system. The modified e-Loran system could be designed in an analogous way. Thus, there could be GPS chains covering the United States and cooperating nations, Galileo chains for Europe, Beidou chains for China and associates, Glonass chains for those collaborating with Russia, and, perhaps, others. The loran message can contain information identifying the system associated with a particular chain.

HOW TO PROCEED

For any system, such as this, for which complete operation has not been verified, it is illogical to attempt to field a complete system without further verification. The first step should be confirmation as a research and development project. It appears that e-Loran will be funded, and built. If so, the first two stations could be a master and a secondary station in the same chain. These stations can be configured as described above. At the same time an integrated receiver can be designed and built. After the performance has been verified, a series of jamming experiments should be done to demonstrate resistance to jamming, thus, ending the R&D project and justifying construction of the entire system. No doubt, some modifications of the ideas will be required.

WHO CAN DO IT?

The selection of the government agency to oversee the R&D work and, if justified, the following system construction, is an important task. The agency selected must be devoted to the successful completion of the development and construction. It should have experience in the technical area of positioning, navigation, and timing. The program should be considered by the agency as one of its most important.

In my opinion, the only agency in the United States that meets all the requirements is the United States Coast Guard (CG).

The Coast Guard was an exemplary steward of the loran system during the entire time of its existence. The CG has been a leader in innovation in the PNT area with its National Differential system, and it has a strong technical legacy in loran and e-Loran in the engineering department of the Coast Guard Academy. The department may have to be expanded, somewhat, to take in this program, but that is, certainly, possible.

Other agencies have some shortcomings. The Air Force will, quickly, realize that the system is not an F-35, and may consider it a competitor to big ticket items, such as GPS III, since it obviates the need for that system. The Navy is in the process of attempting to increase its number of ships, and it would, very likely consider the GLI program a distraction. The Naval Research Laboratory (NRL) and the Naval Observatory (USNO) have the necessary technical abilities, but little experience in the large system construction and operation areas. The CG may choose, however, to use the capabilities of these organizations to solve some of the problems that are sure to arise.

CONCLUSIONS

A system which integrates the GPS and e-Loran systems in a single receiver has been described. It appears that under benign operating conditions, the integrated system produces performance better than either system standing alone. Under conditions of strong interference, performance greatly exceeds that of GPS alone and is, for practical purposes, unjammable.

The technologies necessary for constructing the GLI system have all been demonstrated, separately, but their proper operation when integrated must be verified. The process for verifying integrated performance would be, first, to simulate the system operation, and, then, to activate one, or two e-Loran stations which have the proper signaling, and monitoring, capabilities, and to design, and build an integrated receiver that operates as described above. This can be done as a research and development program. E-Loran stations, with monitoring systems attached can, then, be added one at a time or at least, one chain at a time. At the end of the process, a complete North American e-Loran chain will exist as a GPS backup even if the integration process fails. In the event of a complete failure fo the GPS, the e-Loran system will continue to operate in its

well-understood way. In the process of development and construction a significant store of GPS and e-Loran technology will be collected, even in the event of failure, and compared to the cost of satellite launches, the cost will be modest. The USCG was identified as the best agent for pursuing the program.

The time to begin is now!

References

Axelrad, P. *et al*. (2011). Collective Detection and Direct Positioning Using Multiple GNSS Satellites. *Journal of the Institute of Navigation*. 58. 305–321.

Brown, A. *et al*. (2008). Test Results from a Precise Positioning and Attitude Determination System for Microsatellites using a Software-Defined Radio. *Proceedings of the 21st International Technical Meeting of the Satellite Division of The Institute of Navigation (ION GNSS 2008)*. Savannah, September 16th – 19th. pp. 769 –774.

Burke, M. M. (2016). *Stars and Stripes Newspaper*, 29 January 2016.

Cameron, A. (2017). *GPS World*, 27 March 2017.

Chadwick, D. J. and Kim, T. (2006). An Evaluation of the Effectiveness of Intentional Interference on E-Loran. *Military Communications (MILCON) Conference*. October 23rd – 25th, 2006.

Defense Science Board (DSB). (2005). *The Future of the Global Positioning System*. Washington, D.C: DSB.

Department of Homeland Security (DHS). (2017). *Presidential Policy Directive (PPD-21)*. Available at: at www.dhs.gov.

European GNSS Agency (GSA). (2017). STRIKE3 Project. Available at: http://www.gnss-strike3.eu/

Federal Aviation Administration (FAA). (2014). *GPS SPS Performance Analysis (Report No. 86)*. Washington, D.C: FAA.

Helwig, A. *et al*. (2011). *e-Loran System Definition and Signal Specification Tutorial (ILA-40)*. London: International Loran Association.

House Armed Services Committee (HASC). (2017). *Strategy and Forces subcommittee*. Availale at: https://armedservices.house.gov/

Ipatov, V. P. (2005). *Spread spectrum and CDMA: Principles and applications*. Hoboken: Wiley Publishing.

Izvestia, 23 October 2016.

Jammer From China (JFC). (2017). Available at: www.jammerfromchina.com

Lo, S., and Enge, P. (2002). WAAS performance in the 2001 Alaska Flight Trials of the high speed Loran data channel. *Proceedings of IEEE Position, Location, and Navigation Symposium 2002*. Palm Springs, April 15th – 18th, 2002. pp. 328–335.

Misra, P. and Enge, P. (2010). *Global Positioning System, Signals, Measurements, and Performance*. Lincoln: Ganga-Jamuna Press.

Niekerk, A. and Combrinck, L. (2012) The use of civilian-type GPS receivers by the military and their vulnerability to jamming. *South African Journal of Science*. 108. pp. 1–4.

Ohlmeyer, E. J. (2006). Analysis of an Ultra-Tightly Coupled GPS/INS System in Jamming. *Proceedings of IEEE Position, Location, and Navigation Symposium 2006*. Coronado, April 25th – 27th, 2006. pp. 44–53.

Parkinson, B. W. *et al*. (eds.) (2001). *Global Positioning System: Progress in Astronautics and Aeronautics*. Vol. 163, Lincoln: AIAA.

Partridge, R. E. (1991). Timing system for firing widely spaced test nuclear detonations (Los Alamos Report LA-UR-91-3749, 1991). *Proceedings of the 23rd NASA GSFC Annual Precise Time and Time Interval (PTTI) Applications and Planning Meeting.* Pasadena, California, December 3th–5th, 1991. pp. 119–126.

Peterson, B. B. *et al*. (2000). Enhanced LORAN- C data channel project. *Proceedings of the International Symposium on Integration of LORAN-C/Eurofix and EGNOS/ Galileo*. pp. 186–197.

Petovello, M., O'Driscoll, M. and Lachappelle, C. (2008). Weak Signal Carrier Tracking Using Extended Coherent Integration with an Ultra-Tight GNSS/IMU Receiver. *Proceedings of the 12th ENC-GNSS Conference*. Toulouse, April 23rd–25th, 2008. p. 11.

Liang, Q., Xiong W. and Li, Y. (2012). Research on Modulation Technique of High Speed Loran-C Data Channel. *Proceeedings of 8th International Conference on Wireless Communications, Networking and Mobile Computing (WiCOM)*. Shanghai, September 21st – 23rd, 2012, pp. 1–3.

Sun, J. *et al*. (Eds.) (2016). *Proceedings of China Satellite Navigation Conference (CSNC) 2016*. Volume 3. Changsha, May 18th–20th, 2016.

The Economist, 27 July 2013.

The Korean Herald (KH), 31 March 2016.

Ward. P. W., Betz, J. W. and Hegarty, C. J. (2006). Satellite Signal Acquisition, Tracking, and Data Demodulation (Chapter 5). In: Kaplan, E. D. and Hegarty, C. J. (eds.*). Understanding GPS: Principles and Applications, Second Edition*. Norwood: Artech House. pp. 153–241.

Technical co-sponsors

Satellite Navigation University Network

Sveučilište u Rijeci
TEHNIČKI FAKULTET

Media coverage

Coordinates
A monthly magazine on positioning, navigation and beyond